REPORT 2014 - 14

VERMONT AGENCY OF TRANSPORTATION

Materials & Research Section
Research Report

STATISTICAL ANALYSIS OF WEIGH-IN-MOTION DATA FOR BRIDGE DESIGN IN VERMONT

Report 2014 – 14

December 2014

STATISTICAL ANALYSIS OF WEIGH-IN-MOTION DATA FOR BRIDGE DESIGN IN VERMONT

Report 2014 – 14

DECEMBER 2014

Reporting on SPR-RAC-729

STATE OF VERMONT
AGENCY OF TRANSPORTATION

RESEARCH & DEVELOPMENT SECTION

BRIAN R. SEARLES, SECRETARY OF TRANSPORTATION
CHRIS COLE, DIRECTOR OF POLICY, PLANNING AND INTERMODAL DEVELOPMENT
JOE SEGALE, P.E./PTP, PLANNING, POLICY & RESEARCH
WILLIAM E. AHEARN, P.E., RESEARCH & DEVELOPMENT

Prepared By:

University of Vermont, Transportation Research Center
Eric M. Hernandez, Ph.D., Assistant Professor, School of Engineering

Transportation Research Center
Farrell Hall
210 Colchester Avenue
Burlington, VT 05405
Phone: (802) 656-1312
Website: www.uvm.edu/transportationcenter

The University of Vermont

The information contained in this report was compiled for the use of the Vermont Agency of Transportation (VTrans). Conclusions and recommendations contained herein are based upon the research data obtained and the expertise of the researchers, and are not necessarily to be construed as Agency policy. This report does not constitute a standard, specification, or regulation. VTrans assumes no liability for its contents or the use thereof.

Technical Report Documentation Page

1. Report No.	2. Government Accession No.	3. Recipient's Catalog No.
2014-05	- - -	- - -

4. Title and Subtitle	5. Report Date
STATISTICAL ANALYSIS OF WEIGH-IN-MOTION DATA FOR BRIDGE DESIGN IN VERMONT	October 2014
	6. Performing Organization Code

7. Author(s)	8. Performing Organization Report No.
Eric M. Hernandez, Assistant Professor, School of Engineering	2014-09

9. Performing Organization Name and Address	10. Work Unit No.
UVM Transportation Research Center Farrell Hall] 210 Colchester Avenue Burlington, VT 05405	11. Contract or Grant No. RSCH017-729

12. Sponsoring Agency Name and Address		13. Type of Report and Period Covered
Vermont Agency of Transportation Materials and Research Section 1 National Life Drive National Life Building Montpelier, VT 05633-5001	Federal Highway Administration Division Office Federal Building Montpelier, VT 05602	Final 2012 – 2014
		14. Sponsoring Agency Code

15. Supplementary Notes

16. Abstract

This study investigates the suitability of the HL-93 live load model recommended by AASHTO LRFD Specifications for its use in the analysis and design of bridges in Vermont. The method of approach consists in performing a statistical analysis of weigh-in-motion (WIM) data collected between the years 2000-2012 at 12 stations across the state of Vermont. In total 36,754,819 individual WIM events were analyzed in this study. We compared the statistics of the lane moment and shear induced by the WIM data to the corresponding lane moment and shear induced by the HL-93 live load model. This analysis was performed on two types of very common bridge decks: (i) steel girders and concrete slabs and (ii) concrete girders with concrete slabs. In all cases the decks were considered to be acting fully composite. We considered span lengths in the range of 5-60 meters (~ 16-200 ft). The mains findings of this study are: (i) The probability that the lane moment and shear induced by the WIM data exceeds the corresponding values induced by the HL-93 model, decreases with span length. Averaged over all years considered in this study, the largest probability of exceedance was found to be approximately 1%. (ii) For span lengths exceeding 10 m, the annual probability of failure induced by the WIM data analysis did not exceed the annualized AASHTO target probability of failure. This indicates that for typical bridge decks with span length exceeding 10 meters, the HL-93 live load model is adequate for its use in Vermont. (iii) We propose that a more detailed study be carried out for short span structures such as culverts. Evidence from our study suggests that for very short spans (< 10 m), the HL-93 live load model might not be conservative.

17. Key Words	18. Distribution Statement
Statistical Analysis, Weigh-in-Motion, Bridge Design, LRFD,	No Restrictions.

19. Security Classif. (of this report)	20. Security Classif. (of this page)	21. No. Pages	22. Price
- - -	- - -		- - -

Form DOT F1700.7 (8-72) **Reproduction of completed pages authorized**

Acknowledgements

The author would like to acknowledge funding from the Vermont Agency of Transportation and the USDOT thru the University Transportation Center (UTC) program at the University of Vermont.

Disclaimer

The contents of this report reflect the views of the authors, who are responsible for the facts and the accuracy of the data presented herein. The contents do not necessarily reflect the official view or policies of the University of Vermont. This report does not constitute a standard, specification, or regulation.

ABSTRACT

This study investigates the suitability of the HL-93 live load model recommended by AASHTO LRFD Specifications for its use in the analysis and design of bridges in Vermont. The method of approach consists in performing a statistical analysis of weigh-in-motion (WIM) data collected between the years 2000-2012 at 12 stations across the state of Vermont. In total 36,754,819 individual WIM events were analyzed in this study. We compared the statistics of the lane moment and shear induced by the WIM data to the corresponding lane moment and shear induced by the HL-93 live load model. This analysis was performed on two types of very common bridge decks: (i) steel girders and concrete slabs and (ii) concrete girders with concrete slabs. In all cases the decks were considered to be acting fully composite. We considered span lengths in the range of 5-60 meters (~ 16-200 ft). The mains findings of this study are: (i) The probability that the lane moment and shear induced by the WIM data exceeds the corresponding values induced by the HL-93 model, decreases with span length. Averaged over all years considered in this study, the largest probability of exceedance was found to be approximately 1%. (ii) For span lengths exceeding 10 m, the annual probability of failure induced by the WIM data analysis did not exceed the annualized AASHTO target probability of failure. This indicates that for typical bridge decks with span length exceeding 10 meters, the HL-93 live load model is adequate for its use in Vermont. (iii) We propose that a more detailed study be carried out for short span structures such as culverts. Evidence from our study suggests that for very short spans (< 10 m), the HL-93 live load model might not be conservative.

EXECUTIVE SUMMARY

This study investigates the suitability of the HL-93 live load model recommended by AASHTO LRFD Specifications for its use in the analysis and design of bridges in Vermont. The method of approach consists in performing a statistical analysis of weigh-in-motion (WIM) data collected between the years 2000-2012 at 12 stations across the state of Vermont. In total 36,754,819 individual WIM events were analyzed in this study. The statistics of the lane moment and shear induced by the WIM data was compared with the corresponding lane moment and shear induced by the HL-93 live load model. This analysis was performed on two types of very common bridge decks: (i) steel girders and concrete slabs and (ii) concrete girders with concrete slabs. In all cases, the decks were considered to be acting fully composite. Span lengths in the range of 5-60 meters (~ 16-200 ft) were considered. As a general trend it was found that as the span length increases, the probability that the lane moment and shear induced by the WIM data exceeds the values induced by the HL-93 model, decreases. Averaged over all years considered in this study, the largest probability of exceedance was found to be approximately 1%, this occurred in 5 meter spans. The largest probability of exceedance in any single year and station was found to be 2.5%, again for 5 meters span lengths.

In terms of structural reliability, an analysis that included the variability in loading (using the statistical analysis of WIM data) and the variability in strength of the bridge deck (using values from the literature) were performed. This analysis was done for steel girder and concrete slab decks for span lengths in the range of 10-60 meters (~ 16-200ft). The results were compared with the AASHTO LRFD target reliability index of 3.5 in 75 years (probability of failure of 0.023% in 75 years). In this analysis it was found that the annual probability of failure induced by the WIM data analysis did not exceed the annualized AASHTO target probability of failure. This indicates that for typical bridge decks with span length exceeding 10 meters, the HL-93 live load model is adequate for its use in Vermont.

Based on our statistical analysis of the available WIM data and the subsequent reliability analysis, it is proposed that a more detailed study be carried out for short span structures such as culverts. Evidence from our study suggests that for very short spans (< 10 m), the HL-93 live load model might not be conservative, in the sense that it is not consistent with the target reliability index of 3.5 in 75 years. This requires a separate study since culverts have a different type of structural system in comparison with typical bridge decks.

Contents

List of Figures

List of Tables

Chapter 1

Introduction

1.1 History of Design Codes

Civil structures are essential for the social, economic, and political wellbeing of modern society. These structures must be designed such that their use does not pose any danger to people. This has been and continues to be the goal of all design codes: to ensure the safety of those who use the structure(s). The earliest known building code is contained in the Code of Hammurabi, written in 1772 BC in Mesopotamia (modern day Iraq). Although the standards set forth in this code are extremely simple and somewhat drastic compared to modern codes, the underlying concepts remain valid:

> *228. If a builder builds a house for someone and complete it, he shall give him a fee of two shekels in money for each sar of surface.*
> *229 If a builder builds a house for someone, and does not construct it properly, and the house which he built fall in and kill its owner, then that builder shall be put to death.*
> *230. If it kills the son of the owner the son of that builder shall be put to death.*
> *231. If it kills a slave of the owner, then he shall pay slave for slave to the owner of the house.*
> *232. If it ruins goods, he shall make compensation for all that has been ruined, and inasmuch as he did not construct properly this house which he built and it fell, he shall re-erect the house from his own means.*

> *233. If a builder builds a house for someone, even though he has not yet completed it; if then the walls seem toppling, the builder must make the walls solid from his own means.*

From these simple lines we can appreciate important concepts such as risk, reward, and failure criteria. Fast forward several thousand years: the industrial revolution created a much greater need for infrastructure, particularly bridges. The invention of the car further increased this need, as people began to travel greater distances with more frequency. In the 20^{th} century engineers began to develop design codes that mandate a common load to be used in design of any structure of a given type. These codes started operating on a local or state level. One of the first design loads for bridges was suggested in 1912 by Henry Seaman [1]. The first load models were uniform loads, but engineers soon realized that these were not a reflection of reality. L.R. Manville and R.W. Gastmeyer first noted this in 1914 when they used statistics of existing trucks to suggest that live load with a concentration should be used to better represent a typical heavy vehicle [2]. In the 1920s and 30s many load models that were suggested were considered to represent heavy trucks. These load models incorporated both uniform and point loads. In the 1944 the H20 load was adopted. This load included a uniform load and a vehicle load with a variable axle spacing to more accurately model the trucks on the road at that time. However, the debate continued over which live load model was best. As the United States became more industrialized, different types of heavy trucks became more commonplace on the roads. A tradeoff between the cost of building and maintaining highway bridges and the cost of transporting goods by trucks caused changes in the regulations regarding axle configurations and weight limits of trucks. This further fueled the debate over the live load model because design had to accommodate more than one type of truck. The variety of trucks in use made the problem more statistical in nature.

Recently, this statistical nature has been realized and accounted for. Over the past several decades there has been an initiative to nationalize bridge design standards. The result is the AASHTO LRFD Bridge design specifications. The goal of this code is to ensure a satisfactorily low probability of failure for any bridge structure designed using it. This code uses probabilistic design methods. This type of design has emerged as an alternative to factor of safety design, a school of thought that some might argue is inadequate.

1.2 Probabilistic Design vs. Allowable Stress Design

The basic equation that governs LRFD, a probabilistic design philosophy, is that the sum of the factored load effects shall be less than or equal to the factored resistance:

$$\sum \gamma_i Q_i \leq \phi R_n \tag{1.1}$$

In this equation $\gamma_i > 1$ are load factors, statistically based multipliers that correspond to the load effects Q_i. $\phi \leq 1$ is also a statistically based factor that is applied to the nominal resistance to determine the factored resistance. This contrasts with the deterministic approach of Allowable Stress Design (also called Factor of Safety Design). The equation that governs the deterministic approach says that the sum of the load effects must be less than the elastic resistance divided by a safety factor:

$$\sum Q_i \leq R_E/FS \tag{1.2}$$

The first problem with his method is that exact calculation of elastic resistance is frequently impossible. This value depends on things such as elastic modulus, which cannot be determined exactly in some cases, making the value of elastic resistance an estimate. The second problem is that it assumes the same safety factor independent of the statistical variability of the loads. This generates structures with potentially large differences in effective safety factors. To more accurately characterize loads and resistances, a statistical approach is necessary.

The basic idea of probabilistic design is depicted in fig. 1.1. Data and prior knowledge are used to form statistical models of both loads (Q) and structure resistance (R). From this, the probability distribution of the resistance minus the loads can be determined. The probability to the left of zero represents the failure region and the goal is to control this area to levels acceptable to society. This area can be controlled by selecting the proper combination of loads with load and resistance factors, hence the name Load and Resistance Factored Design (LRFD). β is known as the reliability index. For bridges a target reliability index of 3.5 has been proposed in AASHTO LRFD.

In some instances the loads and resistances can be modeled as normal

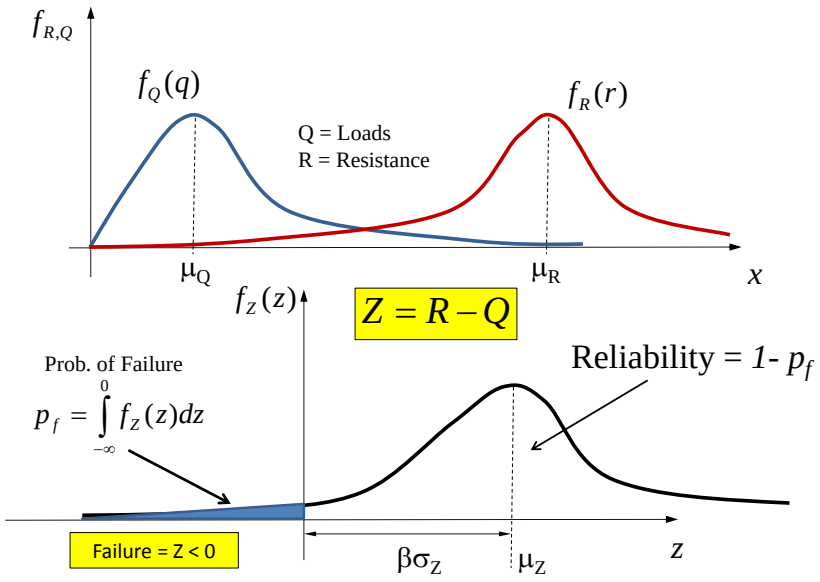

Figure 1.1: Concept of Probabilistic Design

random variables. In this case the random variable that is the subtraction of the loads from resistances is also normally distributed. Such a case is depicted in fig. 1.2. For normally distributed loads and resistance the following equations can be used to calculate both the mean resistance and the resistance factor:

$$\sigma_{(R-Q)} = \sqrt{\sigma_R^2 + \sigma_Q^2} \tag{1.3}$$

$$\beta = \frac{\mu_R - \mu_Q}{\sqrt{\sigma_R^2 + \sigma_Q^2}} \tag{1.4}$$

$$\mu_R = \mu_Q + \beta\sqrt{\sigma_R^2 + \sigma_Q^2} = \lambda R = \frac{1}{\phi}\lambda \sum \gamma_i Q_i \tag{1.5}$$

$$\phi = \frac{\lambda \sum \gamma_i Q_i}{\mu_Q + \beta\sqrt{\sigma_R^2 + \sigma_Q^2}} \tag{1.6}$$

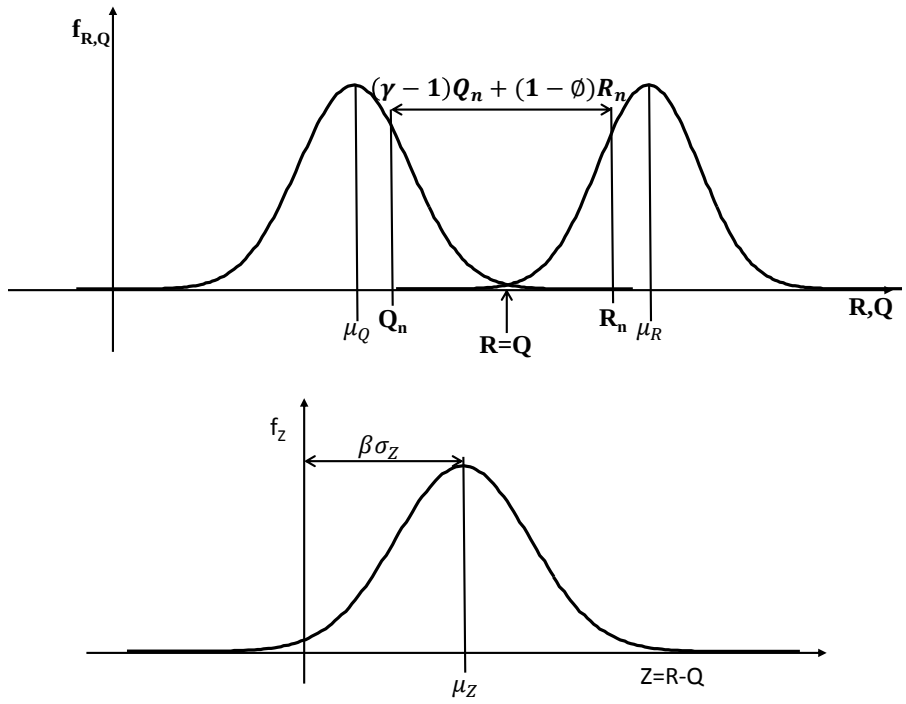

Figure 1.2: Normally Distributed Loads and Resistance

1.3 Evaluation of Live Load Model in AASHTO LRFD

The design loads in the AASHTO Specifications were calibrated in the 1980s and 1990s. Ever since states in the US have been using this code to design bridges, researchers have sought to analyze their performance from the standpoint of bridge reliability. The basic question they are trying to answer is: Does using the AASHTO specified design loading result in the target level of reliability consistent with field data? The goal of this project was to explore this question for the state of Vermont. This project focuses on one type of load, the vehicular live load. For bridges, the primary source of live load is heavy vehicles. The Vermont Agency of Transportation (VTrans) has provided 12 years of Weigh-in-Motion (WIM) data to use for comparison with the AASHTO loads. This is an extensive data set, containing roughly 37 million vehicles. As a comparative reference, the live load in the AASHTO

specifications (HL-93) was calibrated using 9,250 vehicles.

The Vermont data contains many pieces of important information: a timestamp, vehicle gross weight, axle count, individual axle weight and axle spacing. The first step in the data processing was to use structural analysis to determine the maximum stress demand (shear force and bending moment) each vehicle produces in a bridge deck. Once an algorithm that could handle all of the data in a timely manner was developed all of the data was passed through it. What resulted was a distribution of stress demands that can be sorted by time and location.

The next step was to develop models of these distributions to use in reliability calculations. Two different approaches were taken at this stage of the research. The first was to directly model the resulting stress demand distributions, using Lognormal Mixture Models. As the name suggests these models are weighted mixtures of lognormal distributions. These models serve as a flexible and computationally efficient way of modeling the entire stress demand distribution. The model parameters are estimated from the data using the Expectation Maximization (EM) algorithm. This provides an elegant way of modeling the distributions and allows for the fit of the estimated model to be assessed easily.

The second approach was to use extreme value theory and Bayesian statistics to model the distribution of the daily maximum stress demands. Using the time stamps in the data set, the distribution of daily maximum bending moments was found for all years for various WIM stations. Bayes Theorem was used to analyze the fit of potential models to the distribution of these extremes. Bayes Theorem was also used to estimate the optimal parameters of these models. By combining these two procedures into one algorithm the comparison of the models is more robust and can be seen to provide the best fit for the data.

The different statistical models for the load were then combined with statistical models for the resistance to determine bridge superstructure reliability. The resistance models and parameters are taken from existing literature. The resistance models were developed by using the AASHTO Specifications to design sample bridges. In this procedure the structures were designed to be as close as possible to the minimum threshold, so as to minimize the contribution of self-weight, referred to as dead load, to the total load on the structure. Once a design was obtained, finite element analysis (FEA) was used to determine the amount of live load that each girder must support. This allowed for an expression of the total dead and live loads that the

beams in these structures needed to support. With the resistance already calculated in the design phase, the reliability calculations were completed. Examination of the yearly probability of failure for different locations in the state of Vermont is a crucial element of the contents of this report.

Chapter 2

Literature Review

In this chapter the papers relevant to this project topic are reviewed and summarized individually.

2.1 NCHRP Report 368: Calibration of LRFD Bridge Design Code

Published in 1999, NCHRP Report 368 describes the calibration of the design live load, as well as the calculation of load and resistance factors used in the AASHTO LRFD Bridge Design Specifications. Included in this work was the development of load and resistance models, selection of the reliability analysis method, and the calculation of reliability indices for many bridges. The reliability index (β) is the number of standard deviations the mean of the distribution of loads minus resistance is past zero. Another way to think of this is as the inverse standard normal function of the probability of failure. This is the measure of reliability that was used throughout the report. It is a particularly useful measure because it relates to probability of failure, but is easier to calculate. The report set the target reliability index for bridges based on the reliability indices of existing bridges designed using allowable stress and/or load factor design (AASHTO standards before LRDF).

Roughly 200 sample bridges were selected from around the United States as representative of the bridge population. Load effects, such as shear forces and bending moments, and load carrying capacities were calculated for these bridges. Next, the available data regarding loads and resistances

were compiled. This data includes truck weight surveys, material tests, and field measurements among other things. From this data, models of loads and resistances can be made by considering them to be random variables. Reliability indices can be computed from these models considering different limit states (failure modes) using the Rackwitz and Fiessler procedure along with Monte Carlo simulations and other sampling techniques. The target reliability index of 3.5 was determined from the reliability indices calculated for these sample bridges. The load and resistance factors are then determined so that the factored load has a probability of failure based on the target reliability index.

The load models treated all dead loads as normal (Gaussian) random variables. The report includes tabulated bias factors and coefficients of variation (COV) for various dead load components. The live load effects (stress demands) that were examined were shear force, positive moment, and negative moment (for continuous spans). These effects were determined using data from a truck data survey performed in 1975 in Ontario. This survey contained about 10,000 trucks that appeared to be heavily loaded. This report holds that, at the time of the survey, the truck population in Ontario was similar enough to the truck population in the US to use the survey for code calibration purposes. The maximum stress demands from these vehicles were then extrapolated to various return periods using the assumption that the truck data represented a 2 week time period. The mean and COV of these stress demands were computed for the various return periods.

The single vehicle stress demands were then combined to obtain maximum stress demands for multiple vehicle and multiple lane scenarios. This combination was done using data regarding headway distance, multiple truck presence, and degree of correlation between trucks. The report acknowledges that there is little data available to verify the statistical parameters used to account for presence of multiple heavy vehicles. Ultimately, the mean maximum stress demands for one or multiple lanes was determined for various return periods.

The live load model that was selected was calibrated using the maximum 75 year stress demands. A 75 year time period was thought to correspond to the service life of a bridge. The objective of selecting a new load model was to achieve a uniform ratio of the nominal, or design, value to the maximum 75 year demand. It was determined that the load model that best accomplished this used the maximum of: i) a combination of the HS-20

truck and a lane load of 64 pounds per square foot, ii) a tandem of two 25 kip axles spaced 4 feet apart plus the lane load for short spans, or iii) 90% of two HS-20 trucks plus 90% of the lane load effect. This load model was designated HL-93 vehicular live load for use in the AASHTO LRFD Bridge Design Specifications.

Resistance models were also developed for various types of construction materials. Since bridges usually contain multiple types of materials that act simultaneously to resist the load, material test data and numerical simulations were used to determine the statistical parameters of resistances. This was done for steel girders (composite and non-composite), reinforced concrete T-beams, and pre-stressed concrete AASHTO-type girders. Expressions for shear and moment capacity for these types of members were used to consider limit state functions in the reliability analysis. The report defines limit states as the boundaries between safety and failure. These limit state functions have many variables: load components, resistance parameters, and material properties to name a few.

Direct calculation of the probability of failure is difficult because these limit states are highly complex due to their dependence on so many variables. Therefore, an iterative procedure was used to calculate the reliability index. This procedure, developed by Rackwitz and Fiessler, uses normal approximations to non-normal distributions at the point of maximum probability on the failure boundary, called the design point. Initially this design point is estimated and a reliability index is calculated. This is an iterative procedure because a new design point is determined based on the previously calculated reliability index. This procedure is repeated until the design point converges [3].

2.2 Characteristic Traffic Load Effects from a Mixture of Loading Events on Short to Medium Span Bridges

This paper focuses on site specific load effect assessment. As previously established, Monte Carlo methods are useful for representing synthetic traffic when the statistics of the traffic are available. The conventional approach is to identify the maximum load effect during a loading event and fit these

maxima to an extreme value distribution. This approach assumes that the loading events are independent and identically distributed (iid). However, loading events from multiple vehicles are much more complex than single vehicle events, because they involve considerably more variables. Mixing the effects from these two different types of events violates the iid assumption necessary to use extreme value analysis, and can therefore result in errors.

A new way of combining the non iid loading events is proposed. This method combines the effects of multiple mechanisms that operate on the same random variables. The assumption that the individual loading events converge to an extreme value distribution is used to achieve a closed form for the joint distribution of the load effects. This method is shown to be less conservative than the conventional approach of using extreme value theory. One noteworthy finding is that loading events of more than 2 vehicles can govern the design of short to medium span bridges. This does not agree with the theory that the 2 vehicle situation governs, as postulated in the calibration of the AASHTO LRFD specifications [4].

2.3 Probabilistic Characterization of Live Load Using Visual Counts and In-Service Strain Monitoring

This paper argues that conservative assumptions are made about the multiple presence of vehicles in the calibration of the AASHTO LRFD design code. The basis of this argument is that no field data on multiple presence probability and truck weight correlation were provided in the calibration. For this study, multiple and single presence occurrences were visually observed along a highway close to a bridge. A Poisson process-based occurrence model is used to achieve a closed form result for side-by-side vehicle occurrence rates. The key assumptions made in this formulation are that occurrence of trucks in each lane can be modeled by a Poisson pulse process and that these processes are independent for each lane. Although these assumptions may not hold true, this allows for a simple model that is shown to provide adequate results compared to the data.

Strain data was obtained from gauges positioned on the bridge girders. This strain data was used to compare an estimated 75 year design load from the data with the AASHTO load. The largest strain observed from each data

collection was converted into a bending moment based on girder geometry. The maximum 75 year effect was computed using statistical extrapolation of the data set to the 75 year time period. It is shown that the design moment using HL93 live loading is about 3.5 times that of the estimated maximum 75 year value obtained from data for a particular bridge [5].

2.4 WIM Based Live Load Model for Bridge Reliability

This study uses a WIM data set of 47 million vehicles from California, Florida, Indiana, Mississippi, New York, and Oregon to compare with the data set used to calibrate the HL93 live load. The maximum load effect for each vehicle in the data set was determined. The comparison of the new and old data suggested that, on average, the Ontario trucks (data used in the calibration of HL93) were heavier than the vehicles in the WIM data set. It was also concluded that extrapolation of the maximum values of the live load effects from the WIM data would result in the same maximum values as found when the HL93 load was calibrated. The correlation between truck weights was also obtained from the WIM data so multiple presence analysis could be performed.

Six steel girder bridges were designed according to the AASHTO LRFD code. The WIM data was used in conjunction with FEM analysis to calculate the reliability indices of these bridges for live load. The calculated reliability indices are higher than the AASHTO target of 3.5, leading to the conclusion that the HL93 live load is still generally valid across the United States. However, it was noted that a further analysis of New York is necessary because of the observation of extreme loads at some sites [6].

2.5 Calibration of Live-Load Factor in LRFD Bridge Design Specifications Based on State-Specific Traffic Environments

This paper proposes recalibrating the live load factor based on state-specific traffic and bridge information. Moving load analyses were conducted for sample bridges selected from the state of Missouri. The loads considered in

the analysis came from a WIM data set of approximately 41 million vehicles. The moving load analysis was performed on the heaviest 5% of vehicles because a strong correlation between maximum load effect and gross vehicle weight (GVW) were observed. Multiple presence of vehicles was considered and the daily maximum demand was computed. Girder distribution factors computed using AASHTO were used to compute the portion of live load supported by the girders in the sample bridges. A Gumbel Type I distribution was fitted to the daily maximum values and extreme value theory was used to determine the mean maximum 75 year demand.

The reliability index of these sample bridges was calculated using FORM (First Order Reliability Method). For these calculations it was assumed that the resistance and dead load followed normal and lognormal distributions respectively. The reliability indices calculated showed that the AASHTO specifications resulted in over designed bridge superstructures in Missouri. A method for calibrating the live load factor that results in the target reliability index (3.5) is suggested. This method modifies the current live load factor (1.75) by using a modification factor based on ADTT (average daily truck traffic) [7].

2.6 Using Weigh-In-Motion Data to Determine Aggressiveness of Traffic for Bridge Loading

This study uses WIM data from highways in the Netherlands, Czech Republic, Slovenia, Slovakia, and Poland as a basis for Monte Carlo simulation of bridge loading by two lane traffic. The simulation model was optimized so it could run thousands of years of traffic to obtain the characteristic bridge load effects, which are compared to design values for bridges as specified by the Eurocode Load Model 1 for bridge traffic loading. This comparison serves as the basis for calculating a BAI (bridge aggressiveness index). The BAI is to be used to provide an estimate of the magnitude of the characteristic load effect based on WIM data. This is intended as a rating system for the traffic, not to provide an estimate of the reliability of the bridge. It is determined that the BAI can be calculated based on the maximum weekly GVW [8].

2.7 Reliability of Highway Girder Bridges

This paper discusses procedures for reliability calculations for girder bridges. The various types of girder bridges considered are steel girder (both composite and non-composite), reinforced concrete T-beams, and prestressed concrete girder bridges. Load models are used, but not discussed. Lognormal resistance models are developed using simulations based on material tests results and are used in reliability calculations. Individual girder behavior is described using a moment curvature relationship. Bridge carrying capacities are found by determining the maximum truck load before failure. In this procedure single unit and semi-trailer truck configurations are used. The axles are positioned so they cause the maximum load effect and then the axle loads are increased until they cause deformations that exceed acceptable values.

Girder reliability is computed using the iterative procedure developed by Rackwitz and Fiessler for typical slab on girder bridges. The reliability of the bridge system is calculated using the bridge carrying capacity. The reliability of the system is shown to be higher than the reliability of the individual girders, reflecting the redundancy built into such structures. The fact that the system reliability is higher than reliability of the individual components shows that girder bridges exhibit behavior of parallel systems. A sensitivity analysis revealed that accurately characterizing the resistance parameters, such as yield stress or steel area, is particularly important when determining bridge reliability [9].

2.8 Locality of Truck Loads and Adequacy of Bridge Design Load

This paper focuses on the high variation of loading conditions between bridge sites. From WIM data obtained in the state of Michigan, it is apparent that truck weights greatly vary from site to site. The high amount of variation suggests that the national and state design codes do not account for localized risk. WIM data consisting of roughly 46,000 vehicles from 9 sites are used to develop statistical representations of live load effects in the sample bridges at critical cross sections. The reliability indices for a randomly selected sample of new bridges from the state of Michigan are based on these statistical models.

The results show that the Michigan design load used in 2005 (HS25) does not consistently attain the desired reliability index in the Detroit Metro Region. The results also show significant variation in the reliability indices among both bridge sites and types. This suggests that a site specific live load calibration using WIM data could help achieve more uniform reliability indices across the state [10].

2.9 Buckling Reliability of Deteriorating Steel Beam Ends

This paper proposes a reliability-based damage assessment for deteriorating steel beam ends that become susceptible to shear buckling as a result of material deterioration in the beam webs. The objective was to develop reliability charts for web buckling based on real time data instead of simply the design load. The load model in this procedure is based on a WIM data set from 42 WIM stations in the state of Michigan. A detailed finite element model is used to determine the resistance of the weekend sections. A detailed case study is presented for one bridge. Varying levels of deterioration are considered to examine the effect of web thinning on point-in-time reliability indices. The results of this study can be used to eliminate unnecessary bridge closures as a result of overestimating the risk resulting from web deterioration [11].

2.10 Evaluation of a Permit Vehicle Model Using Weigh-In-Motion Truck Records

This study evaluates the Wisconsin permit vehicle based on a WIM data set of 6 million vehicles collected in 2007. The heaviest 5% of vehicles in the data set were used to find the maximum demand (shear and bending moment) in 2 and 3 span continuous girders. The demand values were found using a moving load analysis in SAP2000, a finite element analysis program. Multiple presence and distributed lane loads were not included in this analysis. The ratios of these maximum demands to the Wisconsin permit vehicles were computed. An extreme value distribution was used to fit the resulting distribution of ratios. The results showed that some short single-unit trucks could exceed bridge responses forecasted using the Wisconsin permit vehi-

cle. A new permit vehicle is proposed based on the 95^{th} percentile of the corresponding axle weights and spacing observed in the WIM data [12].

2.11 Applying Weigh-In-Motion Traffic Data to Reliability Based Assessment of Bridge Structures

This study identifies evaluation of the effects increasing traffic volumes on short to medium span bridges as a critical area of study. These types of bridges are important because they make up most of the bridge population; these span lengths make up 85% of the bridge population in France, the area where the study was conducted. The effects of time variation of traffic loading on reliability of bridge structures are investigated. A model for the loss of strength in a reinforced concrete bridge is used in the reliability analysis. Extreme value theory is used to model the effects of the traffic in the WIM data set. Extrapolation from daily to yearly maximum values is achieved by raising the daily extreme distribution to the power of the number of days in a year. The change in these yearly values is modeled using data on traffic growth, both in weight and volume. Annual reliability is used as a metric to quantify the influence of traffic evolution on the reliability of a sample reinforced concrete bridge [13].

2.12 Site Specific Probability Distribution of Extreme Traffic Action Effects

This paper seeks to find an empirical relationship between site characteristics and parameters of a Type III extreme value distribution that is used to model traffic effects on a bridge. Random traffic is simulated by using different parameters for distributions of traffic characteristics that correspond to different traffic scenarios. These characteristics include traffic composition, axle group weights, vehicle geometry, and axle spacing. The maximum load effects from the simulated traffic are computed using influence lines. Many different site characteristics are included in the analysis, including multiple spans, multiple lanes, different span lengths, and various traffic flow conditions.

It was found that a Type III distribution best fits the distribution of maximum load effects. This was expected because the maximum values are sampled from distributions with an upper bound. The relationships between the distribution parameters and traffic load parameters are derived. Reliability calculations are performed using the load effect distributions from the simulated load effects and using the distributions obtained using the derived relationships. The reliability calculations were done using the FOSM (first order second moment) method. The reliability indices calculated using the simulated data and are shown to be very close to the corresponding indices using the previously mentioned relationships. This shows that the relationships between site characteristics and distribution parameters can be used to perform site specific reliability calculations for bridges [14].

2.13 Monte Carlo Simulation of Extreme Traffic Loading on Short and Medium Span Bridges

This paper is a critical review of the assumptions made in the process of using statistical distributions as the basis of Monte Carlo simulations used to predict maximum lifetime traffic load effects. A model for Monte Carlo simulation of bridge loading from free flowing traffic that can be applied to different sites is presented. Particular attention is paid to modeling axle layout, as the estimate of maximum lifetime load effect is particularly sensitive to assumptions regarding axle spacing and wheelbase. For instance, two trucks with similar GVWs and different lengths can result in a 50 Such a model gives a more realistic estimate of lifetime loading than others. Vehicles that cause demands larger than any vehicle in the data set may be used in the model because of its probabilistic nature. This approach allows for determination of which loading scenarios can cause the lifetime maximum demands. It also gives information about which types of vehicles are involved in those loading scenarios. When a single vehicle occurrence results in a characteristic load effect, it is often the result of a truck significantly heavier than any observed truck. This highlights the importance of controlling the presence of these specially loaded vehicles on highways [15].

2.14 Information Regarding WIM Data Sets Used in Reviewed Studies

Table 2.1: Number of Vehicles and Time Period Represented in the WIM Data Sets

Study	Approximate Number of Vehicles	Time Frame
1	9,250	2 weeks
2	no WIM data used	
3	no WIM data used	
4	47,000,000	3 years
5	41,000,000	5 years
6	2,700,000	4 years
7	no WIM data used	
8	46,000	N/A
9	101,000,000	5 years
10	6,000,000	1 year
11	600,000	6 months
12	no WIM data used	
13	2,700,000	4 years
Our Study	36,000,000	**2 years**

Chapter 3

Identification of Mixture Models from Weigh-in-Motion Data with Application to Bridge Deck Reliability Analysis

This paper proposes the use of mixture models to represent the aleatoric variability of internal forces in bridge decks induced by vehicular loads. The proposed mixture models are identified from vehicle axle data measured in 12 weigh-in-motion (WIM) stations across the state of Vermont, USA during a period of 12 consecutive years. The temporal and spatial variability of the parameters that define the mixture models is investigated. The paper presents a comparison between the demands induced by the WIM data and the AASHTO HL-93 live load model. The identified mixture models are used to compute the annual probability of failure of simply supported bridge decks of various span lengths under normal operating conditions.

3.1 Introduction

A mixture model is a probabilistic model that specifies the probability distribution of a random variable Y as a countable sum of distributions $f_{X_i}(x, \theta)$ weighted by corresponding scalars $w_i \in \mathbb{R}$

$$f_Y(x) = \sum_{i=1}^{n} w_i f_{X_i}(x, \theta_i) \tag{3.1}$$

where $n \in \{1, 2, ...\}$. The only restriction being that $\sum w_i = 1$ in order to garantee that $\int f_Y(x)dx = 1$. The distributions $f_{X_i}(x, \theta_i)$ are uniquely defined by the parameter vector θ_i. Mixture models are extensively used in diverse engineering fields [1], including traffic modeling [4]. In this paper we are concerned with using mixture models to describe the probability distributions of the traffic induced stress demands in the main load carrying elements of a typical bridge deck. Specifically we are interested in the inverse problem of identifying mixture models from the vehicle axle data measured by weigh-in motion (WIM) stations. In this paper we implement the expectation maximization (EM) algorithm to perform the identification of the mixture models from WIM data. The data for the statistical analysis presented in this paper corresponds to axle weight and spacing data of vehicles obtained from 12 WIM stations spread across the state of Vermont, USA. The data was collected over the years 2000-2012. In total $36,754,819$ vehicle events were recorded by the WIM system and analyzed in this study.

This study is motivated by current efforts at the Vermont Agency of Transportation (VTrans) to assess the reliability of their bridge inventory and to determine if the AASHTO live load model [5] provides stress demands consistent with the demands that can be inferred from processing the WIM data. The current HL-93 live load model used in AASHTO LRFD Brige Design Specifications was originally calibrated by Nowak [11]. The vehicle data used to formulate the model was obtained from a truck survey conducted in Ontario, Canada over a span of approximately two weeks in the 1970's. Since its adoption, several studies have been carried out to determine the validity of the model in various geographical settings, especially across the United States. Remarkably, despite its simplicity and considering that a relatively small amount of data was used for its initial formulation, most of the studies typically conclude that the HL-93 is adequate, although potentially conservative, and remains valid under most situations [8, 9]. The intent

of the current AASHTO LRFD Bridge Design Specifications is, as stated in NCHRP 368 (Nowak 1999), to provide load and resistance factors that are consistent with a reliability index (β) of 3.5 for a service life of 75 years.

Identification of the proposed mixture models from WIM data can have various applications. One of the most common is for the development of site specific live load models [2, 3, 22]. In that application the argument is that significant savings can be achieved in design of new bridges and assessment of aging bridges if local traffic conditions are used instead of a "one size fits all" approach such as the HL-93. In the study by [3], the standard permit vehicle in Wisconsin was evaluated by using six million WIM truck records collected in 2007. The evaluation was on the basis of statistical analyses of the maximum moments and shear in simply supported, 2-span, and 3-span continuous girders in the selected heaviest 5% of trucks in each vehicle class/group. The comparisons showed that 5-axle, short, single-unit trucks may cause larger moment/shear in bridge girders than the standard permit vehicle, and a 5-axle truck model was proposed to supplement the standard permit vehicle for possible use in bridge design and rating in Wisconsin.

Existing literature focuses mainly on identifying generalized extreme value distributions (GEV) from the WIM data and extrapolating these distributions, sometimes along with deterioration models, to estimate the reliability index of the bridge deck as a function of time. Consider as a representative example a recent paper by Zhou, et al. [13]. This paper reports the use of WIM data during a span of 6 months in highway system in southern France. The data is used to identify a GEV distribution and then extrapolate it to 100 years using linearly increasing trend of traffic growth. The study investigated the specific case of short span reinforced concrete bridges and the main source of strength degradation was chloride induced corrosion. They found that with the effect of proyected traffic growth of 0.002% per year, the reliability droped from an initial value of 3.9 to 3.5 in 40 years and to 2.8 in 90 years. Given that the data was of a relatively short amount of time, it was not possible to assess if the GEV was adequate. In [4] it was found that significant errors are incurred if standard methods for extreme value modeling are used without accounting for the fact the the parent distributions are not independent and identically distributed (iid). One of the objectives of this paper is to quantify the temporal and spatial variability of the parent distribution on the basis of data measured by WIM stations.

In summary, the main contribution of this paper is the identification of time-variant mixture models from WIM data measured at various locations

and during a significantly long period of time. This allow us to validate(or invalidate) the independent and identically distributed (iid) assumption typically used whenever deriving GEV for reliability analysis of bridge structures. A less significant, but potentially interesting application of the statistical analysis developed in the paper is that instead of extrapolating the identified probability model into the future, we deduce from the data a yearly probability of failure. This allows for the use of failure rate as a potential critieria for reliability design and assessment of bridges. In this paper we focus on the operational failure rate, i.e. the period where the structure has surpassed the infant mortality phase and has not yet began the wareout phase.

3.2 AASHTO Live Load Model

To place our work in context, in this section we briefly present the AASHTO vehicular live load model. The HL-93 live load model is the latest in an evolving sequence of models that can be traced as far as the early 20th century with the work of Seaman [18] and Manville and Gastmeyer Manville. The AASHTO vehicular live load to be applied on roadways of bridges, designated as HL-93, consists of a combination of a design truck or a design tandem, and a design lane, whichever produces the largest effect (see Fig.3.1).

Transverse to the direction of travel, both the truck and the tandem loads are spaced 1.8 m apart and they can be placed anywhere in a 3.6 m wide lane as long as a clearance of 0.6 m to the lane boundary is maintained (0.30 m in the case of a deck overhang). The lane load should be spread over a width of 3.0 m inside a standard lane [5]. In the case of bending moment in simple spans, for very short spans (≤ 10 m) the tandem combination governs, however for longer spans, the truck combination is more critical. For lane shear, the truck load will typically govern independent of the bridge span. The HL-93 load model is typically referred to as notional because it is not intended to represent any particular truck to be found on the interstate highways. In essence the objective of the HL-93 live load model is to induce stress demands on a bridge structure which are consistent with low probability stress demands generated by heavy vehicles.

One of the partial objectives of this study is to compare the stress demands in the form of lane shears and lane moments obtained from AASHTO HL-93 with the ones obtained by applying the measured vehicles on simu-

lated one span bridges of varying length. Recent studies on the subject have also proceeded in a similar fashion. In one such study a small set of WIM data (about 40,000 trucks) was analyzed to evaluate the adequacy of the HS-25 truck [22]. The HS-25 design truck is used in the HL-93 live load model. A similar study used WIM records coupled with finite element analysis to examine maximum live load shear in deteriorating steel beams [23]. Others compared the girder design moments according to AASHTO standards with girder moments from WIM data [6].

3.3 Description of Data and Pre-Processing

The Vermont Agency of Transportation currently maintains 12 WIM stations spread across various roads within the state (See Fig. 3.2). These stations have been operational since the year 2000. The total number of vehicles recorded by the system each year during the period 2000-2012 is shown in Fig. 3.3. Note that significant variation regarding the total number of recorded vehicles per year can be observed. A typical data file from the WIM system contains the following information: station identification, time stamp, vehicle class, axle weight, and axle spacing. We performed an initial quality control check on the WIM data and eliminated spurious measurements prior to initiating the statistical analysis.

Our approach was to select each data point (measured vehicle) for a given station and year and determine the maximum lane bending moment and shear that it would induce on various simple span bridges of varying length (5-60 meters). For the case of bending moment this was efficiently carried out by invoking a well-known theorem from structural analysis. The theorem states that the location of maximum bending moment results from the maximum of n possible moments, each one of these corresponds to placing the axles such that in each case one of the loads is equidistant from the center of the beam with the resultant of the forces [7]. For short spans and vehicles with many axles, it can occur that only a portion of the axles are within the span of the beam, therefore an iterative approach is needed in order to find a stable position of the axles where the resultant of the loads inside the beam is equidistant from the load considered (Fig.3.4). The analysis for shear is simpler since the maximum shear is equal to the maximum reaction corresponding to n possible axle positions where one of the axle loads is placed immediately adjacent to one of the supports. All the algorithms were

efficiently implemented and all $36,754,819$ vehicle measurements were individually analyzed. This is in contrast with recent studies that only examine the heaviest portion of vehicles [3]. Our approach allows the computation of probabilities interpreted as a fraction of cases of interests to the total number of cases.

Historgrams such as the ones shown in Figs. 3.6 and 3.7 were generated after transforming the data from axle weights to lane shears and moments for each station in a given year for the various lengths considered. These histograms support our hypothesis that the distribution of the lane bending moment and shear follows a mixture distribution and does not fit any standard distribution. As a starting point we determined for each station and each year the proportion of vehicles that generated lane bending moments or shears which exceeded the lane moments and(or) shear generated by the AASHTO HL-93 live load. The values depicted in Fig.3.5 are averaged over all of the years. Although there is significant inter-station variation, shorter span lengths tend to exhibit a larger fraction of demands over the AASHTO HL-93 value. Other trends that can be observed is that all stations in the eastern part of the state (X073, X249, N001, E020) have a consistently smaller fraction of cases exceeding AASHTO, as opposed to the stations located in the western portion of Vermont (B379,R001,Y117,R100,A041,A111,D092,G005). This can be explained by population trends and economic activity which varies significantly from east to west in Vermont [24]. In addition, it can be seen that four stations, namely, R100, B379,G005 and R001, present the highest levels of exceedance with respect to AASHTO HL-93 (nearly 1%).

Fig.3.12 shows the yearly variation of the probability of exceedance for the lane shear and bending moment with respect to the AASHTO HL-93 demands. The results are shown for four stations, namely, R100, X249, G005 and R001. Significant variation can be observed from year to year. In the case of R100 there appears to be an upwards trend, while for the case of G005 an increase was verified until 2004 however a decrease thereafter. The other two stations exhibit a more erratic behavior without a clear trend. This contradict the hypothesis that vehicular live load demands are stationarity over a long period of time or that they grow or decrease at a constant rate.

3.4 Statistical Analysis Methods

In this section we present a more detailed spatio-temporal statistical analysis of the WIM data. We describe the mixture models that were postulated and the EM algorithm that was employed. We also show the results obtained for the various stations and years considered.

3.4.1 Mixture Models

A mixture model is a probabilistic model that specifies the probability distribution of a random variable Y as a finite sum of distributions $f_{X_i}(x)$ weighted by corresponding scalars $w_i \in \mathbb{R}$

$$f_Y(x) = \sum_{i=1}^{n} w_i f_{X_i}(x) \tag{3.2}$$

The restriction being that $\sum w_i = 1$. A popular choice for many applications is the Gaussian mixture model (GMM), which as the name suggests, uses

$$f_{X_i}(x) = \frac{1}{\sqrt{2\pi\sigma_i^2}} e^{-\frac{1}{2}\left(\frac{x-\mu_i}{\sigma_i}\right)^2} \tag{3.3}$$

From the histograms of the stress demands (Figs. 3.6 and 3.7) it is apparent that a mixture model is a potentially successful model class to describe the distributions of lane shear or bending moment induced by traffic. In an initial statistical analysis we tested Gaussian and log-normal mixture models to determine their power in explaning the data. We found that the log-normal model is a better fit. We also found that even though a non-parametric framework allows for an increasing number of distributions to be included in the mixture in order to adapt to the data, for the data set considered in this paper, a mixture of three ($n = 3$) distributions is sufficient to attain the desired accuracy. The choice made for our application was a log-normal mixture model (LNMM), which uses

$$f_{X_i}(x) = \frac{1}{\sqrt{2\pi x^2\sigma_i^2}} e^{-\frac{1}{2}\left(\frac{\log x-\mu_i}{\sigma_i}\right)^2} \tag{3.4}$$

3.4.2 Expectation Maximization Algorithm

We employed the Expectation Maximization (EM) algorithm [10] to compute the maximum likelihood estimates (MLE) of the mixture weights (w), means (m), and variances (v). This algorithm can be readily implemented using the following equations:

$$w_j = \frac{1}{N}\sum_{k=1}^{N} 1_{z_k=j} \tag{3.5}$$

$$m_j = \frac{\sum_{k=1}^{N} 1_{z_k=j} x_k}{\sum_{k=1}^{N} 1_{z_k=j}} \tag{3.6}$$

$$v_j = \frac{\sum_{k=1}^{N} 1_{z_k=j} \left(x_k - \mu_j\right)\left(x_k - \mu_j\right)^T}{\sum_{k=1}^{N} 1_{z_k=j}} \tag{3.7}$$

where $1_{z_k=j}$ is the indicator function. The value of z_k for the data x_k is computed as

$$z_k = j \quad \text{if} \quad f_{X_j}(x_k) > f_{X_l}(x_k) \quad \forall l \neq j \tag{3.8}$$

The EM algorithm is guaranteed to converge, however, only convergence to a local maximum is guaranteed so the final estimate is dependent on an initial guess of the model parameters. The initial guess for the values of σ_i and μ_i was based on a visual inspection of the data and by using known relationships between mean m, variance v and the parameters μ and σ of each distribution [21], namely

$$\mu_i = \log\left(\frac{m_i^2}{\sqrt{v_i + m_i^2}}\right) \tag{3.9}$$

$$\sigma_i = \sqrt{\log\left(1 + \frac{v_i}{m_i^2}\right)} \tag{3.10}$$

3.5 Results

Typical results from the implementation of the EM algorithm are shown in Fig.3.8 for various years and stations for a span length of $10m$. The Fig.3.8 shows the match between the normalized histogram constructed using the

maximum bending moment induced by the measured vehicle axles and the identified mixture model using 3 lognormals. As can be seen the match is adequate and similar quality of results were obtained for other stations/years/span length that were analyzed. We proceed to present a spatial and temporal variability analysis on the basis of the identified LNMM,such as the ones presented in Fig.3.8.

3.5.1 Spatial Variability

Table 1 presents results for the identified maximum likelihood value of the LNMM parameters for various stations over all years for which data was available. Significant inter-station variation can be observed specially in the weighting coefficients (w_i) and to a lesser extent in the (σ_i). At the bottom of the table we show the arithmetic average and the coefficient of variation (CoV) for all stations. The identified average and coefficient of variation can be used to postulate a distribution for the model coefficients and subsequently used to generate random synthetic data which can then be used for long term reliability analysis of bridges. This approach, although more computationally intensive, could be more realistic than the more traditional approach of postulating a stationary GEV distribution for the life of the structure. We illustrate this approach in a subsequent section of the paper.

Table 3.1: Maximum Likelihood Estimate of Mixture Model Parameters in eq.3.4 for a 10 m span

Station	w_1	w_2	w_3	μ_1	μ_2	μ_3	σ_1	σ_2	σ_3
R100	0.291	0.419	0.290	6.528	7.297	8.122	0.279	0.254	0.321
X249	0.345	0.374	0.281	6.347	7.209	7.872	0.367	0.226	0.335
G005	0.538	0.347	0.115	5.635	6.544	7.337	0.312	0.308	0.292
R001	0.167	0.412	0.421	6.489	7.301	8.028	0.412	0.223	0.254
Average	0.336	0.387	0.275	6.495	7.321	8.063	0.356	0.260	0.295
CoV	0.596	0.284	0.452	0.041	0.031	0.023	0.307	0.256	0.178

3.5.2 Temporal Variability

In order to illustrate the intra-stational temporal variability of the mixture models, Fig.3.9 shows the variation of the identified weighting coefficients

as a function of time (averaged results for every year). Fig.3.10 shows the variability of the μ parameter and Fig.3.11 the variability of the σ parameter. The parameters (μ_i) do not change significantly, however consistent with the results shown in Table 1, the relative weights (w_i) and the parameters (σ_i) do vary appreciably with time. The variation of the parameters is not monotonic and it does not exhibit any particularlly clear trend and can be described as aleatoric. Using the identified LNMM, Fig.3.12 depicts the probability of any random truck exceding the AASHTO HL-93 induced lane bending moment and(or) shear for each of the stations considered in a $10m$ bridge deck. Note that this is not the probability that the heaviest truck in a given time frame exceeds the AASHTO HL-93 induced lane bending moment and(or) shear.

3.6 Reliability Analysis

One potenial application of the identified LNMM is in reliability analysis of bridges. This involves defining distributions for the dead (D) and total loads ($Q = D + L$). The distribution for the dead load was estimated as normally distributed with the nominal value equal to the dead load calculated on the basis of an AASHTO complying bridge design. As recommended by [11], a bias factor of 1.05 and coefficient of variation (COV) of 0.1 were used to determine the mean and variance of the component dead load distribution. For the wearing surface dead load a mean thickness of 3.5 in and COV of 0.25 were used [11]. Convolving the distribution for the dead load with that of the live load will give is the distribution of the total load ($Q = D + L$) as depicted in Fig. 3.14 for a particular case of a $5m$ and $10m$ span bridge.

$$f_Q(q) = \int_{-\infty}^{+\infty} f_D(x) f_L(q - x) dx \tag{3.11}$$

The nominal resistance (R) was estimated as the resistance of one lane of the bridge. A bias factor of 1.14 and COV of 0.13 were applied to these values to get the means and variance of the resistance [11]. The resistance was estimated as a log-normally distributed random variable. This model does not consider degradation of the bridge or any repair actions that migth be taken during the service life of the structure. In this calculation we are operating under hte premise that the structure is in good condition and no significant degradation has taken place. Once the distribution of the resistance is computed we can proceed to find the distribution of the resistance

minus the total loads $Z = R - Q$. This was done by taking the correlation between the resistance and loads as shown in Fig.9.

$$f_Z(z) = \int_{-\infty}^{+\infty} f_Q(x) f_R(z + x) dx \tag{3.12}$$

The area to the left of zero corresponds to the probability of failure, i.e.

$$p = \int_{-\infty}^{0} f_z(z) dz \tag{3.13}$$

The probability of failure calculated for the particular case shown in Fig.3.15 is 2.83×10^{-9}, significantly lower than the AASHTO underlying target probability induced by a $\beta = 3.5$ (3.1×10^{-6}). A a bias factor of 0.546 for the resistance is necessary to match the AASHTO target reliability index.

Similar calculations can be carried out for all other stations and span lengths. To illustrate one particular case, consider the results shown in Fig.3.16 for $10m$ span length across time. As can be seen the probability of failure varies greatly across five orders of magnitude and it does not exceed the implicit AASHTO target threshold. So even though the behavior is not stationary, it appears to be conservative to assume stationary at the AASHTO target reliability level. These results do not include any degradation of strength the bridge may experience, therefore they constitute a lower bound. However, for the type of structure analyzed (steel-concrete decks) this condition is not unrealistic. This is not the case for reinfroced concrete decks.

3.7 Conclusions and Future Work

This paper proposes the use of mixture models to represent the aleatoric variability of internal forces in bridge decks induced by vehicular live loads. The proposed mixture models were properly identified from vehicle axle data measured in 12 weigh-in-motion (WIM) stations across the state of Vermont, USA during a period of 12 consecutive years. The temporal and spatial variability of the parameters that define the mixture models were investigated. It was found that significant variation exists within and among stations. The identified mixture models were used to compute the time-varying reliability of simply supported bridge decks of various span lengths.

Future work on this subject will involve the formulation of a probabilistic model for the random process that defines the variability of the mixture model parameters. We will also look at the formulation of extreme value distribution that represent the mixture models that have been found through this study. Finally we will also investigate the applicability of using WIM data for bridge structural health monitoring and asset management.

3.8 Acknowledgement

This research was carried out thanks to the financial support of the Vermont Agency of Transportation. Their support is gratefully acknowledged.

3.9 Figures

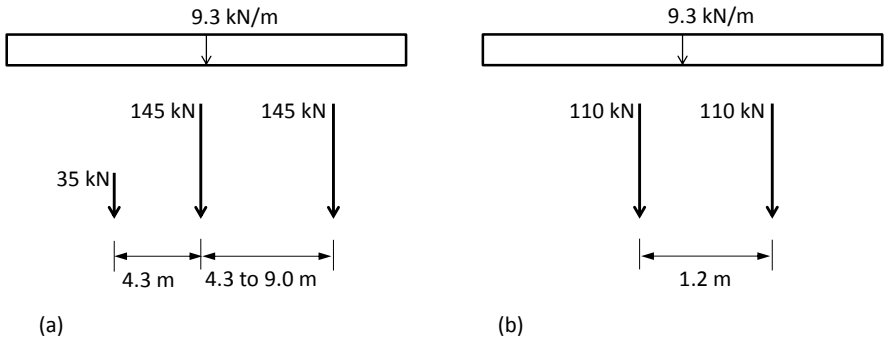

Figure 3.1: AASHTO HL-93 live load model per lane of traffic.

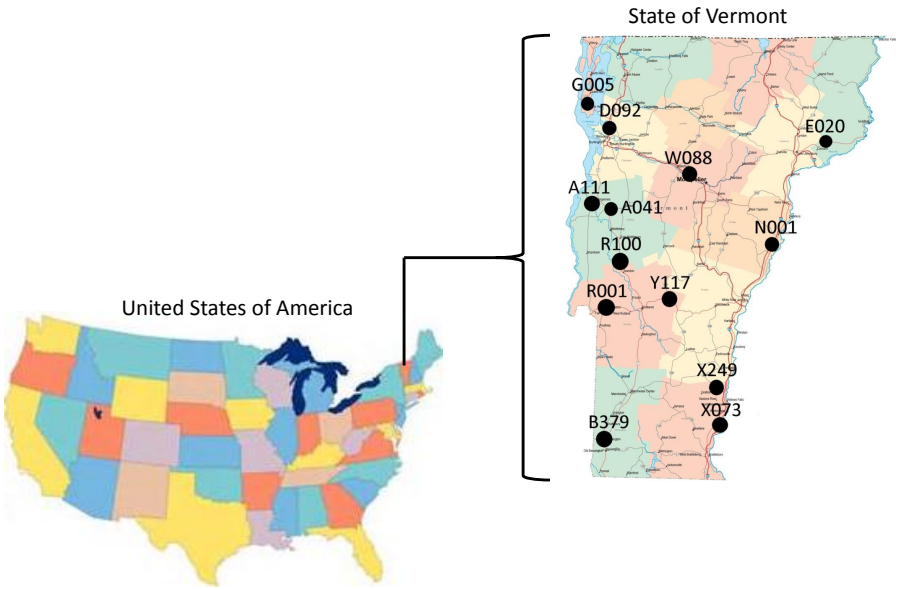

Figure 3.2: Geographical location and designation of WIM stations in Vermont.

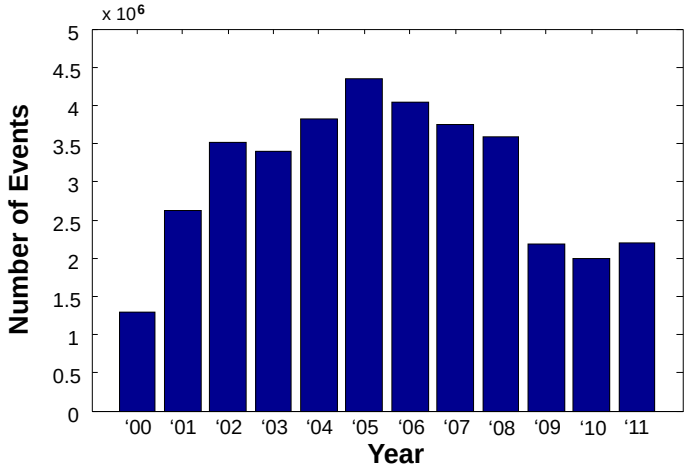

Figure 3.3: Total number of measured vehicles per year in all WIM stations

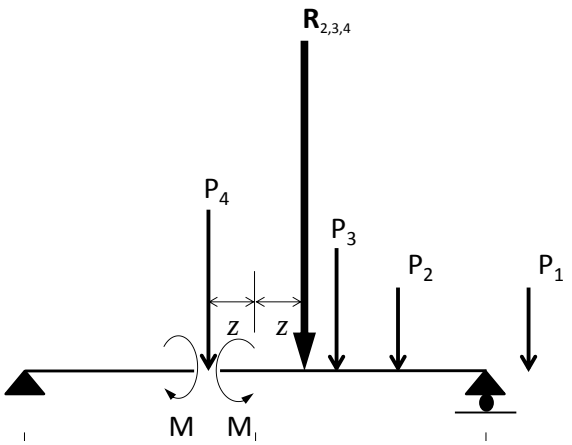

Figure 3.4: Illustration of a potential axle location within a simply supported span.

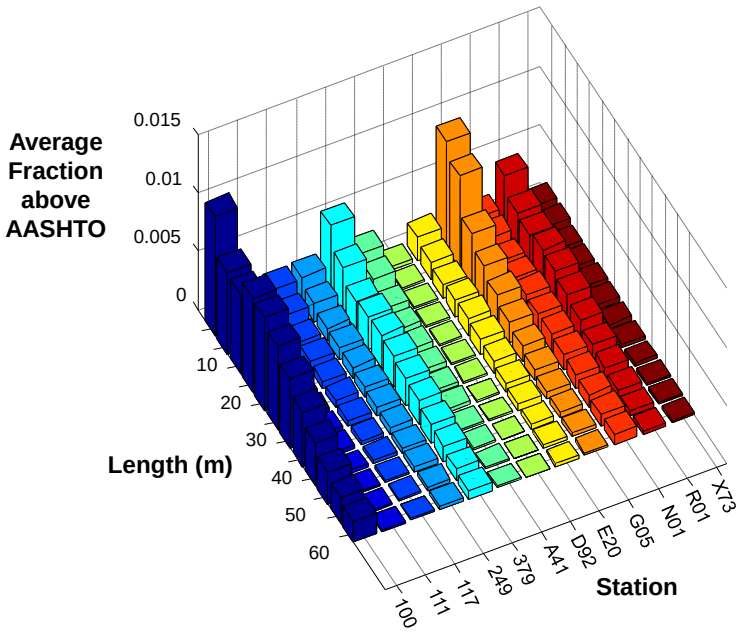

Figure 3.5: Proportion of measured vehicles that generate moments and(or) shears that exceed HL-93 induced moments and(or) shears as a function of stations and averaged over all years.

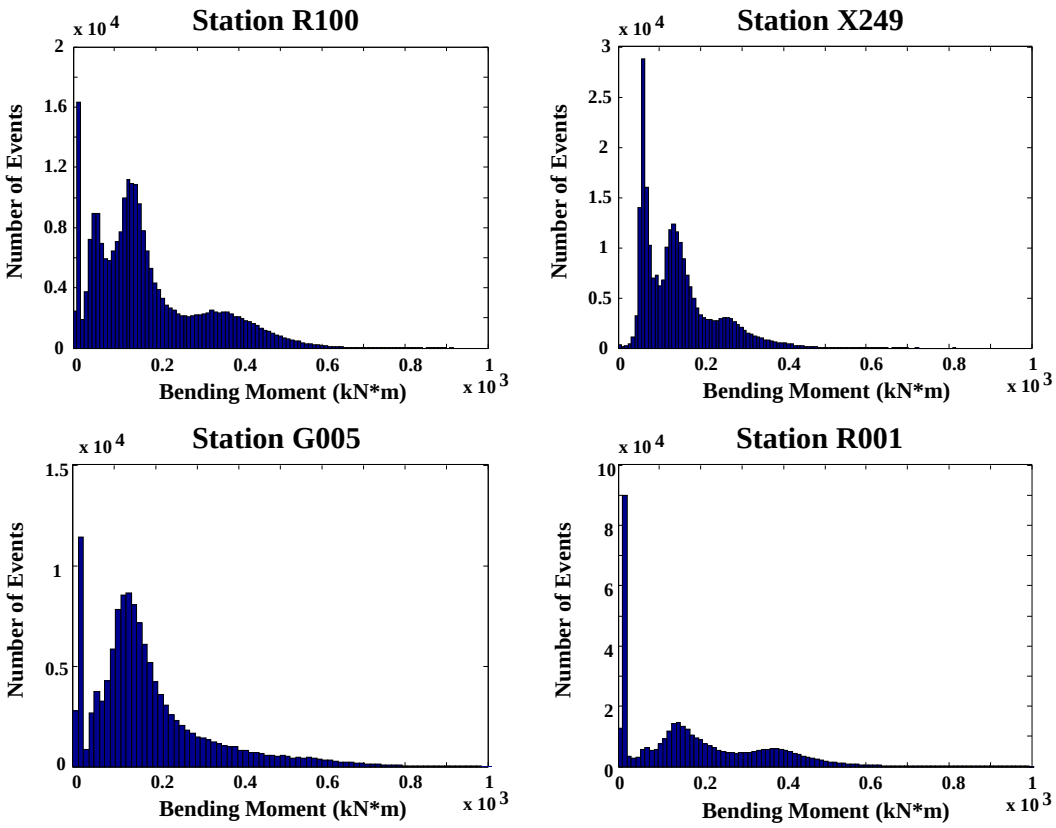

Figure 3.6: Histogram of lane bending moments generated by measured vehicles at 4 stations in 2004 for a span length of 10 m.

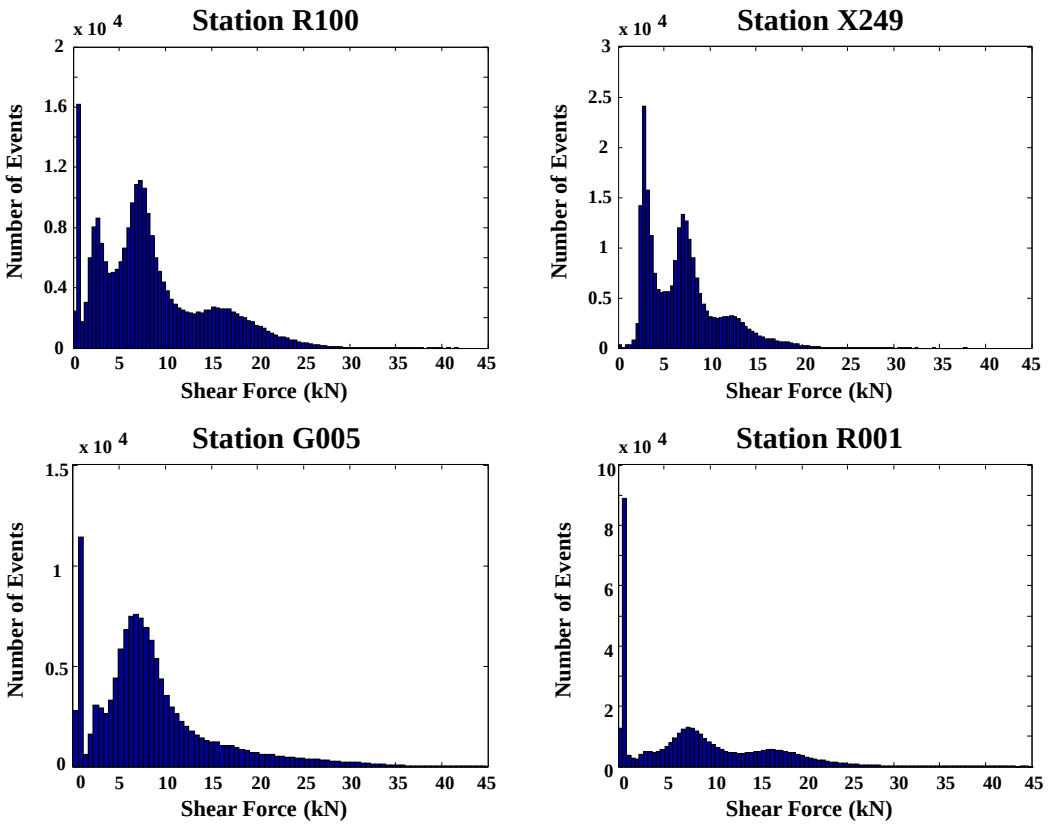

Figure 3.7: Histogram of lane shear force generated by measured vehicles at 4 stations in 2004 for a span length of 10 m.

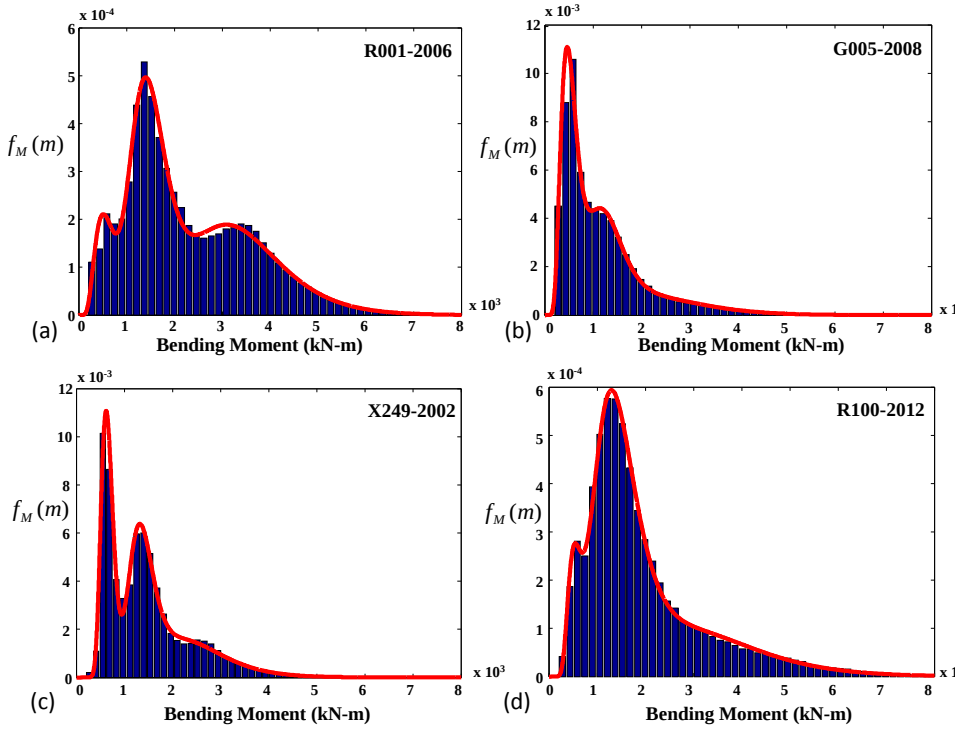

Figure 3.8: Quality of mixture model fit for various stations/years for a 10 m span

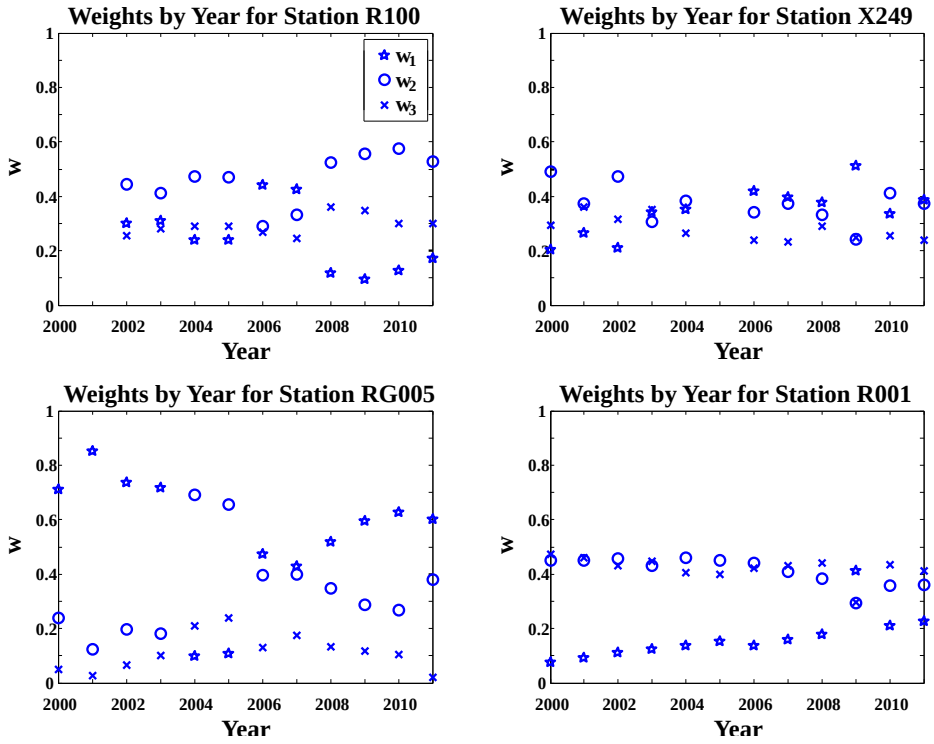

Figure 3.9: Mixture model weight parameters by station for 10 m length

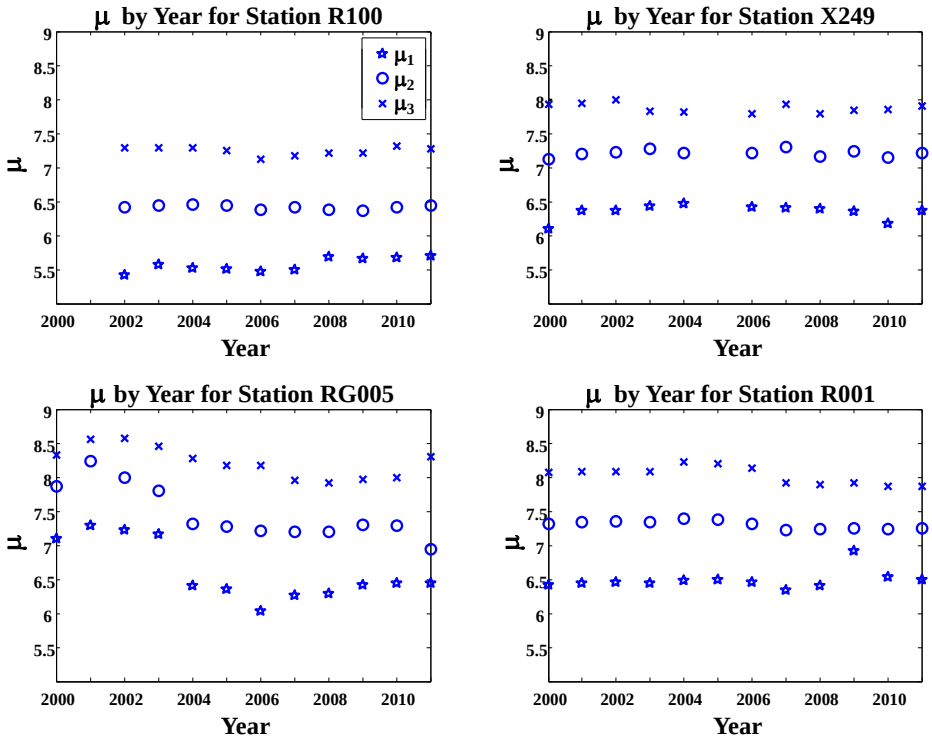

Figure 3.10: Mixture model mean parameters by station for 10 m length

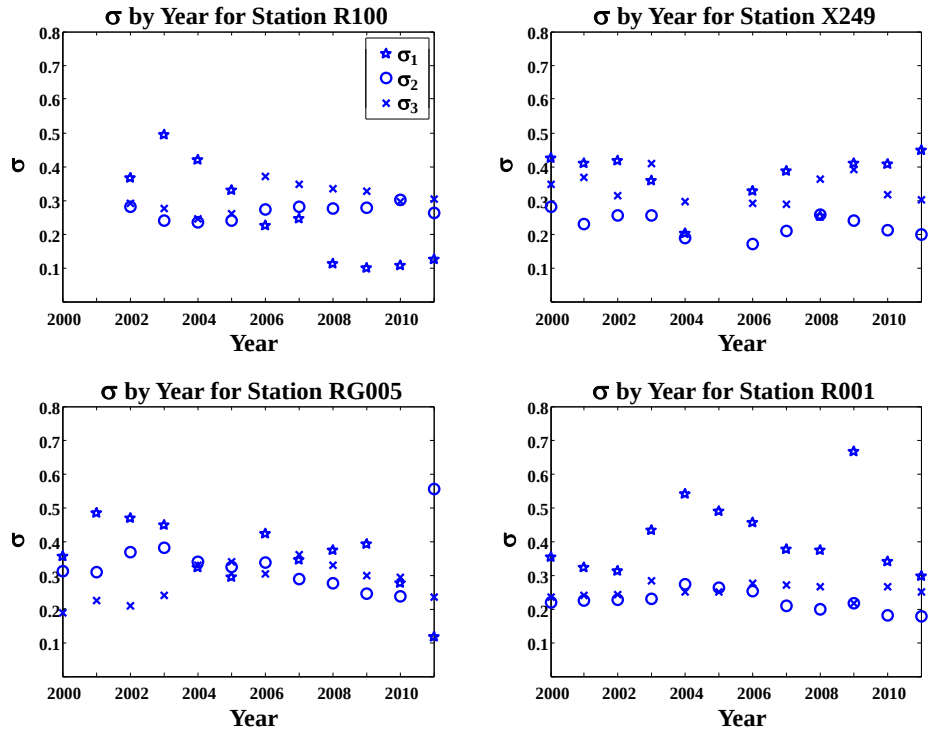

Figure 3.11: Mixture model standard deviation parameters by station for 10 m length

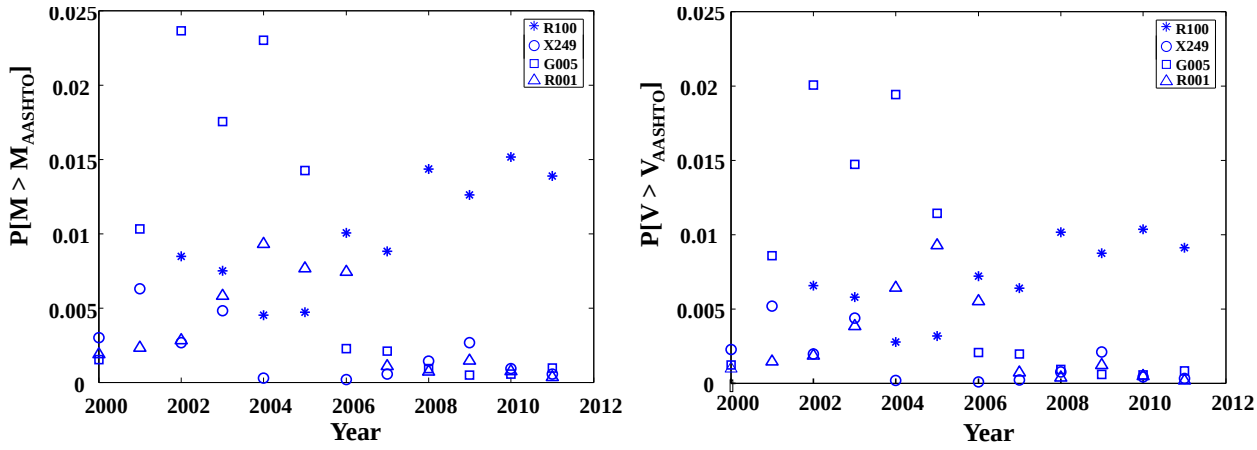

Figure 3.12: Probability of lane bending moments and shear forces exceeding AASHTO HL-93 induced lane values for a simply supported span of 10 m

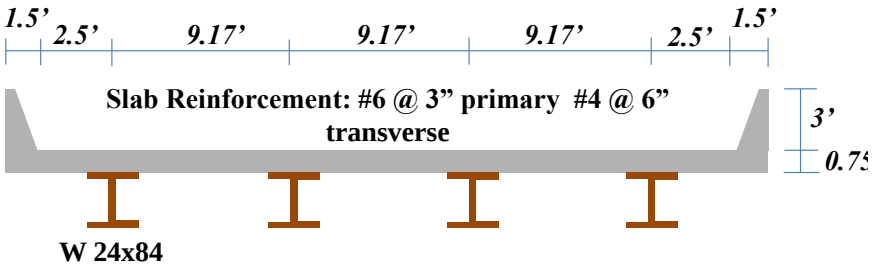

Figure 3.13: Cross section

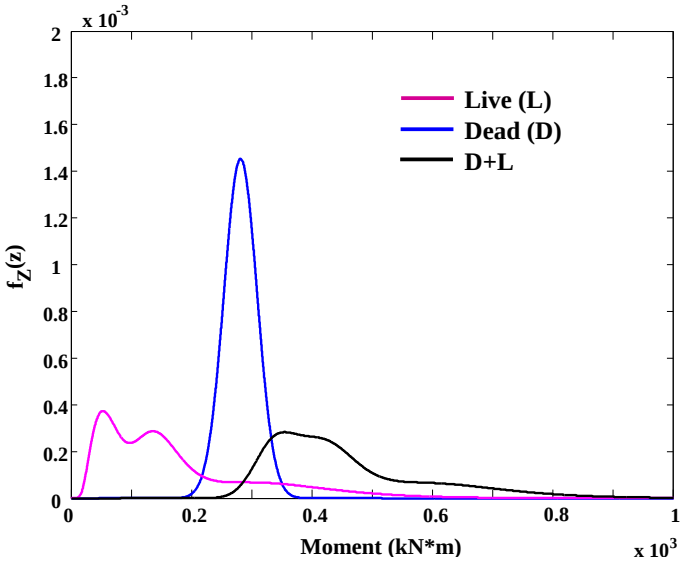

Figure 3.14: Probability distribution for dead plus live load lane bending moment, Station R100, year 2002, 10 m length

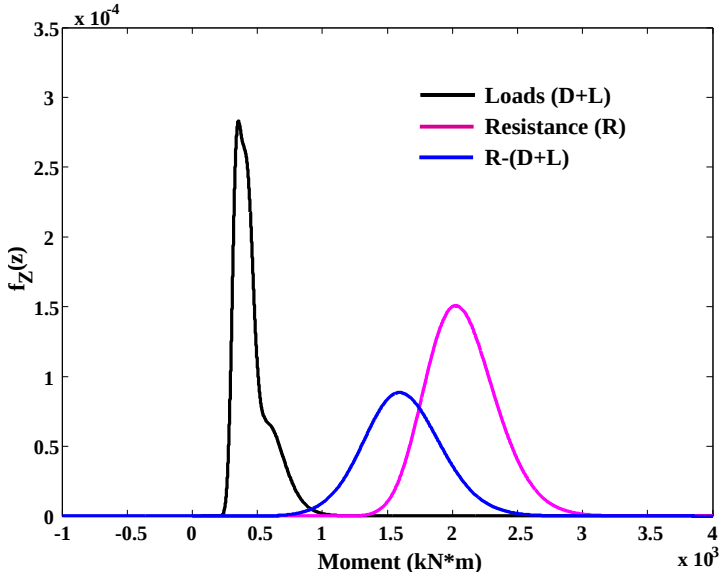

Figure 3.15: Probability distribution loads, resistance, and resistance minus loads, Station R100, year 2002, 10 m length

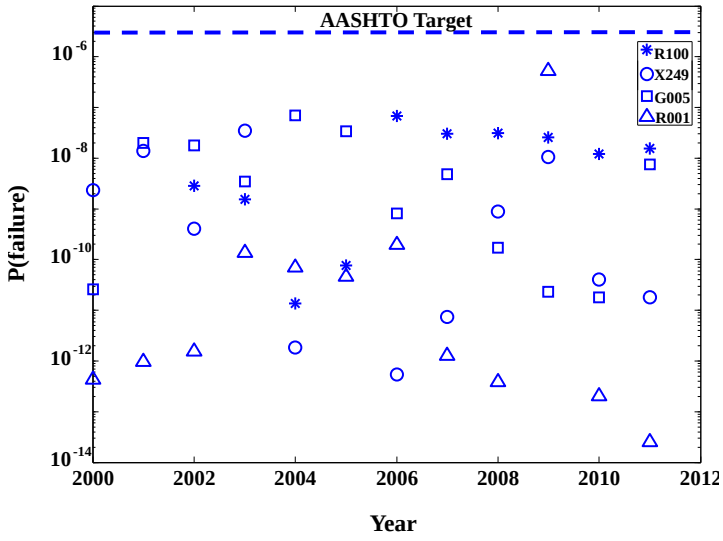

Figure 3.16: Probability of failure by station and year, 10 m length

Bibliography

[1] Zhuang, X., Huang, Y., Palaniappan, K. and Zhao, Y. (1996). "Gaussian Mixture Density Modeling Decomposition, and Aplications" *IEEE Trans. Imag. Proc.* 5(9): 1293-1302.

[2] Pelphrey, J.M. (2007)."An Investigation of Oregon Weigh-In-Motion Data for Bridge Rating Implementation and Evaluation." Thesis Oregon State Univ.

[3] Zhao, J. and Tabatabai, H. (2012). "Evaluation of a Permit Vehicle Model Using Weight-in-Motion Truck Records." *J. Bridge Engr.,*, ASCE, 17(2): 389-392.

[4] Caprani, C., OBrien, E. J., and McLachlan, G. (2007). "Characteristic Traffic Load Effects from a Mixture of Loading Events on Short to Medium Span Bridges." *J. Struct. Safety,* Elsevier, 30: 394-404.

[5] American Assoiation of State Highway and Transportation Officials (AASHTO). (2010).*AASHTO LRFD Bridge Design Specifications,* Washington, DC.

[6] Guzda, M., Battacharya, B., and Mertz, D. (2007). "Probabilistic Characterization of Live Load Using Visual Counts and In-Service Strain Monitoring." *J. Bridge Engr.,* ASCE, 121(1): 130-134.

[7] Hibbeler, R. C. (2009). "Chapter 6: Influence Lines for Statically Determinate Structures." *Structural Analysis (7^{th}),* McGraw-Hill, New York, 250-251.

[8] Kozikowski, M. (2009). *WIM Based Live Load Model for Bridge Reliability.* Ph.D. Dissertation, Univ. of Nebraska, Lincoln, NE.

[9] Kwon, O., Kim, E., and Orton, S. (2011). "Calibration of Live Load Factor in LRFD Bridge Design Specifications Based on State-Specific Traffic Environments." *J. Bridge Engr.,* ASCE, 121(1): 130-134.

[10] McLachlan, G. and Basford, K. (1988) *Gaussian Mixture Models,* Marcel Dekker, New York.

[11] Nowak, A. S. (1999). *NCHRP 368: Calibration of LRFD Bridge Design Code,* NCHRP, Washington, DC.

[12] OBrien, E. J. and Enright, E. (2013). "Using Weight-In-Motion Data to Determine Agressiveness of Traffic for Bridge Loading." *J. Bridge Eng.,* ASCE, 16, Special Issue: 812-819.

[13] Zhou, X., Schmidt, F., Toutlemonde, F. and Jacob, B. (2013). "Applying weigh-in-motion traffic data to reliability based assessment of bridge structures." ICOSSAR 2013, NY, NY.

[14] Tabsh, S. W., and Nowak, A. S. (1991). "Reliability of Highway Girder Bridges." *J. Struct. Eng.,* ASCE, 117(8): 2372-2388.

[15] Frangopol, D.M. and Lin, K.Y. (1997). "Reliability of reinforced concrete girders under corrosion attack." *J. Struct. Eng.,* ASCE, 123(3): 286-297.

[16] Val, D.V. and Melchers, R.E. (1997). "Reliability of Deteriorating RC Slab Bridges." *J. Struct. Eng.,* ASCE, 123(12): 1638-1644.

[17] Kulicki, J.M. (2010). "Evolution of the AASHTO bridge design specifications." University of Buffalo, Bridge Engineering Distinguished Speaker Series.

[18] Seaman, H.B. (1912). "Specifications for the design of bridges and highways." *Transactions of the American Society of Civil Engineers* 75(1): 313-352

[19] Manville, R. and Gastmeyer, R.W. (1914). "comparative figures on trucks and road rollers." *Engineering News* 71(35):492-507

[20] Ma, Y., Zhang, J., Wang, L. and Liu, Y. (2013). "Probabilistic prediction with Bayesian updating for strength degradation of RC bridge beams." *J. of Structural Safety,* Elsevier, 44: 102-109.

[21] Melchers, R.E. (1999). Structural Reliability Analysis and Prediction. John Wiley and Sons, Ltd. West Sussex, England

[22] van de Lindt, J.W., Fu, G., Zouh, Y., and Pablo, R. (2005). "Locality of Truck Loads and Adequacy of Bridge Design Load." *J. Bridge Engr.,*, ASCE, 10(5): 622-629.

[23] van de Lindt, J.W. and S., Pei. (2006). "Buckling Reliability of Deteriorating Steel Beam Ends." *Electronic Journal of Struct. Engineering,* 2006(6): 1-7.

[24] http://www.census.gov/census2000/states/vt.html

[25] Stewart, M.G. and Rosowki, D.V. (1998) "Time-dependent reliability of deteriorating reinforced concrete bridge decks." *J. Structural Safety,* Elsevier, (20):91-109

Chapter 4

Bayesian Model Averaging Methods for Identifying Live Load Stress Demand Extreme Value Distributions in Bridges

This paper proposes the use of the Bayesian Model Averaging to identify the optimal model of the extreme values of internal forces in bridge decks from weigh-in-motion (WIM) data. The identified models are used for reliability analysis of bridge decks. The weigh-in-motion data was collected by the Vermont Agency of Transportation during a period of 12 years. The paper presents a comparision between the demands induced by the WIM data and the AASHTO HL-93 live load model.

4.1 Introduction

The study of the occurrence of low probability/high consequence events is a crucial aspect of developing a probabilistic design code. The AASHTO LRFD Bridge Design Specifications were generated through such studies. The goal of this code is to provide load and resistance factors consistent with a reliability index (β) of 3.5 for a service life of 75 years [7]. In order to do this, the occurrence of extreme loading events needs to be carefully considered. Since 75 years of continuous data are not available, methods for

extrapolating smaller periods of data to the 75 year design life are necessary. This extrapolation often involves making assumptions about the behavior of traffic that can influence the results [3, 4]. Despite this, it is generally agreed upon that extreme value theory provides an adaquate method for this extrapolation.

Many researchers have been able to use extreme value analysis to calculated lifetime characteristic load effects for bridge spans [2, 10]. Others [9] modeled truck loads by using the most extreme trucks by weight. Although this may not be completely consistent with extreme value theory, the analysis was able to show that using only extreme values by weight to evaluate truck load models is possible. A strong correlation between gross vehicle weight (GVW) and and a vehicle producing a maximum stress demand has been observed [6]. However, axle layout has a more significant effect on this outcome [4]. This is especially true in short and medium span bridges ($L \leq 50m$) where the length of a truck might exceed the length of the span. These types of bridges are important because they constitute the largest part of the bridge population. This study focuses on bending moment demand in short and medium span bridges.

The data for this study comes from 4 Weigh-In Motion (WIM) stations in the state of Vermont taken over a twelve year period (2000-2011). These stations collect truck axle weights and spacing data, among other things. From this data the maximum bending moment each truck produces in a simple span can be calculated using structural analysis algorithms. The data were also time stamped so the moments can be sorted by day of ocurrence. However, no data on speed or headway between vehicles was recorded, so multiple presence can not be assessed. The maximum bending moment produced by a vehicle in each day was attained because it was of interest to develop a probability model that describes the occurrence of the largest (extreme) bending moments. This paper describes the various probability models that were tested, as well as the methods used to test their adaquacy to represent the data. The best fitting model is then used to perform reliability calculations for sample bridge superstructures of varying lengths.

The estimated probability of failure is computed using resistance models developed by others [7, 8]. The estimated probability of failure can be compared with the target value from AASHTO. A reliability index (β) of 3.5 for 75 years corresponds to a probability of failure of 0.000233. Since there is only 12 years of data available, and less for some stations, we must postulate a probabilistic model for the yearly probability that is consistent with the

desired probability for a 75 year service life. To calculate the desired yearly probability a binomial model is postulated. If one assumes that the process is stationary and the probability of failure is constant every year, one finds that a Bernoulli process would result in a probability of at least one failure given by

$$P[Z < 0] = 1 - (1 - p)^{75} \tag{4.1}$$

where p is the yearly probability of failure. Setting $P[Z < 0] = 0.000233$ one can solve the previous equation and obtain the corresponding yearly probability of $p = 3.1 \times 10^{-6}$. This can then be used to find the 12 (or 10) year failure probability by

$$P[Z < 0] = 1 - (1 - p)^{12} \tag{4.2}$$

resulting in a 12 year probability of $p_{12} = 3.72 \times 10^{-5}$ and a 10 year probability of $p_{10} = 3.1 \times 10^{-5}$. These probabilities will be compared to the estimates of the probability of failure computed using WIM data.

4.2 The Data

The data was extracted by taking the maximum value from a certain each day over the data set. This is different from what has been done in the past [6, 9]. Commonly, the heaviest or largest 5% of the data is taken and used for the data. This is not consistent with extreme value theory, and the potential issues with this are not discussed in this paper, for more detail see [5]. A histogram of the data is shown in fig. 4.1. The difference between the distribution of the data in fig. 4.1 and figs. 4.2 and 4.3 is drastic. Fig. 4.2 shows the histogram of the largest 5% of moments with the AASHTO value denoted by a red line, along with the percent of cases over AASHTO. Fig. 4.3 shows the bending moments that resulted from the heaviest 5 % of trucks. It is clear that selecting data in either of these manners will lead to very different conclusions about design values of bending moments than selecting the daily extreme value. This can be seen in two key ways. The first is the extreme difference in the fraction of cases that exceeded the AASHTO value, this value is three times greater when using the daily maximum moments. The second is the difference in the shape of the distributions. If one were to fit a distribution to the maximum daily moments it would be a completely

different fit from the largest 5% of the moments. In order to be consistent with extreme value theory the maximum daily moments were used for this study.

4.3 Extreme Value Theory

Extreme value theory states that one of three extreme value distributions, Gumbel, Frechét, or Weibull, will describe the distribution of extreme (maximum or minimum) values of independent and identically distributed (iid) variates. These distributions are all part of a family called the Generalized Extreme Value (GEV) distribution. Formally, the GEV distribution is a limiting distribution of the extrema of n iid random variables, X_i, as n $\rightarrow \infty$. Each X_i was the maximum daily bending moment. Which of the three distributions best describes the maxima/minima depends on the parent distribution of the variates. In the case of the bending moments, the parent distribution of the daily bending moment is unknown. Therefore other methods to evauluate the appropriateness of each distribution were used and are discussed later in this paper.

For the Gumbel, the parent distribution of the X_i is in the form of $f_x(x) = e^{-g(x)}$ with $\frac{dg}{dx} > 0$. The normal, exponential, and gamma distributions all have this form. An important aspect to consider is that in reality random variables are hardly ever independent or identical. According to Gumbel this condition does not need to completely satisfied in order to use this distribution (Gumbel, 1958). This is particularly helpful in the case of the bending moment data, since it is virtually impossible to prove that the truck data is independent or identicaly distributed when examined from a daily persepctive.

For the Frechét, the distribution of the X_i is of the form $f_x(x) = kAx^{-(k+1)}$, where $x > 0$ and A is a constant. Distributions of this family include the Cauchy and Pareto. This distribution is one sided, an important aspect because the bending moments considered are all the same sign. The underlying, or parent, distributions for the type II usually have longer tails than those of the type I. The distribution of the maximum bending moments produced by every truck has a very long tail, further suggesting this is a strong potential candidate distribution.

For the Weibull the parent distribution is $f_x(x) = Ak(w - x)^{k-1}$, with $x \leq w$ and A a constant. Examples of these types of distributions are the

uniform, triangular, and gamma. This distribution is typically used when X_i is limited in the tail of interest to a maximum value w. Like the type II, this is also a one sided distribution. Although the Weibull dsitribution is typically used for failure, the flexibility of the distribution to fit a wide variety of data makes it useful for this situation. The thought here is that if Weibull analysis can provide good failure forecasts with little data, it can also forecast the occurrence of large stress demands with similar accuracy (Abernathy, 2006).

4.4 Daily Maximum Bending Moments and Extreme Value Theory

The condition that populations from which the extremes are being sampled are iid needs to be met in order to use extreme value theory. If this does not hold then none of the asymptotic distributions will suffice to represent the extremes. This is because the derivation of the asymptotic distributions is based on the iid asumption. This assumption is such that probability of the extremes being less than a certain value is a function of the cumulative distribution of the population which the extremes came from:

$$P[X_1, X_2, ..., X_n \leq x] = F_X(x)^n \tag{4.3}$$

If this does not hold true the stability postulate cannot be applied so the asymptotic distribution of the extremes does not converge to a GEV distribution [5]. Therefore examination of the distribution of the daily bending moments is necessary.

From fig. 4.4 it is clear that the daily bending moments do not have the same parent distribution. Although they all appear to be mixture distributions, the weights, means, and standard deviations of the moxture components appear to be completely different from day to day. Clearly this violated the iid assumption necessary to invoke extreme value theory. Therefore we will consider other distributions, as well as the GEV distributions, as potential proabbility models for the daily maximum bending moments.

4.5 Probability Models

The following sections describe the various probability distributions that were tested for their fit to the data. Six probability distributions were tested to fit the data in this study. Since the iid condition necessary to use extreme value theory was not satisfied 3 additional distributions were tested. These other diustributions, the Gaussian, log-normal, and Gamma distributions, were selected based on the shape of the data histogram. These three were thought to have the most potential to fit the data outside of the three GEV distributions because of their shape. The following sections explain how the parameters for each model were estimated.

4.5.1 Normal Models

Gaussian (normal) and log-normal distributions were considered as potential models because of their shape. In fig. 1 the data appear to have a similar shape to these types of distributions. The mean and variance of the data are the parameters for the Gaussian and are easily obtained. For the log-normal distribution the parameters were transformed using the following equations, with m and v representing the mean and variance of the data respectively. Plots of these distributions over the data are shown in fig. 2.

$$\mu = \log\left(\frac{m^2}{\sqrt{v+m^2}}\right) \tag{4.4}$$

$$\sigma = \sqrt{\log(1+\frac{v}{m^2})} \tag{4.5}$$

4.5.2 GEV Models

As previously stated, all three types of GEV distributions were tested. The GEV Type I distribution is descibed by the following PDF:

$$f_y(y) = \alpha e^{-\alpha(y-u)-e^{-\alpha(y-u)}} \tag{4.6}$$

The parameters α and u are estimated from the data using the following equations (γ is Euler's constant):

$$E[y] = \mu_y = u + \frac{\gamma}{\alpha} \tag{4.7}$$

$$Var[y] = \sigma_y^2 = \frac{\pi^2}{6\alpha^2} \tag{4.8}$$

The GEV Type II distribution is described by the following PDF:

$$f_y(y) = \frac{k}{y}\left(\frac{u}{k}\right)^k e^{-(u/y)^k} \tag{4.9}$$

The parameter estimation for this distribution is less straightforward. This is because the definition of the moments involves using the gamma function. The estimation is done using the following equations:

$$E[y] = \mu_y = u\Gamma(1 - 1/k) \tag{4.10}$$

$$Var[y] = \sigma_y^2 = u^2[\Gamma(1 - 2/k) - \Gamma^2(1 - 1/k)] \tag{4.11}$$

These can be combined to eliminate u and k can be estimated by the guess and test method using the following equation:

$$\frac{\mu_y^2}{\sigma_y^2} = \frac{\Gamma(1 - 2/k)}{\Gamma^2(1 - 2/k)} - 1 \tag{4.12}$$

The Weibull distribution is described by the following PDF:

$$f_y(y) = \frac{\beta}{\alpha}\left(\frac{y}{\alpha}\right)^{\beta-1} e^{-(y/\alpha)^\beta} \tag{4.13}$$

The shape parameter β is estimated iteratively using the following equation:

$$\frac{1}{\beta} = \frac{\sum_{i=1}^N (y_i^k \ln y_i - y_N^k \ln y_N)}{\sum_{i=1}^N (y_i^k - y_N^k)} - \frac{1}{N}\sum_{i=1}^N \ln y_i \tag{4.14}$$

Once the shape parameter has been obtained the definition of the first moment, or expected value, can be used to estimate the scale parameter α. Like the GEV type II, the expected value is defined as:

$$E[y] = \alpha\Gamma(1 + \frac{1}{k}) \tag{4.15}$$

This leads to:

$$\alpha = \frac{E[y]}{\Gamma(1 + \frac{1}{k})} \tag{4.16}$$

4.5.3 Gamma Model

A gamma distribution was also considered as a model for the data. This is mainly because of the shape of this distribution. This distribution has a PDF described by:

$$f_y(y) = \frac{\beta^\alpha}{\Gamma(\alpha)} y^{\alpha-1} e^{-\beta y} \tag{4.17}$$

Where $\Gamma(\alpha)$ represents the gamma function evaluated at α. The parameters α and β are estimated using the following equations:

$$E[y] = \mu_y = \frac{\alpha}{\beta} \tag{4.18}$$

$$Var[y] = \sigma_y^2 = \frac{\alpha}{\beta^2} \tag{4.19}$$

4.6 Bayesian Parameter Estimation

As previously discussed, methods for computing the maximum likelihood estimates for the parameters of these distributions have been developed and well documented. However, a more robust comparison of the models was deirable. This means statistical distributions for the parameters were neeeded. Bayesian methods can be used to compute the posterior distribution of the parameters and make maximum a posteriori (MAP) estimates of them. The MAP is a mode of the posterior distribution, $f(\theta|y)$, of the parameters, θ, that has been computed based on the data, y. The joint posterior distribution is computed using Bayes' Theorem in the following manner:

$$f(\theta|y) = \frac{f(y|\theta)g(\theta)}{\int_\Theta f(y|\tau)g(\tau)d\tau} \tag{4.20}$$

In this expression $f(y|\theta)$ is the likelihood function. The likelihood function for a data point is the probability density function evaluated at that

point for all values being considered in the parameter space Θ. The expression for the evidence, in the denominator, arises due to the total probability theorem. This term is a normalizing constant that ensures the expression integrates to one, and is therefore a valid probability density function. The term $g(\theta)$ is the prior distribution of the parameters. This prior distribution reflects the belief in the values the parameters take before the Bayesian analysis has been performed. A logical choice for the prior is an uncorrelated jointly gaussian distribution centered at the maximum likelihood estimates (MLE's). Jointly Gaussian random variables are distributed acccording to the equation ($\mathbf{K}$ is the covariance matrix, $\mathbf{m}$ is the vector of means, and n is the number of random variables):

$$f_x(x) = \frac{1}{(2\pi)^{n/2}|\mathbf{K}|^{\mathbf{1/2}}} e^{-\frac{(\mathbf{x}-\mathbf{m})^{\mathbf{T}}\mathbf{K}^{-\mathbf{1}}(\mathbf{x}-\mathbf{m})}{2}} \tag{4.21}$$

The means used for each parameter were the MLE's that were calculated as discussed in the probability models section. A coeffecient of variation (COV) of 0.2 was applied to get the standard deviations and variances for each parameter. Before proceeding it was checked that the jointly Gaussian priors integrated to 1. A sample PDF of a jointly gaussian prior is shown in fig. 4.5.

The posterior computed from one data point is used as the prior for the next. The entire data set ($\vec{y}$) is then run through the algorithm to compute the full posterior, $f(\theta|\vec{y})$. The MAP can be computed at each step so convergence of the parameter estimates can be tracked and verified. This is of particular interest because computation time can be saved by minimizing the amount of data that needs to be run through the algorithim. Fig. 4.6 shows the path the parameters take as the dats is evaluated for the various distributions.

From the previous plots it can be seen that the parameters do converge, although some faster than others. The fact that convergence can be observed strengthens the conclusions regarding the parameter estimates for these distributions. The normal distribution was also run through this alrorithm, but the MAP estimates of the parameters were simply the mean and variance of the data. This was expected and used to verify the algorithm before other distributions were tested.

An in depth analysis of the posterior is important becausse it gives insight into the strength of the conclusions drawn from it. Another area of interest is observing how the posterior changes as more data is analyzed. This shows

how the belief goes from a spread out jointly gaussian prior into a much sharper and more precise estimate of the parameters. Fig. 4.7 shows the evolution of the posterior distribution of the GEV type I parameters as more data us evaluated. This contour plot was generated every 350 data points throughout the entire data set analysis.

These two figures are important for examing the behavior of the posterior, because this gives us informatuion about the accuracy of the parameter estimates. The contours are significantly stretched along the α direction. This means that this parameter converges slower, which can also be seen in the previous figure that traces the MAP estimate of α. This behavior remains constant throughout the evolution of the posterior. Although the peak becomes much sharper throughout this process, this means that there is more uncertainty on the true value of α than u. The higher uncertainty can also be seen in the ranges of the credible intervals. A credible interval represents the interval that the true value of the parameter has a certain probability of falling within. The 95% credible interval for α is $7.0171\times10^{-4}-7.4735\times10^{-4}$ and $5.6798\times10^{3}-5.8345\times10^{3}$ for u.

Fig. 4.8 shows a similar behavior for the GEV Type II posterior. Here, the difference in uncertainty is less pronounced, but the uncertainty on the true value of u is still significantly less than than than of k. The credible itnerval for u is $5.4876\times10^{3}-5.6640\times10^{3}$ and $3.5441-3.7352$ for k. It only takes about 500 data points for u to converge within 5% of its MAP value, while k appears to be trending thowards a MAP value, but does not appear to have completely converged for the total amount of data available. This was the only instance where a parameter appeared to not completely converge. In fig. 4.6 all parameters for all other distributions appear to have leveled off in the neighborhood of the MAP estimates.

The difference in uncertainty on the Weibull parameters is noticably less, as shown in fig. 4.9. However, there is still more uncertainty on the true value of β than on α. The 95 % credible interval for α is $6.96341\times10^{3}-7.1418\times10^{3}$ and $4.5790-4.8564$ for β. This was expected since fig. 4.6 shows α converging faster than β. The value of α gets to and stays within 5% of the MAP roughly 550 points before the value of β does.

The uncertainty on the gamma parameters was shared evenly between the parameters α and β. This can be seen by the almost one-to-one line formed by the posterior in fig. 4.10. When looking at the convergence of these parameters this shared uncertainty makes sense. Both parameters appear to have coverged at an alomst identical rate, suggesting that the uncertainty

on them is similar. The MAP estimates were only slightly different than the MLE estimates. The MAP estimate for α was 20.69, while the MLE was 20.92. The 95% credible interval was $18.0931 - 20.1947$. For β the MAP and MLE were $7.24x10^{-4}$ and $7.32x10^{-4}$ respectively. The 95 % credible interval was $2.7820 \times 10^{-3} - 3.1109 \times 10^{-3}$.

The uncertainty on the log-normal and Gaussian parameters was virtually nonexistent, the credible intervals were roughly $\pm 1\%$ of the MLE's. This means that the posterior modes were very sharp and decayed quickly moving away from the MLE's.

4.7 Evaluation of Probability Models

Two tools were used to evaluate the adaquacy of the possible probability models. These are the Chi-Square test and Bayesian model comparison, both of which are discussed in this section. The chi-square test is a frequently used frequentist method of testing the fit of a probability model to data. Bayesian model comparison is a newer method of model evaluation that is ideal for applications with large amounts of data, such as this.

4.7.1 Chi-Square test

The chi-square test is commonly used to determine the goodness of fit of a distribution to a data set. The basic idea is to determine the chance of observing a result as extreme as the data if it does come from the postulated distribution. If it turns out that this chance, called the observed significance level, is greater than a desirted and pre-dtermined significance level (α, typically 0.01 or 0.05) then the data cannot be described by the proposed model. The steps to carry out the test are as follows:

1. Divide the sample space S_X into K disjoint intervals (bins).
2. Calculate the probability b_k than an outcome falls within the k^{th} interval based on the assumption that X has the postulated CDF. Set $m_k = nb_k$ where m_k is the expected number of outcomes that fall in the k^{th} interval if the experiment is repeated n times.
3. Calculate the chi-square statistic as the weighted difference between the observed number of outcomes in each interval (N_k) and the expected number (m_k) using the following equation:

$$D^2 = \sum_{k=1}^{K} \frac{(N_k - m_k)^2}{m_k}$$

4. D^2 is then compared to a threshold value (t_{alpha}). If $D^2 > t_\alpha$ the proposed distribution is an acceptable model for the data. This threshold value is determined from a chi-square PDF with $K-1$ degrees of freedom and follows the following equation:

$$P[X \geq t_\alpha] = \alpha$$

This test was performed on each of the proposed probability models. Each distribution is shown over the data in fig. 4.11. The Chi-Square statistic for each distribution is also shown on these plots. The threshold value for a 0.05 significance level using 30 bins is 42.56. This means that the test showed that none of the models was a particularly good fit for the data. Therefore another means for evaluating the models was needed.

4.7.2 Bayesian Model Averaging

Since the chi-square test was incinclusive, Bayesian model averaging provided an alternative and more conclusive way of comparing the models for the data. This method for model comparisson uses Bayesian methods to compute the belief that each model is a propper fit for the data. To start, first consider what is occurring onthe individual model level. Bayes' theorem is used to calculate the probability of observing the data if each model were correct ($P[y|M_i]$). For a given model and set of parameters $\boldsymbol{\theta}$, the probability density function of the parameters given the data is found using Bayes' Theorem (eq. 17). The evidence is proportional to the predictive strength of the model. This leads to:

$$P[y|\mathcal{M}_i] = \int_\Theta f(y|\boldsymbol{\theta}) f(\boldsymbol{\theta}) d\theta \tag{4.22}$$

The models can be compared using the probability of observing the data given each model. This requires a probability mass function that defines the prior belief in each model ($P[\mathcal{M}_i]$). Bayes theorem is used again here to develop an expression for the probability of the model being the best fit given the data ($P[\mathcal{M}_i|y]$):

Table 4.1: Results of Model Averaging

Distribution	**Probability**
Log-Normal	0.0
Gaussian	0.3495
GEV Type-I	0.0
Gamma	0.6505
GEV Type-II	0.0
Weibull	0.0

$$f(\mathcal{M}_i|y) = \frac{P[y|\mathcal{M}_i]P[\mathcal{M}_i]}{\sum_{j=1}^{m} P[y|\mathcal{M}_j]P[\mathcal{M}_j]} \tag{4.23}$$

Again, to compare multiple models, the jointly gaussian distribution centered at the parameter MEL's were used for the parameter priors. The likelihood for a data point was simply the probability model evaluated at that point for all possible values of the parameter. Numerical integration was used to compute the evidence.

The prior for each model was considered to be 1/6 since it was not clear which model would be the best fit from the previous analysis performed. For the model comparison, the evidence calculated for each model at a given point was used as the likelihood for that model. The total evidence for at each point was then computed as the sum of the individual likelihoods times the corresponding model priors, as shown in the denominator of equation 19. The posterior probability was therefore the likelihood of the model times the prior for the model divided by the evidence. This process was repeated for every point in the data set with the posterior being used as the new prior. The belief in each model is then updated every time a new data point is considered. Afrter running through the entie data set the model that best fits will have the highest posterior value. Different values for the COV were used after the initial analysis was performed. This was to examine the effect that the COV had on the results. It was determined that a 100% increase in the COV resulted in less than a 1% change in the results.

The results of the Bayesian model averaging are shown in table 1. The Gaussian and Gamma distributions are overwhelmingly favored: the belief

in all other models rounds to zero from over 10 decimal places. The data was run sequentially starting with the maximum bending moment from the first day of data. The belief in each probability model that was found using Bayes' rule can be used as weights to form a mixture distribution. The evolution of these weights, or mixing coeffecients, as the data was run are shown in fig. 4.12. It can be seen that the belief that the Log-Normal, GEV Type-I, GEV Type-II, and Weibull models diminishes quickly, while the belief in the Gaussian and Gamma models fluctuates throughout the process.

These beliefs can be thought of as weights for a mixture distribution. In this case the mixture is of Gaussian and Gamma distributions. The Log-Normal and GEV Type-I distributions are excluded from this because of their large chi square statistics and virtually zero belief as found using Bayes' Theorem. Since it is not evident that the belief in the Gamma and Gaussian coverged, different weights were tested ranging between 0.3-0.7 for each distribution. The mixture distribution is shown over the data in fig. 4.13 along with the Chi-Square statisitc for this distribution. This mixture distribution is a better fit visually and mathematically than to the other distributions (shown in fig. B.3), as seen through the Chi-Square statistic. The critical value for the 0.05 significance level is 42.6, so the distribution passes the test.

4.8 Results

The purpose of this project was to combine the credible intervals on the parameters and model comparisson results to model the live load stress demands. To do this, the distributions, with each combination of parameter estimates, were mixed according to the model comparrison results. Using the lower bound of α with corresponding value of β found using equation 15 gave values of .3860 of cases over AASHTO, while using the upper bound of α and corresponding value of β gave a value of .3809 of cases over AASHTO. Repeating the same procedure for the upper and lower values of β led to results within 2% of the values for when the upper and lower bounds of α were used. This showed that the uncertainty on the parameter values results in minimal uncertainty on the probability of exceeding AASHTO. These distributions can then be used to perform reliability calculations on bridge girders.

In order to complete a full live load reliability analysis for the superstructure, the dead load and girder resistances needed to be calculated. This was done by using AASHTO to design bridges that were as close to the minimum

Table 4.2: Results of Reliability Analysis

	Estimated Probability of Failure	
Station	L=10m	L=20m
R100	4.86×10^{-8}	1.89×10^{-6}
X249	7.45×10^{-8}	5.83×10^{-8}
G005	1.30×10^{-7}	1.39×10^{-5}
R001	1.84×10^{-7}	2.11×10^{-6}

Table 4.3: Results of Reliability Analysis Using GEV Distribution for the Live Load

	Estimated Probability of Failure	
Station	L=10m	L=20m
R100	1.75×10^{-5}	6.95×10^{-5}
X249	1.55×10^{-6}	3.66×10^{-5}
G005	1.42×10^{-5}	6.44×10^{-5}
R001	4.69×10^{-6}	2.21×10^{-5}

requirements for strength as possible. From the superstructure design, the dead load and resistances could be calculated. The dead load and resistance were then assigned distributions based on available literature [7]. SAP2000 was used to model the bridge decks to determine the maximum amount of live load that each girder would need to support.

Table 2 shows the estimated probability of failure for the 4 WIM stations considered for both 10 and 20 meter length spans. The probability model used for the live load was the mixture determined using Bayesian Model Averaging. The values here are all at least one order of magnitude smaller than the 10 and 12 year target values given in the introduction. Table 3 shows the estimated probability of failure using a GEV type I distribution for the live load. In all cases there is a noticable difference in the estimated probability of failure, with the estimate using a GEV distribution for the live load much larger. In all but one case this difference is greater than one order of magnitude.

This large difference in estimated probability of failure can be attributed to the shape of the tail of the GEV type I distribution. The GEV type I with MAP parameters and the best fitting distribution are shown in fig. 4.14. The tail of the GEV distribution is noticably heavier than the tail of the best fit. A convolution is used to add the dsitribution of the live load effects to the distribution of the dead load effects. A cross corelation is then used to subtract the distribution of the load effects from the distribution of the resistance. These two processes compound the effect of the heavier tail, as can be seen in the difference in estimated probability of failure.

4.9 Conclusion

The results of this study show that using extreme value theory to model live load effects in bridge spans can lead to over estimating the probability of failure. Other distributions, or mixtures of other distributions, have been shown to better fit the extreme values of the live load effects. The reason for the difference in probability of failure is that these other distributions have lighter tails than the GEV dsitributions. Furthermore, it has been shown that the parent distributions that the extreme load effects come from are not identical. This violates one of the necessary conditions to use extreme value theory.

Bayes' Theorem has been shown to be a powerful method for determining the optimal probability model for these load effects have been developed. We have shown that this method result in better fitting probability models than simply using extreme value theory. Furthermore, the optimal parameters for these probability models vary from the maximum likelihood estimates. Bayesian methods also provide suitable methods for determining the parameters.

4.10 Figures

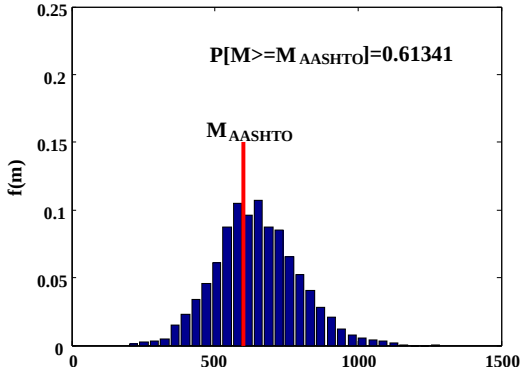

Figure 4.1: Histogram of Daily Maximum Bending Moments, Station R100 10m Span

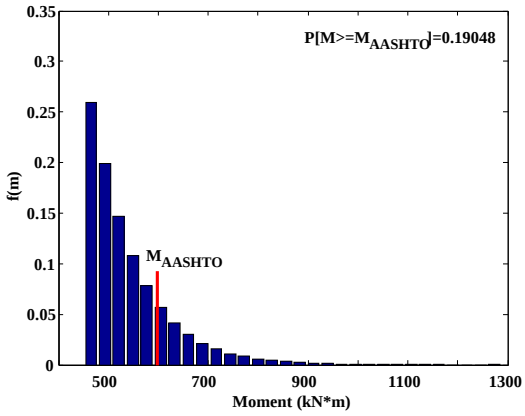

Figure 4.2: Histogram of 5% Largest Maximum Bending Moments, Station R100 10m Span

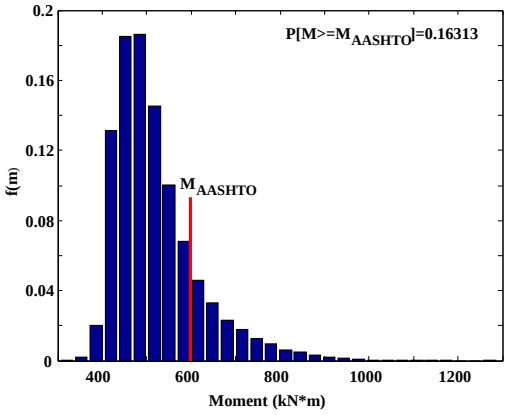

Figure 4.3: Histogram of Maximum Bending Moments from 5% Heaviest Vehicles, Station R100 10m Span

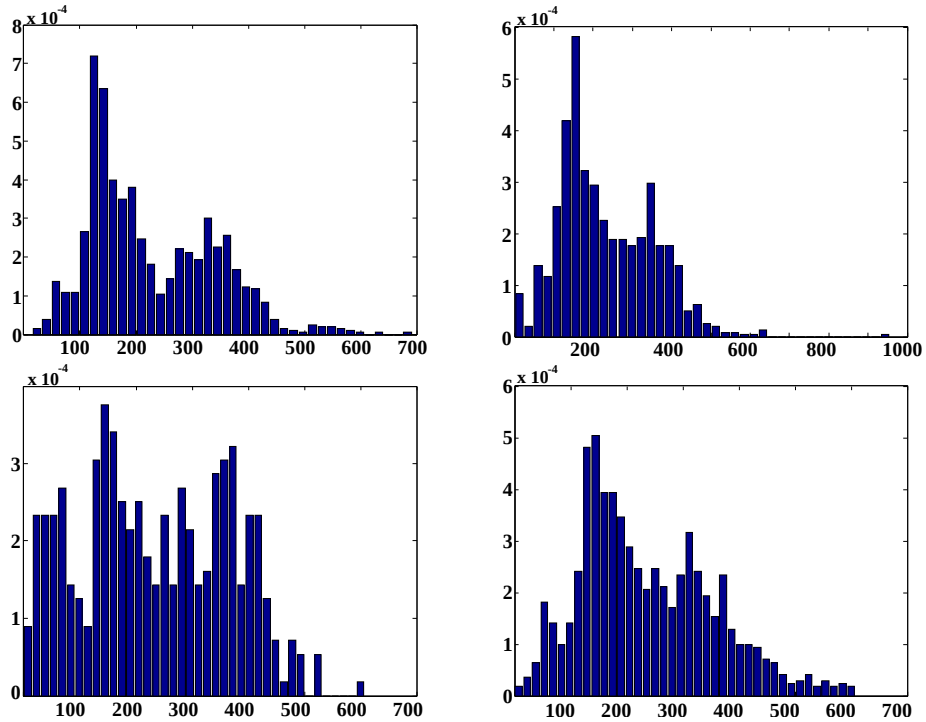

Figure 4.4: Histograms of Maximum Bending Moments for Randomly Selected Days from Station R001 in 2006

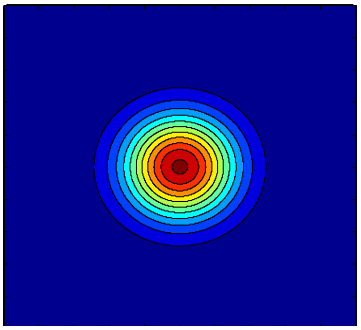

Figure 4.5: Independent Jointly Gaussian PDF

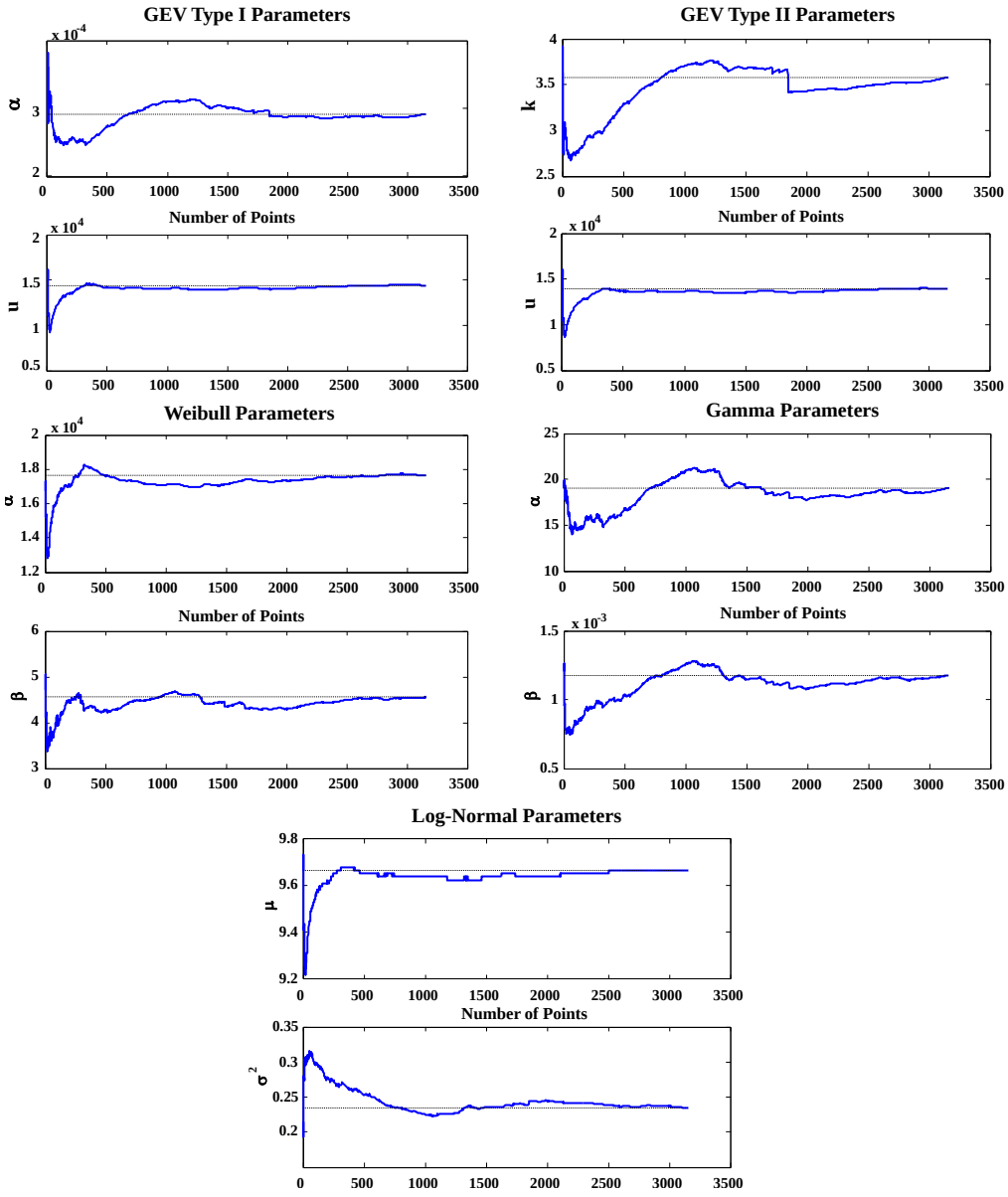

Figure 4.6: Behavior of Parameters as Data is Evaluated

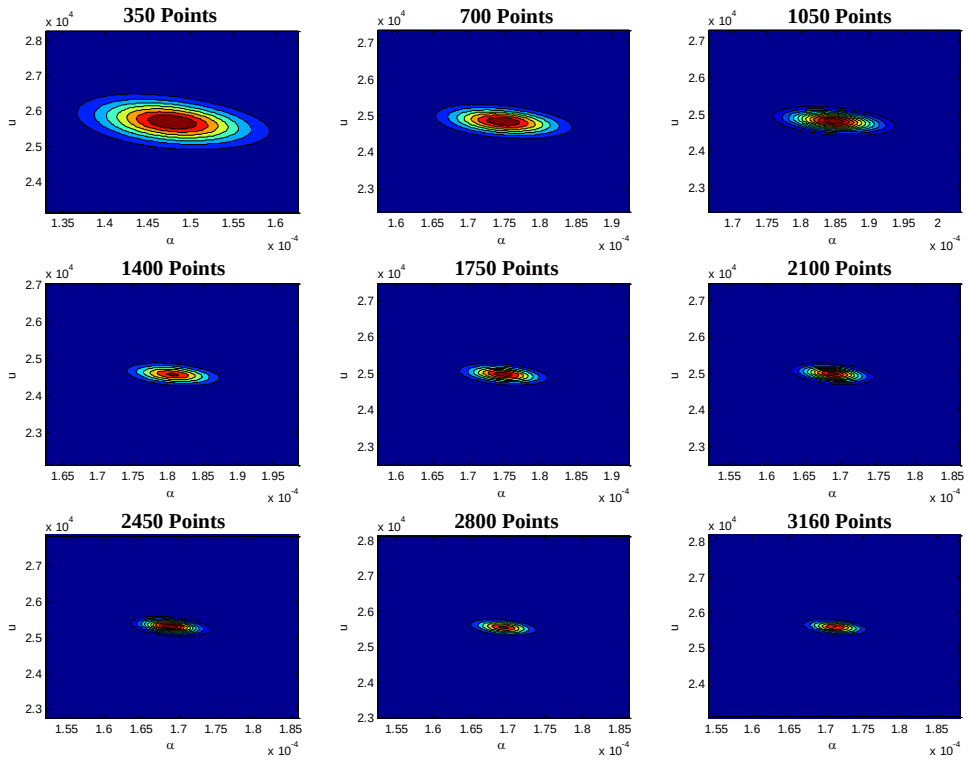

Figure 4.7: Evolution of GEV Type I Posterior

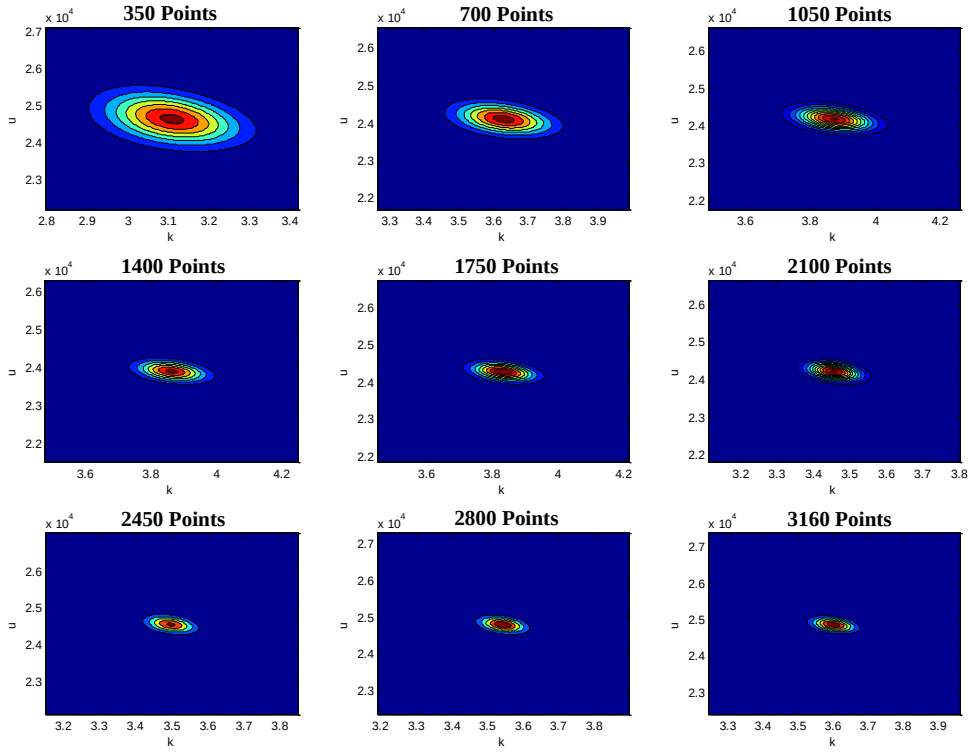

Figure 4.8: Evolution of GEV Type II Posterior

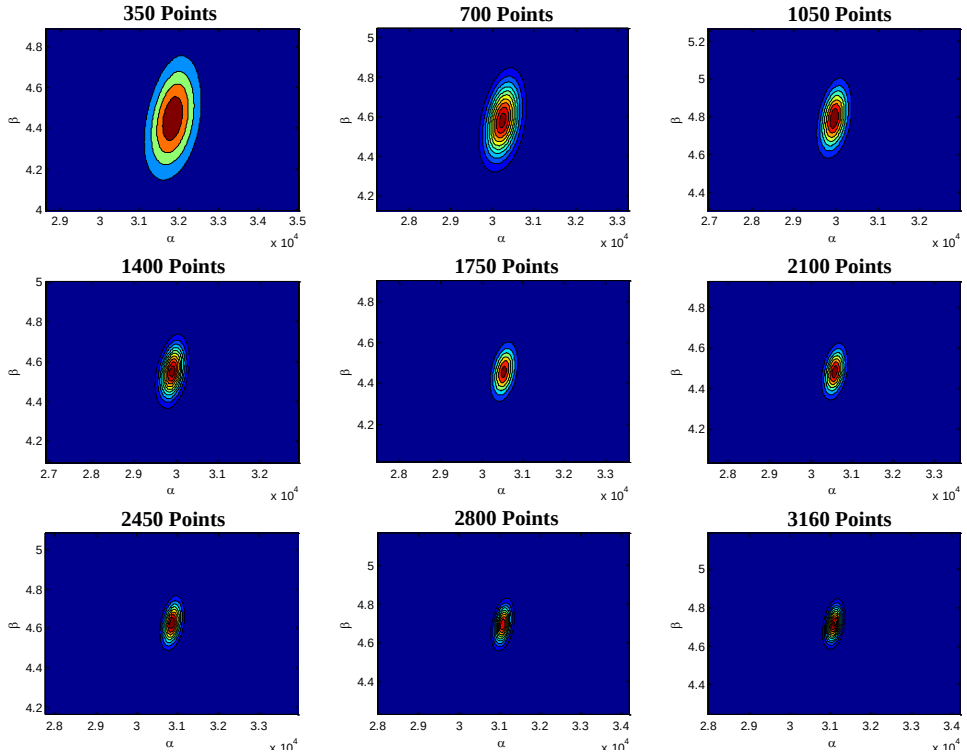

Figure 4.9: Evolution of Weibill Posterior

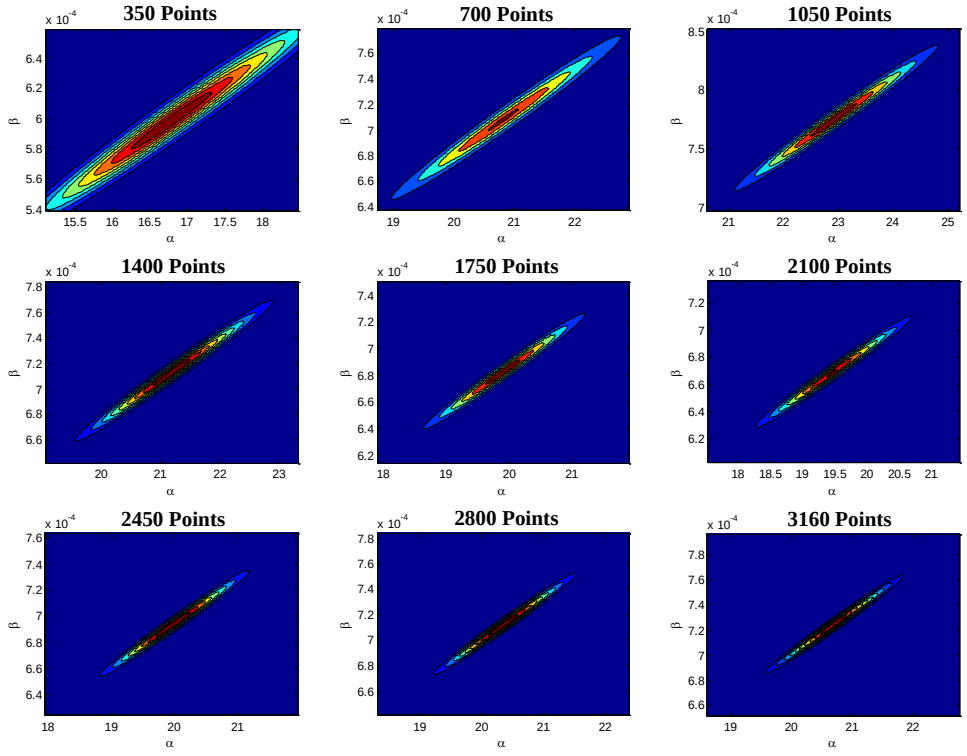

Figure 4.10: Evolution of Gamma Posterior

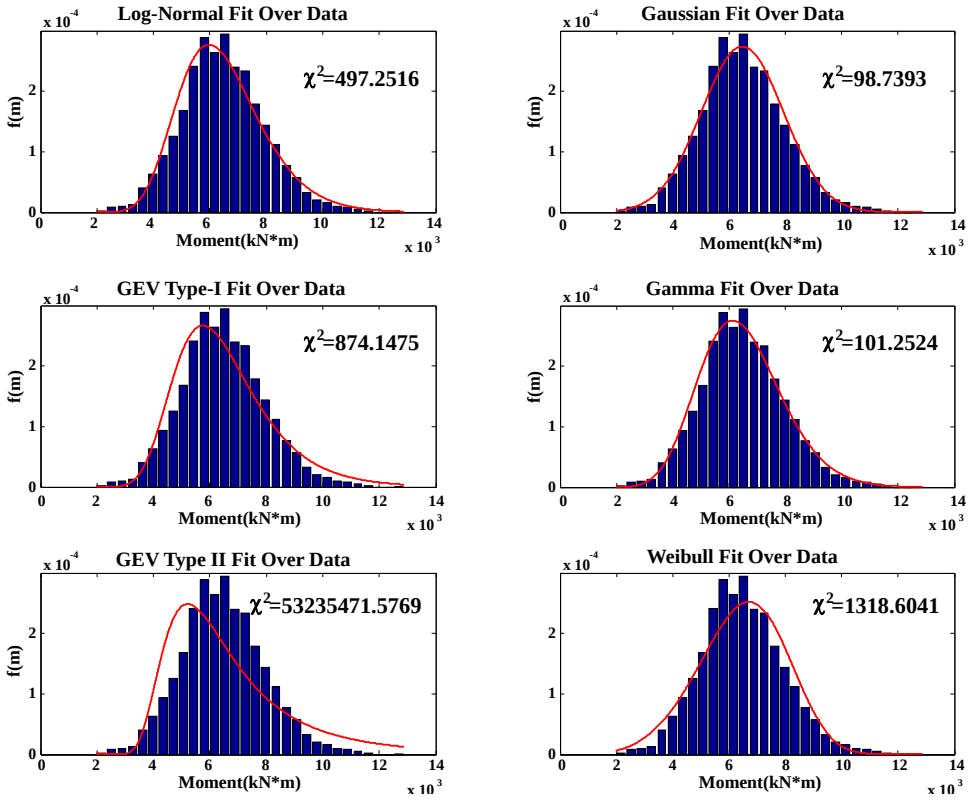

Figure 4.11: Probability models plotted over the data with their respective Chi-Square statistic

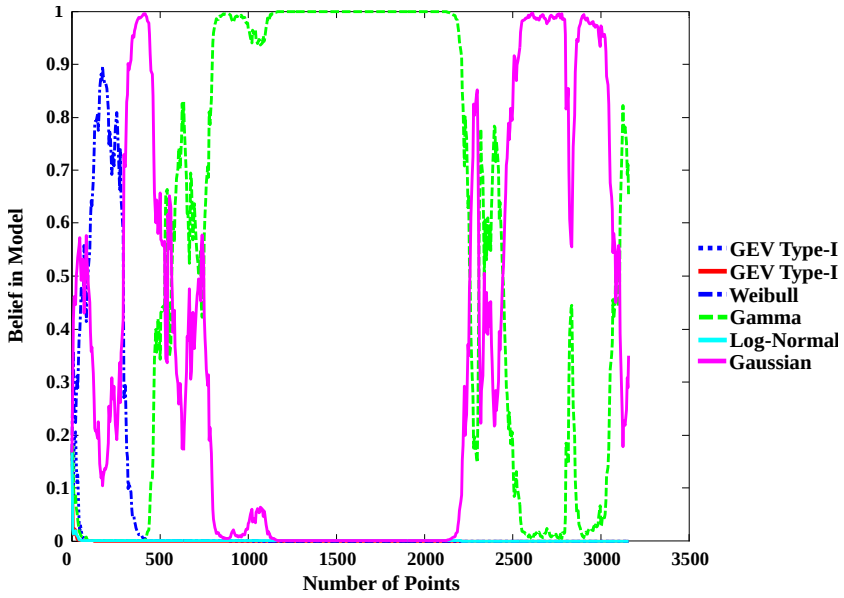

Figure 4.12: Evolution of Mixing Coeffecients as Data is Run

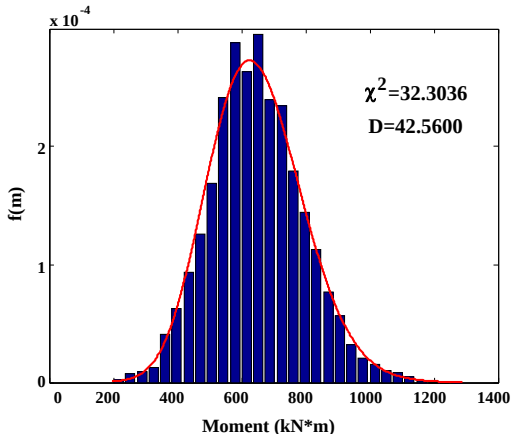

Figure 4.13: Gaussian/Gamma Mixture Fitted Over Data χ^2 Statistic

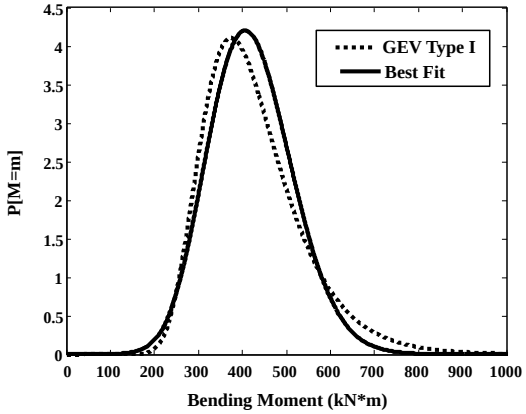

Figure 4.14: Comparison of GEV to Best fitting Distribution

Bibliography

[1] Abernethy, RB. "Ch. 1: An Overview of Weibull Analysis." *The New Weibull Handbook,* (5th), North Palm Beach, FL, 2006.

[2] Bailey, S. and Bez, R. (1999) "Site Specific Probability Distribution of Extreme Traffic Action Effecs." *J. Probabilistic Engineering Mechanics,* Elsevier, 14, 19-26.

[3] Caprani, C., OBrien, E. J., and McLachlan, G. (2007). "Characteristic Traffic Load Effects from a Mixture of Loading Events on Short to Medium Span Bridges." *J. Struct. Safety,* Elsevier, 30, 394-404.

[4] Enright, B. and O'Brien, E.J. (2012) "Monte Carlo Simulation of Extreme Traffic Loading on Short and Medium Span Bridges." *Structure and Infrastructure Engineering,* Taylor and Francis, 9(12), 1267-1282.

[5] Gumbel, E.J. (1958) *Statistics of Extremes,* Columbia University Press, New York.

[6] Kwon, O., Kim, E., and Orton, S. (2012). "Calibration of Live-Load Factor in LRFD Bridge Design Specifications Based on State-Specific Traffic Environments." *J. Bridge Eng.,* ASCE, 16, SPECIAL ISSUE: AASHTO-LRFD Bridge Design and Guide Specifications: Recent, Ongoing, and Future Refinements, 812819.

[7] Nowak, A. S. (1999). *NCHRP 368: Calibration of LRFD Bridge Design Code,* NCHRP, Washington, DC.

[8] Tabsh, S. W., and Nowak, A. S. (1991). "Reliability of Highway Girder Bridges." *J. Struct. Eng.,* ASCE, 117(8), 2372-2388.

[9] Zhao, J. and Tabatabai, H (2012). "Evaluation of a Permit Vehicle Model Using Weight-In-Motion Truck Records." *J. Bridge Eng.,* ASCE, 17(2), 389-392.

[10] Zhou, X., Schmidt, F., Toutlemonde, F., and Jacob, B. "Applying Weight-In-Motion Data to Reliability Based Assessment of Bridge Structures." *ICOSSAR2013,* 11^{th} *International Conference on Structural Safety & Reliability, France.*

Bibliography

[1] Henry Seaman. Specifications for the design of bridges and highways. *Transactions of the American Society of Civil Engineers*, 1912.

[2] L.R. Manville and R.W. Gastmeyer. Motor trucks: Loads on highway bridges. *Engineering News*, 1914.

[3] A.S. Nowak. Nchrp report 368: Calibration of lrfd bridge design code. Technical report, NCHRP, 1999.

[4] O'Brien E.J. Caprani, C. and G. McLachlan. Characteristic traffic load effects from a mixture of loading events on short to medium span bridges. *J. Structural Safety, Elsevier*, 2007.

[5] Battacharya B. Guzda, M and D. Mertz. Probabilistic characterization of live load using visual counts and in-service strain monitoring. *J. Bridge Engineering, ASCE*, 2007.

[6] M. Kozikowski. *WIM Based Live Load Model for Bridge Reliability*. PhD thesis, University of Nebraska, 2009.

[7] Kim E. Kwon, O. and S. Orton. Calibration of live load factor in lrfd bridge design specifications based on state-specific trafic environments. *J. Bridge Engineering, ASCE*, 2011.

[8] E.J. O'Brien and B. Enright. Using weight-in-motion data to determine agressiveness of traffic for bridge loading. *J. Bridge Engineering, ASCE*, 2013.

[9] S.W. Tabsh and A.S. Nowak. Reliability of highway girder bridges. *J. Struct. Engineering, ASCE*, 1991.

[10] Fu G Zouh Y. van de Lindt, J.W. and R. Pablo. Locality of truck loads and adequacy of bridge design load. *J. Bridge Engineering, ASCE*, 2005.

[11] J.W. van de Lindt and S. Pei. Buckling reliability of deteriorating steel beam ends. *Electronic Journal of Structural Engineering*, 2006.

[12] J. Zhao and H. Tabatabai. Evaluation of a permit vehicle model using weight-in-motion truck records. *J. Bridge Engineering, ASCE*, 2012.

[13] Schmidt F. Toutlemonde F. Zhou, X. and B. Jacob. Applying weight-in-motion traffic data to reliability based assessment of bridge structures. In *ICOSSAR2013, 11th International Conference on Structural Safety and Reliability*.

[14] S.F. Bailey and B. Rolf. Site specific probability distribution of extreme traffic action effects. *J. Probabilistic Engineering Mechanics, Elsevier*, 1999.

[15] B. Enright and E.J. O'Brien. Monte carlo simulation of extreme traffic loading on short and medium span bridges. *J. Structure and Infrastructure Engineering, Taylor & Francis*, 2013.

[16] American Association of State Highway and Transportation Officials, Washington, D.C. *AASHTO LRFD Bridge Design Specifications*, 2010.

[17] R.C. Hibbeler. *Structural analysis*. Pearson Prentice Hall, Upper Saddle River, NJ, 7 edition, 2009.

[18] G. McLachlan and K. Basford. *Mixture Models: Inference and Applicationsto Clustering*. Marcel Dekkerl, New York, 1989.

[19] E.J. Gumbel. *Statistics of Extremes*. Columbia University Press, New York, 1958.

Appendix A: Axle Statistics by Station

This section displays the axle statistics for vehicles categorized by WIM station. The percentage of vehicles with a given number of axles is shown by station in table A.1. The mean axle weights and spacing, as well as the covariance matrix are also presented for the 2-7 axle vehicle groups by station. The covariance matrix contains the variance on the diagnals and is symetric. The axle statistics matricies were formed by taking the covariance of the data organized in vectors with the following format:

$$\left[P_1 ... P_n \, S_1 ... S_{n-1}\right]$$

Table A.1: Fraction of Vehicles by Axle Count by Station

Number of Axles	**Station R100**	**Station X249**	**Station G005**	**Station R001**
2	0.4469	0.5319	0.6705	0.2418
3	0.0736	0.0808	0.0894	.0568
4	0.0577	0.0752	0.0728	.0782
5	0.2937	0.2901	0.1523	0.5773
6	0.1277	0.0216	0.0147	50.0452
7	0.0004	0.0005	0.0003	0.0007
$\sum =$	1.0000	1.0000	1.0000	1.0000

Table A.2: 2 Axle Vehicle Means for Station R100

μ_{p1}	μ_{p2}	μ_{s1}
23.77	29.10	43.12

Covariance Matrix for 2 Axle Vehicles

$$\begin{bmatrix} 178.7 & 255.9 & 87.63 \\ 255.8 & 542.1 & 174.5 \\ 87.6 & 174.5 & 154.8 \end{bmatrix}$$

Table A.3: 3 Axle Vehicle Means for Station R100

μ_{p1}	μ_{p2}	μ_{p3}	μ_{s1}	μ_{s2}
51.75	52.22	45.79	52.88	19.61

Covariance Matrix for 3 Axle Vehicles

$$\begin{bmatrix} 313.9 & 289.3 & 290.8 & 45.0 & -78.6 \\ 289.3 & 770.8 & 602.2 & 68.4 & -2.9 \\ 290.8 & 602.2 & 684.8 & 6.2 & -53.1 \\ 45.0 & 68.4 & 6.2 & 134.4 & 87.2 \\ -78.6 & -2.9 & -53.1 & -87.2 & 340.3 \end{bmatrix}$$

Table A.4: 4 Axle Vehicle Means for Station R100

μ_{p1}	μ_{p2}	$\mu_(p3)$	μ_{p4}	μ_{s1}	μ_{s2}	μ_{s3}
41.57	47.38	37.13	34.33	41.04	57.63	23.22

Covariance Matrix for 4 Axle Vehicles

$$\begin{bmatrix} 376.3 & 256.7 & 449.5 & 395.9 & 35.1 & -203.5 & 30.6 \\ 256.7 & 611.4 & 385.0 & 276.9 & 30.1 & 179.7 & -55.2 \\ 449.5 & 385.0 & 874.0 & 724.8 & 36.0 & -462.7 & 70.1 \\ 395.9 & 276.9 & 724.8 & 737.8 & 2.3 & -365.4 & 23.5 \\ 35.1 & 30.1 & 36.0 & 2.3 & 68.5 & -90.4 & 54.2 \\ -203.5 & 179.7 & -462.7 & -365.4 & -90.4 & 1322.9 & -529.2 \\ 30.6 & -55.2 & 70.1 & 23.5 & 54.2 & -529.2 & 718.9 \end{bmatrix}$$

Table A.5: 5 Axle Vehicle Means for Station R100

μ_{p1}	μ_{p2}	μ_{p3}	μ_{p4}	μ_{p5}	μ_{s1}	μ_{s2}	μ_{s3}	μ_{s4}
45.95	44.52	43.29	37.35	36.69	47.12	13.40	88.48	14.03

Covariance Matrix for 5 Axle Vehicles

$$\begin{bmatrix} 162.4 & 134.0 & 131.3 & 110.8 & 108.0 & 20.1 & -2.7 & 21.8 & 7.7 \\ 134.0 & 455.1 & 434.5 & 413.7 & 407.8 & 27.1 & 0.9 & 34.4 & 10.7 \\ 131.3 & 434.5 & 447.2 & 412.8 & 407.2 & 26.9 & -3.9 & 37.3 & 11.2 \\ 110.8 & 413.7 & 412.8 & 510.5 & 490.9 & 17.5 & -3.2 & 20.4 & 13.2 \\ 108.0 & 407.8 & 407.2 & 490.9 & 500.8 & 16.6 & -3.3 & 26.7 & 8.3 \\ 20.1 & 27.1 & 26.9 & 17.5 & 16.6 & 53.9 & -0.8 & 25.1 & 10.0 \\ -2.7 & 0.9 & -3.9 & -3.2 & -3.3 & -0.8 & 15.9 & -18.3 & -0.6 \\ 21.8 & 34.4 & 37.3 & 20.4 & 26.7 & 25.1 & -18.3 & 218.1 & -14.2 \\ 7.7 & 10.7 & 11.2 & 13.2 & 8.3 & 10.0 & -0.6 & -14.2 & 32.0 \end{bmatrix}$$

Table A.6: 6 Axle Vehicle Means for Station R100

μ_{p1}	μ_{p2}	μ_{p3}	μ_{p4}	μ_{p5}	μ_{p6}	μ_{s1}	μ_{s2}	μ_{s3}	μ_{s4}	μ_{s5}
48.06	68.26	68.13	51.91	59.12	58.87	43.88	13.18	74.68	14.36	13.23

Covariance Matrix for 6 Axle Vehicles

$$\begin{bmatrix} 190.3 & 225.9 & 234.4 & 195.2 & 179.9 & 177.0 & 5.4 & 0.5 & -20.5 & 22.7 & 0.05 \\ 225.9 & 704.9 & 667.2 & 477.7 & 509.5 & 501.0 & 3.0 & 0.4 & 2.0 & 3.6 & -4.0 \\ 234.4 & 667.2 & 715.7 & 501.1 & 520.4 & 512.3 & 5.2 & -0.6 & -21.6 & 23.1 & -1.9 \\ 195.2 & 477.7 & 501.1 & 565.1 & 477.3 & 461.7 & 1.0 & -0.7 & -37.7 & 22.0 & 3.8 \\ 179.9 & 509.5 & 520.4 & 477.3 & 713.2 & 703.2 & 20.0 & -1.9 & -61.6 & -5.2 & 5.6 \\ 177.0 & 501.0 & 512.3 & 461.7 & 703.2 & 763.0 & 23.7 & -2.0 & -66.2 & -4.2 & 6.8 \\ 5.4 & 3.0 & 5.2 & 1.0 & 20.0 & 23.7 & 40.0 & 0.7 & -29.0 & 18.4 & 1.4 \\ 0.5 & 0.4 & -0.6 & -0.7 & -1.9 & -2.0 & 0.7 & 2.1 & -1.7 & 0.7 & -0.02 \\ -20.5 & 2.0 & -21.6 & -37.7 & -61.6 & -66.2 & -29.0 & -1.7 & 134.9 & -65.3 & -4.2 \\ 22.7 & 3.6 & 23.1 & 22.0 & -5.2 & -4.2 & 18.4 & 0.7 & -65.3 & 57.7 & 2.0 \\ 0.04 & -4.0 & -1.9 & 3.8 & 5.6 & 6.8 & 1.4 & -0.02 & -4.2 & 2.0 & 4.1 \end{bmatrix}$$

Table A.7: 7 Axle Vehicle Means for Station R100

μ_{p1}	μ_{p2}	μ_{p3}	μ_{p4}	μ_{p5}	μ_{p6}	μ_{p7}	μ_{s1}	μ_{s2}	μ_{s3}	μ_{s4}	μ_{s5}	μ_{s6}
53.11	53.71	81.10	74.16	61.56	60.80	59.77	45.26	13.73	29.04	73.34	19.74	15.10

Covariance Matrix for 7 Axle Vehicles

$$\begin{bmatrix}
204.1 & 133.1 & 91.0 & 69.2 & 32.8 & 0.9 & 4.9 & 10.1 & 0.4 & 10.28 & -8.8 & 6.7 & -2.5 \\
133.1 & 510.3 & 199.1 & 39.4 & 93.7 & 68.5 & 60.9 & 23.5 & 9.1 & 40.4 & -61.5 & 16.2 & -0.5 \\
91.0 & 199.1 & 969.4 & 950.8 & 627.4 & 585.1 & 574.9 & -33.1 & -10.9 & -69.0 & 209.6 & -15.7 & -2.3 \\
69.2 & 39.4 & 950.8 & 1216.0 & 753.8 & 679.7 & 658.6 & -52.9 & -8.1 & -133.8 & 323.3 & -34.2 & 1.1 \\
32.8 & 93.7 & 627.4 & 753.8 & 772.2 & 677.3 & 658.8 & -35.3 & 0.5 & -81.1 & 227.8 & -14.4 & 2.3 \\
0.9 & 68.5 & 585.1 & 679.7 & 677.3 & 829.8 & 805.4 & -38.0 & 6.4 & -67.7 & 119.4 & -39.5 & -5.2 \\
4.9 & 60.9 & 574.9 & 658.6 & 658.8 & 805.4 & 836.5 & -35.7 & 5.3 & -60.6 & 116.5 & -38.1 & -4.9 \\
10.1 & 23.5 & -33.1 & -52.9 & -35.3 & -38.0 & -35.7 & 107.9 & 2.9 & 70.1 & -205.5 & 79.9 & 3.2 \\
0.4 & 9.1 & -10.9 & -8.1 & 0.5 & 6.4 & 5.3 & 2.9 & 47.2 & -4.3 & -38.3 & -1.6 & -2.2 \\
10.3 & 40.4 & -69.0 & -133.8 & -81.1 & -67.7 & -60.6 & 70.1 & -4.3 & 981.0 & -893.2 & -2.4 & -2.6 \\
-8.8 & -61.5 & 209.6 & 323.3 & 227.8 & 119.4 & 116.5 & -205.5 & -38.3 & -893.2 & 1551.2 & -159.5 & -40.4 \\
6.7 & 16.2 & -15.7 & -34.2 & -14.4 & -39.5 & -38.1 & 79.9 & -1.6 & -2.4 & -159.5 & 179.7 & 0.9 \\
-2.5 & -0.5 & -2.3 & 1.1 & 2.3 & -5.2 & -4.9 & 3.2 & -2.2 & -2.6 & -40.4 & 0.9 & 81.4
\end{bmatrix}$$

Table A.8: 2 Axle Vehicle Means for Station X249

μ_{p1}	μ_{p2}	μ_s
15.71	18.28	42.94

Table A.9: 3 Axle Vehicle Means for Station X249

μ_{p1}	μ_{p2}	μ_{p3}	μ_{s1}	μ_{s2}
47.03	45.79	40.33	48.84	25.97

Covariance Matrix for 2 Axle Vehicles

$$\begin{bmatrix} 151.3 & 201.1 & 45.7 \\ 201.1 & 362.1 & 75.3 \\ 45.7 & 75.3 & 68.5 \end{bmatrix}$$

Covariance Matrix for 3 Axle Vehicles

$$\begin{bmatrix} 214.5 & 187.2 & 193.2 & 55.2 & -113.2 \\ 187.2 & 542.0 & 439.9 & 36.9 & -4.5 \\ 193.2 & 439.9 & 490.9 & 27.5 & -99.0 \\ 55.2 & 36.97 & 27.5 & 139.1 & -145.9 \\ -113.2 & -4.5 & -99.0 & -145.9 & 524.1 \end{bmatrix}$$

Covariance Matrix for 4 Axle Vehicles

$$\begin{bmatrix} 228.1 & 176.3 & 256.8 & 236.3 & 24.8 & -70.5 & 38.6 \\ 176.3 & 407.0 & 229.6 & 178.1 & 14.2 & 185.8 & -20.1 \\ 256.8 & 229.6 & 513.0 & 440.4 & 24.9 & -288.0 & 46.5 \\ 236.3 & 178.1 & 440.4 & 457.6 & 5.7 & -237.7 & 25.2 \\ 24.8 & 14.2 & 24.9 & 5.7 & 55.8 & -74.9 & 47.8 \\ -70.5 & 185.8 & -288.0 & -237.7 & -74.9 & 1063.7 & -266.8 \\ 38.6 & -20.1 & 46.5 & 25.2 & 47.8 & -266.8 & 335.7 \end{bmatrix}$$

Table A.10: 4 Axle Vehicle Means for Station X249

μ_1	μ_2	μ_3	μ_4	μ_{s1}	μ_{s2}	μ_{s3}
36.56	42.05	29.12	28.46	39.11	69.13	16.17

Table A.11: 5 Axle Vehicle Means for Station X249

μ_{p1}	μ_{p2}	μ_{p3}	μ_{p4}	μ_{p5}	μ_{s1}	μ_{s2}	μ_{s3}	μ_{s4}
44.14	44.06	42.47	37.13	37.16	46.77	16.01	88.22	17.06

Covariance Matrix for 5 Axle Vehicles

$$\begin{bmatrix} 97.9 & 81.5 & 84.0 & 76.6 & 77.7 & 18.9 & -15.7 & 30.4 & -8.5 \\ 81.5 & 451.7 & 434.5 & 409.9 & 415.5 & 1.0 & 19.3 & -32.9 & 21.0 \\ 84.0 & 434.5 & 458.4 & 417.8 & 427.0 & 7.4 & -17.8 & 9.5 & -7.8 \\ 76.6 & 409.9 & 417.8 & 484.0 & 477.2 & 2.8 & -15.1 & 4.6 & -0.2 \\ 77.7 & 415.5 & 427.0 & 477.2 & 503.9 & 4.0 & -27.3 & 19.4 & -14.7 \\ 18.9 & 1.0 & 7.4 & 2.8 & 4.0 & 65.6 & -26.5 & 50.3 & -13.0 \\ -15.7 & 19.3 & -17.8 & -15.1 & -27.3 & -26.5 & 154.8 & -184.7 & 132.0 \\ 30.4 & -32.9 & 9.5 & 4.6 & 19.4 & 50.3 & -184.7 & 342.5 & -169.5 \\ -8.5 & 21.0 & -7.8 & -0.2 & 14.7 & -13.0 & 132.0 & -169.5 & 171.1 \end{bmatrix}$$

Table A.12: 6 Axle Vehicle Means for Station X249

μ_{p1}	μ_{p2}	μ_{p3}	μ_{p4}	μ_{p5}	μ_{p6}	μ_{s1}	μ_{s2}	μ_{s3}	μ_{s4}	μ_{s5}
46.49	56.73	56.30	42.65	41.79	41.49	48.43	15.0	66.76	23.87	20.74

Covariance Matrix for 6 Axle Vehicles

$$\begin{bmatrix} 188.6 & 215.9 & 245.1 & 150.0 & 114.8 & 132.9 & 63.9 & 23.1 & -124.1 & 123.7 & -72.4 \\ 215.9 & 718.1 & 697.7 & 382.1 & 412.9 & 442.0 & 91.5 & -1.2 & -122.2 & 120.4 & -178.6 \\ 245.1 & 697.7 & 794.3 & 452.2 & 446.9 & 478.7 & 104.6 & -68.0 & -143.8 & 181.1 & -186.4 \\ 150.0 & 382.1 & 452.2 & 484.4 & 363.8 & 359.6 & 0.6 & -44.7 & -105.7 & 124.9 & -24.4 \\ 114.8 & 412.9 & 446.9 & 363.8 & 450.5 & 433.1 & 20.9 & -44.2 & -0.5 & 15.33 & -46.8 \\ 132.9 & 442.0 & 478.7 & 359.6 & 433.1 & 483.3 & 36.9 & -43.9 & -19.2 & 30.6 & -84.5 \\ 63.9 & 91.5 & 104.6 & 30.6 & 20.9 & 36.9 & 89.9 & -16.3 & -57.9 & 71.8 & -104.2 \\ -23.1 & -1.2 & -68.0 & -44.7 & -44.2 & -43.9 & -16.3 & 153.0 & -91.1 & -14.0 & -15.8 \\ -124.1 & -122.2 & -143.8 & -105.7 & -0.5 & -19.2 & -57.9 & -91.1 & 737.7 & -455.0 & -37.7 \\ 123.7 & 120.4 & 181.1 & 124.9 & 15.3 & 30.6 & 71.8 & -14.0 & -455.0 & 407.0 & 32.2 \\ -72.4 & -178.6 & -186.4 & -24.4 & -46.8 & -84.5 & -104.2 & -15.8 & -37.7 & 32.2 & 368.1 \end{bmatrix}$$

Table A.13: 7 Axle Vehicle Means for Station X249

μ_{p1}	μ_{p2}	μ_{p3}	μ_{p4}	μ_{p5}	μ_{p6}	μ_{p7}	μ_{s1}	μ_{s2}	μ_{s3}	μ_{s4}	μ_{s5}	μ_{s6}
49.75	59.22	73.67	59.98	47.33	46.71	46.28	49.58	17.45	32.65	67.58	15.80	14.06

Covariance Matrix for 7 Axle Vehicles

$$\begin{bmatrix}
285.0 & 196.5 & 193.9 & 102.0 & 36.6 & 16.2 & 27.8 & 60.6 & -11.3 & -17.0 & 6.6 & 0.7 & -1.7 \\
196.5 & 781.0 & 413.6 & 74.5 & 73.2 & 61.6 & 77.0 & 58.1 & -5.5 & -22.0 & 2.9 & -4.8 & -0.9 \\
193.9 & 413.6 & 881.3 & 684.1 & 461.6 & 449.3 & 427.9 & 13.9 & -31.4 & -47.8 & 118.7 & 5.2 & 9.9 \\
102.0 & 74.5 & 684.1 & 926.8 & 592.1 & 570.2 & 530.7 & -37.8 & -13.0 & -30.3 & 126.7 & 1.8 & 9.5 \\
36.6 & 73.2 & 461.6 & 592.1 & 613.1 & 531.9 & 485.1 & -49.2 & -4.3 & 0.8 & 66.5 & 3.9 & 6.8 \\
16.2 & 61.6 & 449.3 & 570.2 & 531.9 & 547.8 & 501.3 & -50.4 & -5.5 & -3.8 & 67.8 & 7.2 & 7.2 \\
27.8 & 77.0 & 427.9 & 530.7 & 485.1 & 501.3 & 516.4 & -48.4 & -13.2 & -0.5 & 70.7 & 7.7 & 6.4 \\
60.6 & 58.1 & 13.9 & -37.8 & -49.2 & -50.4 & -48.4 & 198.1 & -28.0 & -24.7 & -89.4 & 17.2 & -0.6 \\
-11.3 & -5.5 & -31.4 & -13.0 & -4.3 & -5.5 & -13.2 & -28.0 & 348.3 & -95.3 & -213.9 & -19.0 & -13.8 \\
-17.0 & -22.0 & -47.8 & -30.3 & 0.8 & -3.8 & -0.5 & -24.7 & -95.3 & 1306.8 & -1014.5 & 51.5 & -6.2 \\
6.6 & 2.9 & 118.7 & 126.7 & 66.5 & 67.8 & 70.7 & -89.4 & -213.9 & -1014.5 & 1482.6 & -110.9 & 2.9 \\
0.7 & -4.8 & .2 & 1.8 & 3.9 & 7.2 & 7.7 & 17.2 & -19.0 & 51.5 & -110.9 & 178.8 & 13.8 \\
-1.7 & -0.9 & 9.9 & 9.5 & 6.8 & 7.2 & 6.4 & -0.6 & -13.8 & -6.2 & 2.9 & 13.8 & 54.9
\end{bmatrix}$$

Table A.14: 2 Axle Vehicle Means for Station G005

μ_{p1}	μ_{p2}	μ_s
17.99	22.69	42.61

Table A.15: 3 Axle Vehicle Means for Station G005

μ_{p1}	μ_{p2}	μ_{p3}	μ_{s1}	μ_{s2}
51.55	51.59	46.74	47.89	20.81

Covariance Matrix for 2 Axle Vehicles

$$\begin{bmatrix} 167.7 & 250.7 & 57.5 \\ 250.7 & 515.1 & 118.8 \\ 57.5 & 118.8 & 98.5 \end{bmatrix}$$

Covariance Matrix for 3 Axle Vehicles

$$\begin{bmatrix} 279.4 & 291.5 & 313.1 & 22.1 & -111.9 \\ 291.5 & 932.2 & 833.0 & -9.0 & 1.1 \\ 313.1 & 833.0 & 883.2 & -20.0 & -77.1 \\ 22.1 & -9.0 & -20.0 & 91.5 & -79.1 \\ -111.9 & 1.1 & -77.1 & -79.1 & 401.0 \end{bmatrix}$$

Covariance Matrix for 4 Axle Vehicles

$$\begin{bmatrix} 392.6 & 219.4 & 542.6 & 505.6 & 4.3 & -265.2 & 40.9 \\ 219.4 & 592.7 & 300.4 & 265.2 & -2.1 & 225.0 & 2.7 \\ 542.6 & 300.4 & 1084.1 & 1009.3 & -12.2 & -606.2 & 50.6 \\ 505.6 & 265.2 & 1009.3 & 1022.8 & -27.9 & -554.7 & 47.4 \\ 4.3 & -2.1 & -12.2 & -27.9 & 32.1 & -21.6 & 16.8 \\ -265.2 & 225.0 & -606.2 & -554.7 & -21.6 & 1190.0 & -162.5 \\ 40.9 & 2.7 & 50.6 & 47.4 & 16.8 & -162.5 & 186.9 \end{bmatrix}$$

Table A.16: 4 Axle Vehicle Means for Station G005

μ_1	μ_2	μ_3	μ_4	μ_{s1}	μ_{s2}	μ_{s3}
40.47	48.21	38.66	37.19	37.67	63.72	14.09

Table A.17: 5 Axle Vehicle Means for Station G005

μ_{p1}	μ_{p2}	μ_{p3}	μ_{p4}	μ_{p5}	μ_{s1}	μ_{s2}	μ_{s3}	μ_{s4}
45.86	49.21	46.72	41.30	41.13	43.91	16.18	84.13	16.88

Table A.18: 6 Axle Vehicle Means for Station G005

μ_{p1}	μ_{p2}	μ_{p3}	μ_{p4}	μ_{p5}	μ_{p6}	μ_{s1}	μ_{s2}	μ_{s3}	μ_{s4}	μ_{s5}
49.98	66.04	65.13	51.10	51.98	50.93	47.60	13.06	67.29	17.23	15.11

Covariance Matrix for 5 Axle Vehicles

$$\begin{bmatrix}
104.2 & 88.1 & 90.1 & 79.0 * 77.9 & 20.1 & -21.0 & 21.0 & -7.1 & \\
88.1 & 598.7 & 567.4 & 563.2 & 556.2 & 5.5 & 25.0 & -55.7 & 31.0 \\
90.1 & 567.4 & 574.8 & 562.4 & 560.0 & 12.1 & -19.7 & 2.8 & -5.7 \\
79.0 & 563.2 & 562.4 & 692.6 & 670.8 & 9.5 & -25.7 & 8.8 & -13.7 \\
77.9 & 556.2 & 560.0 & 670.8 & 689.5 & 10.7 & -38.6 & 31.9 & -32.2 \\
20.1 & 5.5 & 12.1 & 9.5 & 10.7 & 55.7 & -25.4 & 47.4 & -13.3 \\
-21.0 & 25.0 & -19.7 & -25.7 & -38.6 & -25.4 & 169.4 & -209.7 & 144.7 \\
21.0 & -55.7 & 2.8 & 8.8 & 31.9 & 47.4 & -209.7 & 390.1 & -196.4 \\
-7.1 & 31.0 & -5.7 & -13.7 & -32.2 & -13.3 & 144.7 & -196.4 & 185.2
\end{bmatrix}$$

Covariance Matrix for 6 Axle Vehicles

$$\begin{bmatrix}
160.5 & 53.7 & 59.8 & 67.3 & 43.0 & 21.6 & 7.0 & -0.4 & -79.3 & 33.7 & 3.7 \\
53.7 & 812.7 & 787.1 & 600.4 & 629.7 & 632.2 & 23.0 & -3.5 & 39.5 & -5.2 & -39.3 \\
59.8 & 787.1 & 812.4 & 621.8 & 636.3 & 634.7 & 24.0 & -5.4 & 10.2 & 24.5 & -41.9 \\
67.4 & 600.4 & 621.8 & 802.8 & 645.2 & 581.8 & -10.7 & -4.0 & -80.7 & 28.8 & 13.0 \\
43.0 & 629.7 & 636.3 & 645.2 & 799.9 & 740.2 & -16.6 & -3.2 & -75.8 & -1.8 & 11.5 \\
21.6 & 632.2 & 634.7 & 581.8 & 740.2 & 783.6 & -3.8 & -3.2 & -48.8 & -7.6 & -5.2 \\
7.0 & 23.0 & 24.0 & -10.7 & -16.6 & -3.8 & 0.9 & 0.3 & 9.9 & 15.9 & -20.1 \\
-0.4 & -3.5 & -5.4 & -4.0 & -3.2 & -3.2 & 0.3 & 4.4 & -3.2 & 0.1 & 0.1 \\
-79.3 & 39.5 & 10.2 & -80.7 & -75.8 & -48.8 & 9.9 & -3.2 & 389.2 & -119.5 & -36.7 \\
33.7 & -5.2 & 24.5 & 28.8 & -1.8 & -7.6 & 15.9 & 0.1 & -119.5 & 109.2 & 15.6 \\
3.7 & -39.3 & -41.9 & 13.0 & 11.5 & -5.2 & -20.1 & 0.1 & -36.7 & 15.6 & 66.2
\end{bmatrix}$$

Table A.19: 7 Axle Vehicle Means for Station G005

μ_{p1}	μ_{p2}	μ_{p3}	μ_{p4}	μ_{p5}	μ_{p6}	μ_{p7}	μ_{s1}	μ_{s2}	μ_{s3}	μ_{s4}	μ_{s5}	μ_{s6}
47.36	55.53	82.94	70.21	63.43	63.32	62.01	43.66	13.27	34.55	63.71	18.46	14.79

Covariance Matrix for 7 Axle Vehicles

$$\begin{bmatrix}
152.1 & 29.3 & 76.2 & 74.1 & 9.9 & -4.4 & -4.4 & 9.1 & -3.2 & -0.4 & 20.0 & -4.1 & -2.9 \\
29.3 & 597.4 & 163.4 & -127.0 & 120.7 & 109.2 & 143.7 & 16.5 & -3.3 & 9.7 & -94.7 & 23.5 & -1.1 \\
76.2 & 163.4 & 751.9 & 643.9 & 428.8 & 441.1 & 428.7 & -65.5 & -20.2 & -169.9 & 199.7 & -47.8 & -8.0 \\
74.1 & -127.0 & 643.9 & 1020.3 & 510.7 & 531.4 & 488.8 & -99.3 & -17.3 & -255.9 & 306.3 & -69.8 & -7.8 \\
9.9 & 120.7 & 428.8 & 510.7 & 654.4 & 612.0 & 596.2 & -64.4 & -18.8 & -184.8 & 142.6 & -46.3 & 0.8 \\
-4.4 & 109.2 & 441.1 & 531.4 & 12.0 & 660.8 & 630.6 & -66.4 & -19.1 & -180.3 & 149.4 & -49.2 & 1.4 \\
-4.4 & 143.7 & 428.7 & 488.8 & 596.2 & 630.6 & 652.3 & -62.2 & -17.4 & -163.2 & 119.7 & -45.0 & 2.3 \\
9.1 & 16.5 & -65.5 & -99.3 & -64.4 & -66.4 & -62.2 & 86.7 & 2.1 & 180.3 & -205.8 & 80.3 & 26.2 \\
-3.2 & -3.3 & -20.2 & -17.3 & -18.8 & -19.1 & -17.4 & 2.1 & 38.1 & 6.8 & -49.3 & -1.9 & -0.8 \\
-0.4 & 9.7 & -169.9 & -255.9 & -184.8 & -180.3 & -163.2 & 180.3 & 6.8 & 967.4 & -1007.3 & 165.7 & 27.0 \\
20.0 & 94.7 & 199.7 & 306.3 & 142.6 & 149.4 & 119.7 & -205.8 & -49.3 & -1007.3 & 1583.8 & -246.6 & -40.6 \\
-4.1 & 23.5 & -47.8 & -69.8 & -46.3 & 49.2 & -45.0 & 80.3 & -1.9 & 165.7 & -246.6 & 327.6 & 13.3 \\
-2.9 & -1.1 & 8.0 & -7.8 & 0.8 & 1.4 & 2.3 & 26.2 & 0.8 & 27.0 & -40.6 & 13.3 & 84.2
\end{bmatrix}$$

Table A.20: 2 Axle Vehicle Means for Station R001

μ_{p1}	μ_{p2}	μ_s
16.70	22.54	44.16

Table A.21: 3 Axle Vehicle Means for Station R001

μ_{p1}	μ_{p2}	μ_{p3}	μ_{s1}	μ_{s2}
47.33	50.94	41.12	50.95	21.96

Covariance Matrix for 2 Axle Vehicles

$$\begin{bmatrix} 186.4 & 258.3 & 67.7 \\ 258.3 & 536.8 & 127.9 \\ 67.7 & 127.9 & 100.8 \end{bmatrix}$$

Covariance Matrix for 3 Axle Vehicles

$$\begin{bmatrix} 313.1 & 269.7 & 215.5 & 100.6 & -83.2 \\ 269.7 & 842.3 & 538.2 & 87.5 & 41.7 \\ 215.5 & 538.2 & 569.7 & 16.6 & -13.6 \\ 100.6 & 87.5 & 16.6 & 205.0 & -135.1 \\ -83.2 & 41.7 & -13.6 & -135.1 & 500.5 \end{bmatrix}$$

Covariance Matrix for 4 Axle Vehicles

$$\begin{bmatrix} 300.9 & 249.2 & 295.7 & 264.3 & -23.5 & -8.3 & 35.4 \\ 249.2 & 676.3 & 365.5 & 307.5 & -21.9 & 321.0 & -84.5 \\ 295.7 & 365.5 & 525.1 & 443.8 & -22.8 & -74.7 & 45.3 \\ 264.3 & 307.5 & 443. & 473.8 & -46.8 & -32.5 & 31.8 \\ -23.5 & -21.9 & -22.8 & -46.8 & 87.0 & -81.8 & 52.6 \\ -8.3 & 321.0 & -74.7 & -32.5 & -81.8 & 1012.8 & -422.3 \\ 35.4 & -84.5 & 45.3 & 31.8 & 52.6 & -422.3 & 465.7 \end{bmatrix}$$

Table A.22: 4 Axle Vehicle Means for Station R001

μ_1	μ_2	μ_3	μ_4	μ_{s1}	μ_{s2}	μ_{s3}
38.03	51.10	32.63	31.13	36.77	70.82	18.23

Table A.23: 5 Axle Vehicle Means for Station R001

μ_{p1}	μ_{p2}	μ_{p3}	μ_{p4}	μ_{p5}	μ_{s1}	μ_{s2}	μ_{s3}	μ_{s4}
44.65	49.32	47.77	43.43	43.04	45.32	12.71	88.60	13.41

Table A.24: Six Axle Vehicle Means for Station R001

μ_{p1}	μ_{p2}	μ_{p3}	μ_{p4}	μ_{p5}	μ_{p6}	μ_{s1}	μ_{s2}	μ_{s3}	μ_{s4}	μ_{s5}
46.75	68.36	67.79	48.44	49.0	48.18	47.13	12.99	69.65	15.71	12.70

Covariance Matrix for 5 Axle Vehicles

$$\begin{bmatrix} 99.1 & 91.3 & 88.2 & 85.7 & 84.2 & 16.4 & -0.1 & 6.4 & 2.2 \\ 91.3 & 550.8 & 530.4 & 546.2 & 546.3 & 23.8 & 5.4 & 19.4 & 10.6 \\ 88.2 & 530.4 & 539.6 & 543.1 & 544.1 & 25.1 & -2.3 & 30.7 & 8.8 \\ 85.7 & 546.2 & 543.1 & 676.8 & 653.0 & 27.4 & -2.3 & 29.0 & 18.6 \\ 84.2 & 546.3 & 544.1 & 653.0 & 673.8 & 27.0 & -3.0 & 29.9 & 15.0 \\ 16.4 & 23.8 & 25.1 & 27.4 & 27.0 & 63.6 & -1.5 & 24.2 & 10.9 \\ -0.1 & 5.4 & -2.3 & -2.3 & -3.0 & -1.5 & 25.8 & -24.8 & 8.2 \\ 6.4 & 19.4 & 30.7 & 29.0 & 29.9 & 24.2 & -24.8 & 158.4 & -14.9 \\ 2.2 & 10.6 & 8.8 & 18.6 & 15.0 & 10.9 & 8.2 & -14.9 & 37.1 \end{bmatrix}$$

Covariance Matrix for 6 Axle Vehicles

$$\begin{bmatrix} 161.9 & 190.5 & 206.5 & 120.3 & 118.9 & 127.1 & 34.9 & -2.6 & -81.4 & 57.3 & -0.2 \\ 190.5 & 1015.0 & 969.9 & 661.7 & 706.7 & 701.4 & 38.5 & -3.9 & -57.2 & 27.5 & -10.8 \\ 206.5 & 969.9 & 1031.6 & 717.1 & 728.2 & 725.1 & 41.8 & -18.9 & -104.7 & 76.9 & -10.7 \\ 120.2 & 661.7 & 717.1 & 825.1 & 649.2 & 595.1 & -5.5 & -11.7 & -74.1 & 74.9 & 8.7 \\ 118.9 & 706.7 & 728.2 & 649.2 & 721.8 & 657.7 & -0.3 & -12.8 & -60.0 & 42.2 & 5.0 \\ 127.1 & 701.4 & 725.1 & 595.1 & 657.7 & 709.9 & 8.6 & -13.0 & -80.0 & 52.1 & 1.1 \\ 34.9 & 38.5 & 41.8 & -5.5 & -0.3 & 8.6 & 63.7 & 0.2 & -15.9 & 21.8 & 0.2 \\ -2.6 & -3.9 & -18.9 & -11.7 & -12.8 & -13.0 & 0.2 & 37.0 & -21.0 & 1.4 & 0.3 \\ -81.4 & -57.2 & -104.7 & -74.1 & -60.0 & -80.0 & -15.9 & -21.0 & 357.5 & -177.2 & -4.5 \\ 57.3. & 27.5 & 76.9 & 74.9 & 42.2 & 52.1 & 21.8 & 1.4 & -177.2 & 150.9 & 9.0 \\ -0.2 & -10.8 & -10.7 & 8.7 & 5.0 & 1.1 & 0.2 & 0.3 & -4.5 & 9.0 & 23.6 \end{bmatrix}$$

Table A.25: Seven Axle Vehicle Means for Station R001

μ_{p1}	μ_{p2}	μ_{p3}	μ_{p4}	μ_{p5}	μ_{p6}	μ_{p7}	μ_{s1}	μ_{s2}	μ_{s3}	μ_{s4}	μ_{s5}	μ_{s6}
50.29	63.72	79.09	59.94	57.23	59.29	53.21	43.58	14.72	24.75	61.08	16.83	13.31

Covariance Matrix for 7 Axle Vehicles

$$\begin{bmatrix}
241.5 & 192.2 & 194.1 & 129.4 & 29.7 & 50.9 & 91.4 & -3.3 & 4.5 & -16.7 & -25.2 & -4.0 & 1.4 \\
192.2 & 909.5 & 420.6 & -120.3 & 220.0 & 158.6 & 28.6 & 17.1 & -13.7 & -43.4 & -13.9 & -23.1 & -25.1 \\
194.1 & 420.6 & 831.0 & 526.6 & 421.5 & 452.1 & 414.8 & -16.2 & -18.9 & -40.8 & 26.5 & -3.2 & 1.8 \\
129.4 & -120.3 & 526.6 & 1114.4 & 307.5 & 398.0 & 638.8 & -19.1 & 0.1 & 13.4 & 95.9 & 1.9 & 22.6 \\
29.7 & 220.0 & 421.5 & 307.5 & 815.9 & 534.2 & 301.0 & -26.2 & -23.3 & -57.6 & 112.4 & -15.5 & -11.7 \\
50.9 & 158.6 & 452.1 & 398.0 & 534.2 & 712.4 & 406.2 & -30.4 & -18.3 & -61.4 & 60.6 & 10.8 & -1.3 \\
91.4 & 28.6 & 414.8 & 638.8 & 301.0 & 406.2 & 775.7 & -8.6 & -4.6 & -16.6 & 65.0 & -1.6 & 12.0 \\
-3.3 & 17.1 & -16.2 & -19.1 & -26.2 & -30.4 & -8.6 & 123.1 & 6.5 & 19.5 & -27.1 & -10.8 & -6.1 \\
4.5 & -13.7 & -18.9 & 0.1 & -23.3 & -18.3 & -4.6 & -6.5 & 195.8 & -28.2 & -122.6 & -0.2 & 1.4 \\
-16.7 & -43.5 & -40.8 & 13.4 & -57.6 & -61.4 & -16.6 & 19.5 & -28.2 & 865.7 & -586.1 & -26.1 & -0.9 \\
-25.2 & -13.9 & 26.5 & 95.9 & 112.4 & 60.6 & 65.0 & -27.1 & -122.6 & -586.1 & 1223.6 & -192.2 & -36.2 \\
-4.0 & -23.1 & -3.2 & 1.9 & -15.5 & 10. & -1.6 & -10.8 & -0.2 & -26.1 & -192.2 & 224.8 & 3.2 \\
1.4 & -25.1 & 1.8 & 22.6 & -11.7 & -1.3 & 12.0 & -6.1 & 1.4 & -0.9 & -36.3 & 3.2 & 98.2
\end{bmatrix}$$

Appendix B: Cross Sections of Superstructures Designed using AASHTO LRFD

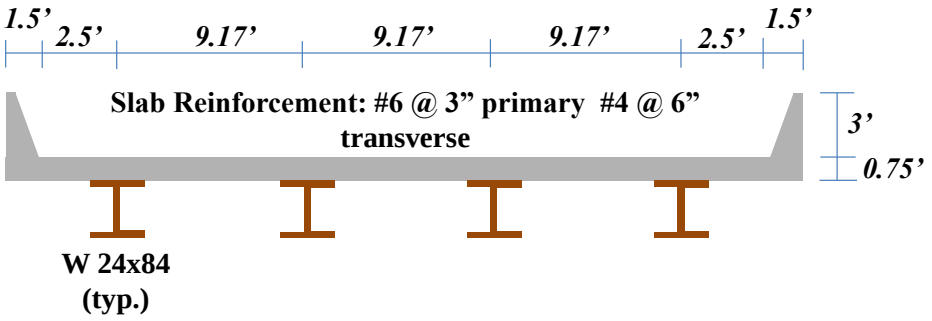

Figure B.1: 10m Bridge Superstructure Cross Section

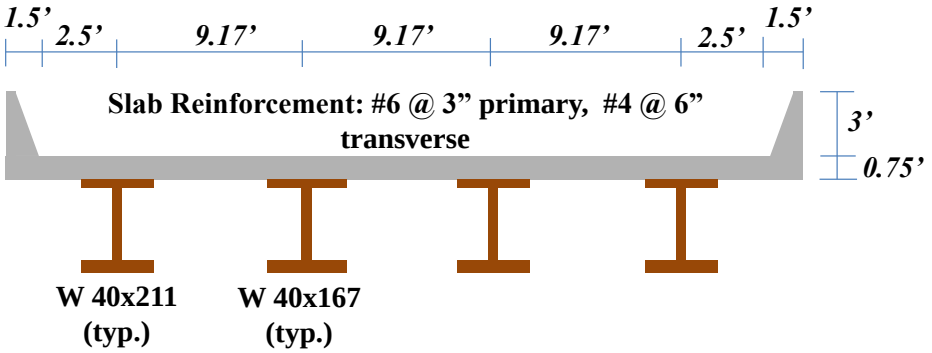

Figure B.2: 20m Bridge Superstructure Cross Section

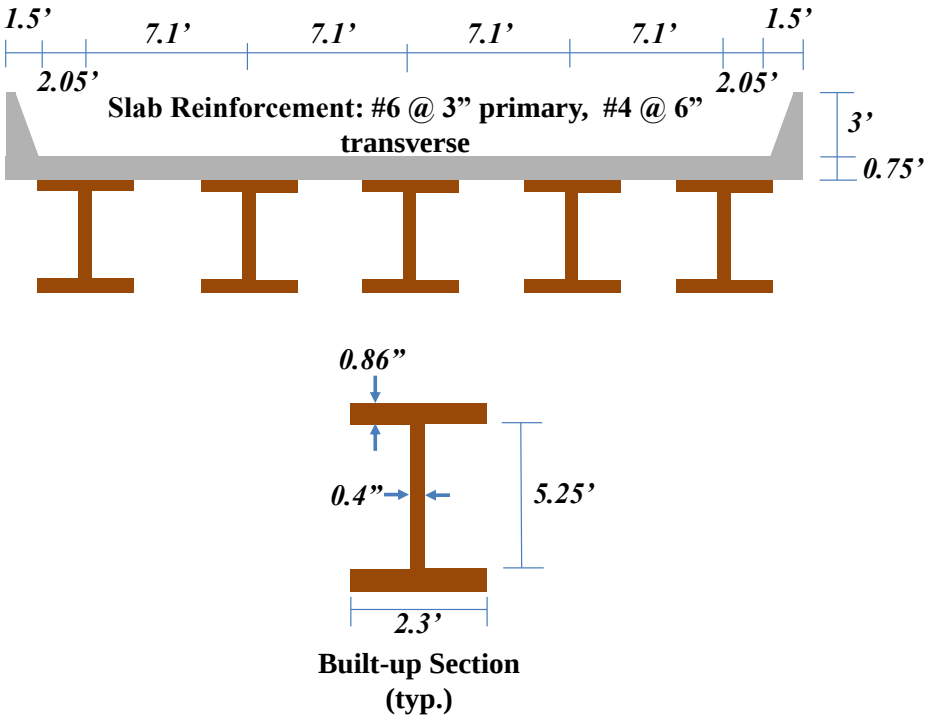

Figure B.3: 30m Bridge Superstructure Cross Section

Appendix C: Bridge Finite Element Models

This appendix shows screen captures of the finite element models of sample bridges. The models were used to verify design calculations, as well as to determine the true proportion of the live load that each girder must support. This was a crucial step for the reliability calculations because the distribution factors calculated using the AASHTO Specifications use the lever rule, which gives a conservative estimate of this proportion. The lever rule is conservative because it does not account for the redundancy due to multiple girders and overall structure stiffness. The models were formulated using the software SAP2000. The parameters that were input include concrete compressive strength, steel yeild strength, reinforcing steel area, as well as the level of composite action between slab and girders.

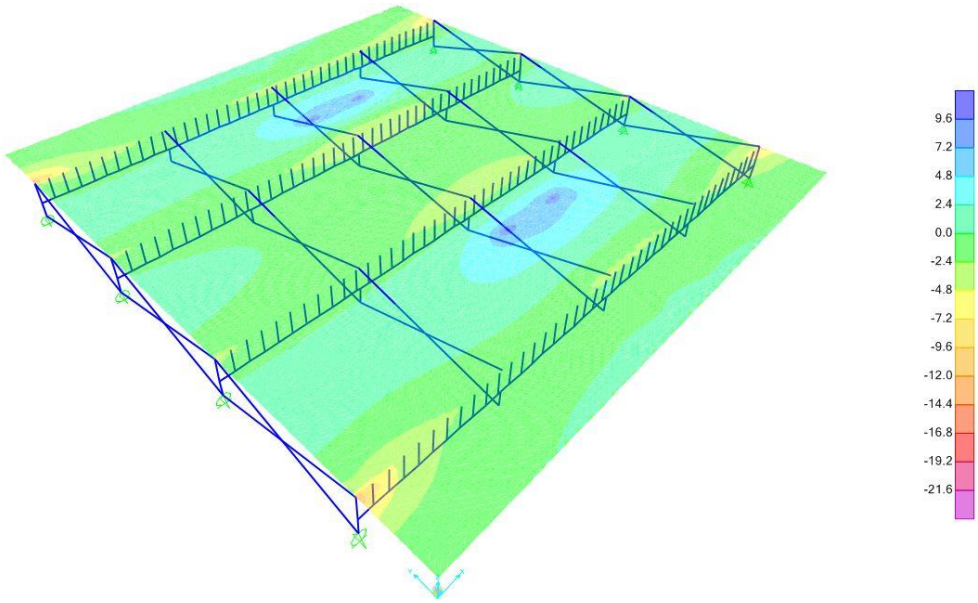

Figure C.1: Finite Element Model Showing Stress Contours in Slab

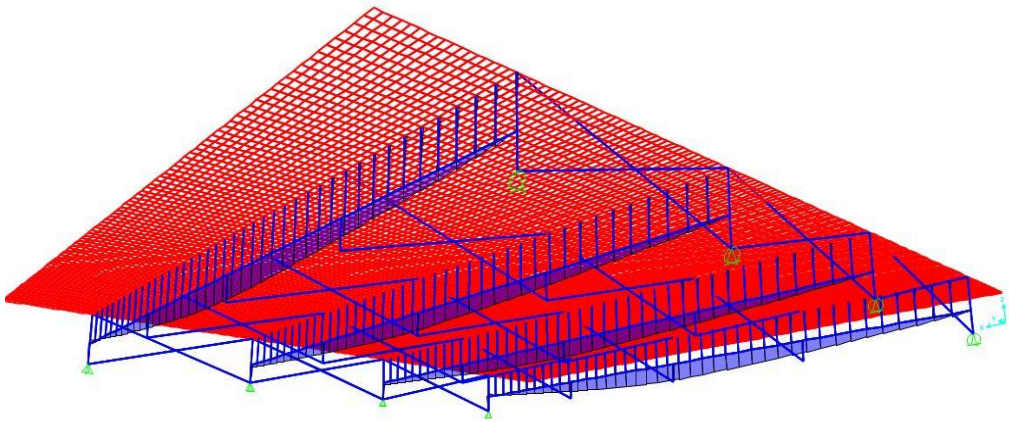

Figure C.2: Finite Element Model Showing Bendimg Moment Diagram on Beams

Appendix D: Fit of Mixture Models to Data

This appendix shows the fitted mixture models plotted over a relative frequency histogram of the bending moments produced by all vehicldes in a given year at the four stations analyzed. The x axis values are bending moments and the y axis represents a probability density or relative frequency.

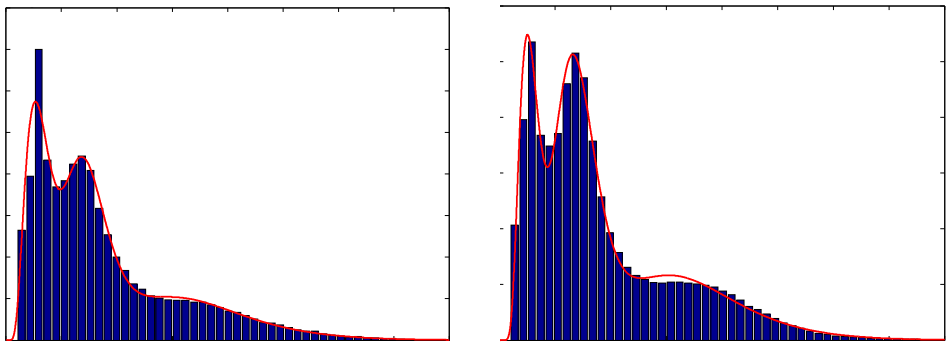

Figure D.1: Station R100 years 2002 (left) and 2003 (right)

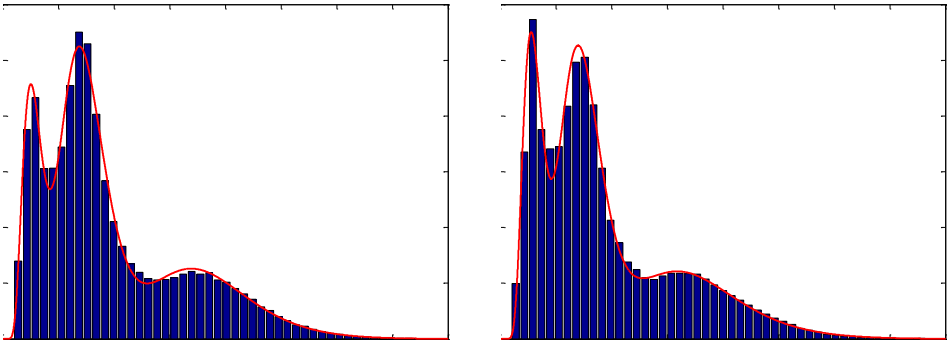

Figure D.2: Station R100 years 2004 (left) and 2005 (right)

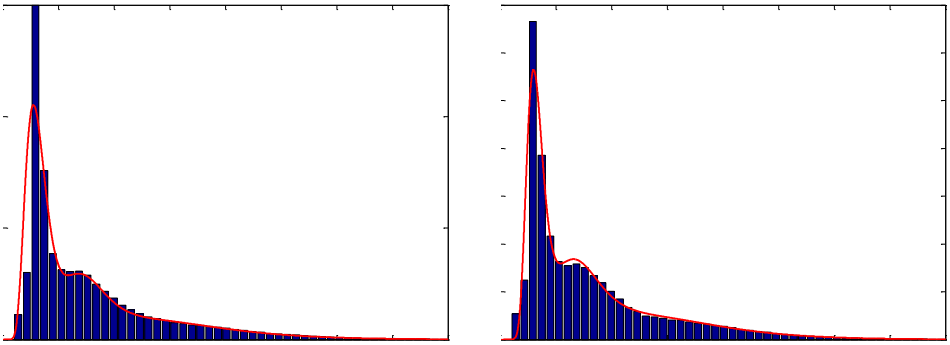

Figure D.3: Station R100 years 2006 (left) and 2007 (right)

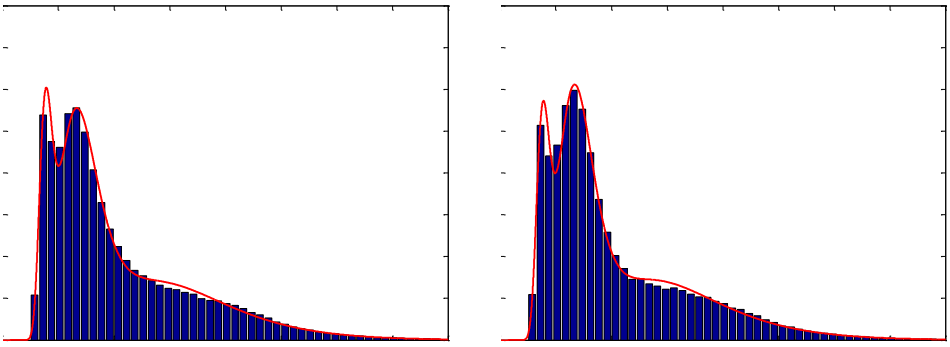

Figure D.4: Station R100 years 2008 (left) and 2009 (right)

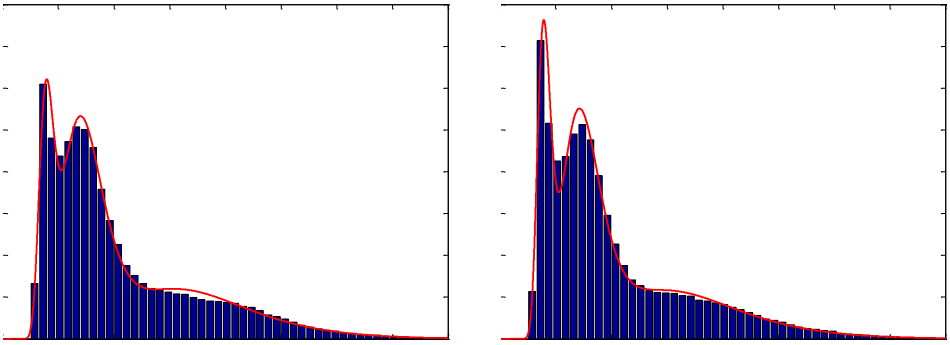

Figure D.5: Station R100 years 2010 (left) and 2011 (right)

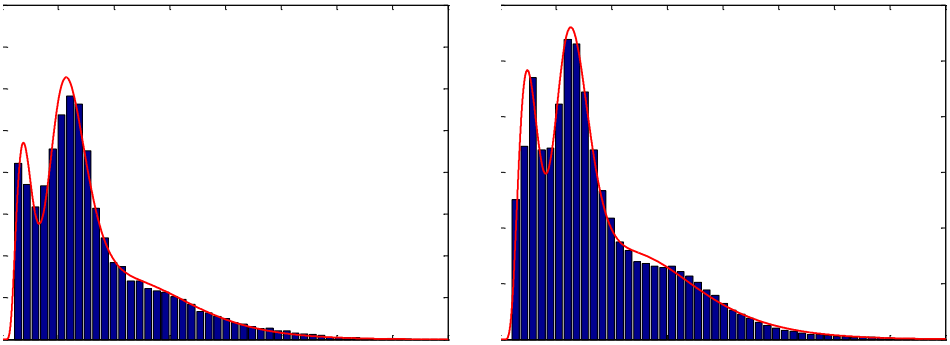

Figure D.6: Station X249 years 2000 (left) and 2001 (right)

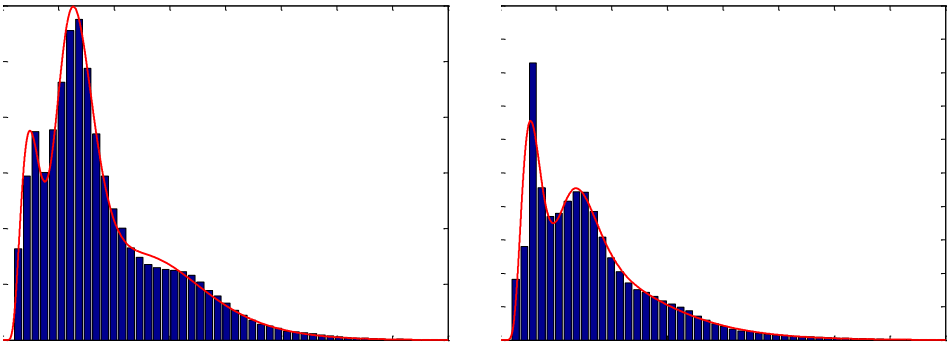

Figure D.7: Station X249 years 2002 (left) and 2003 (right)

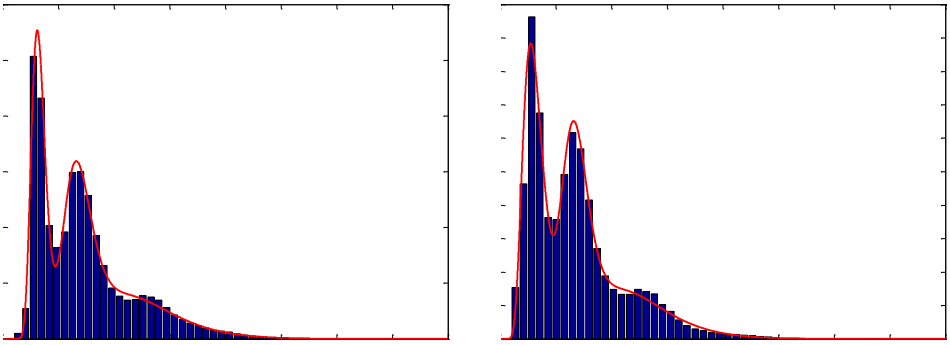

Figure D.8: Station X249 years 2004 (left) and 2006 (right)

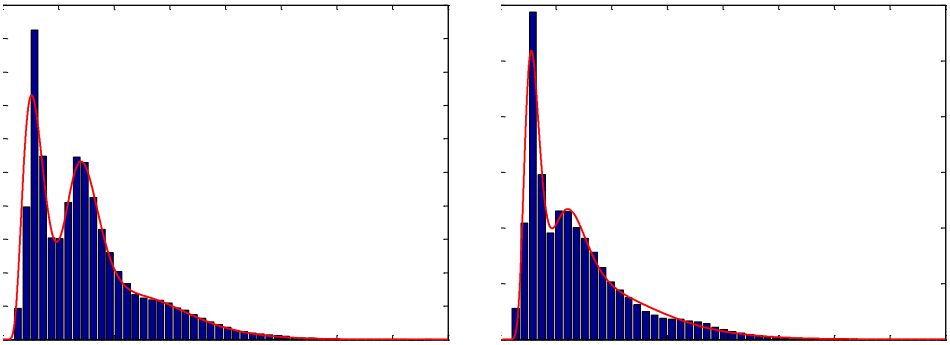

Figure D.9: Station X249 years 2007 (left) and 2008 (right)

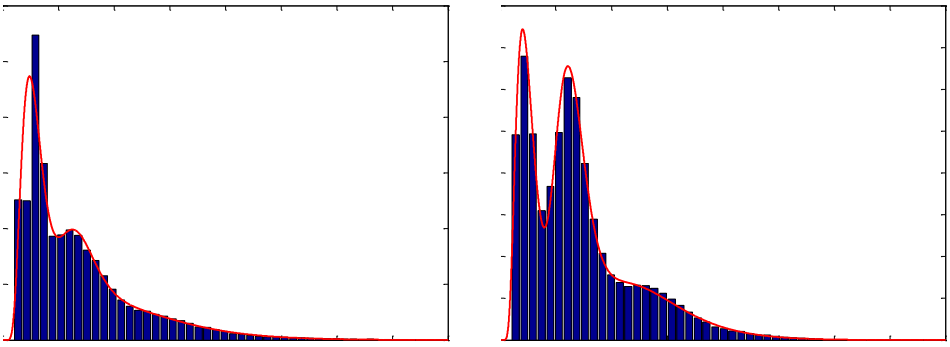

Figure D.10: Station X249 years 2009 (left) and 2010 (right)

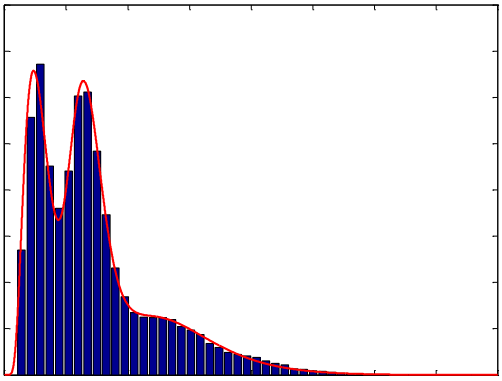

Figure D.11: Station X249 year 2011

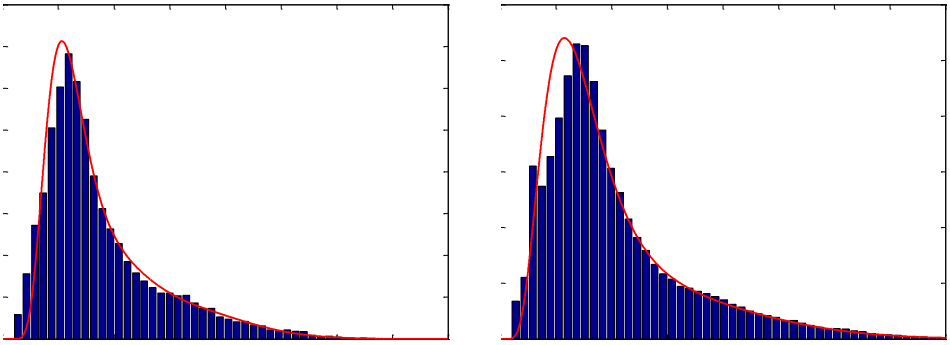

Figure D.12: Station G005 years 2000 (left) and 2001 (right)

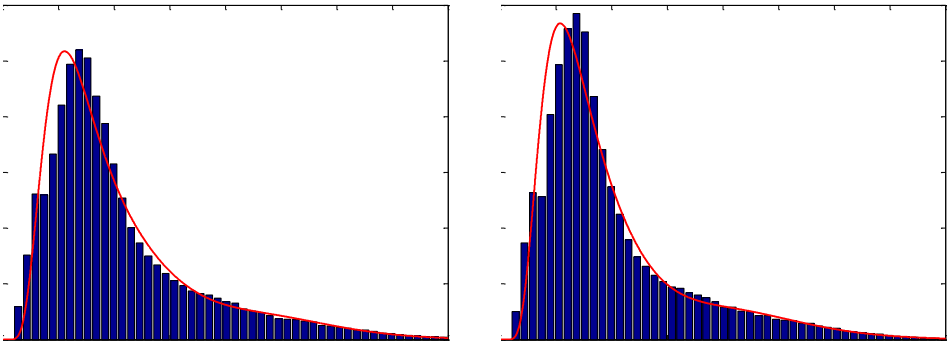

Figure D.13: Station G005 years 2002 (left) and 2003 (right)

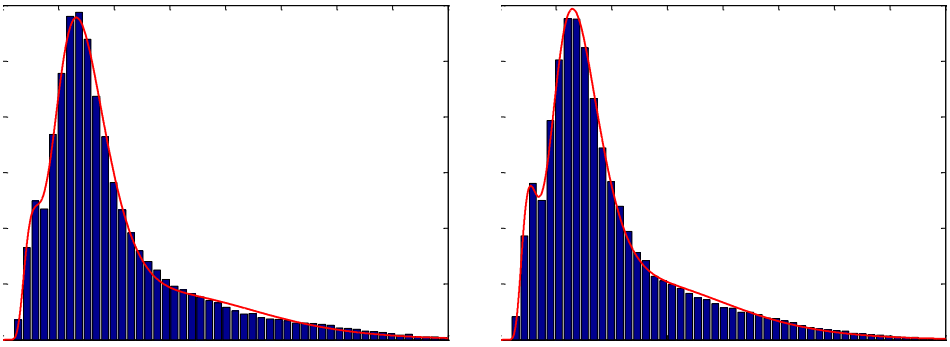

Figure D.14: Station G005 years 2004 (left) and 2005 (right)

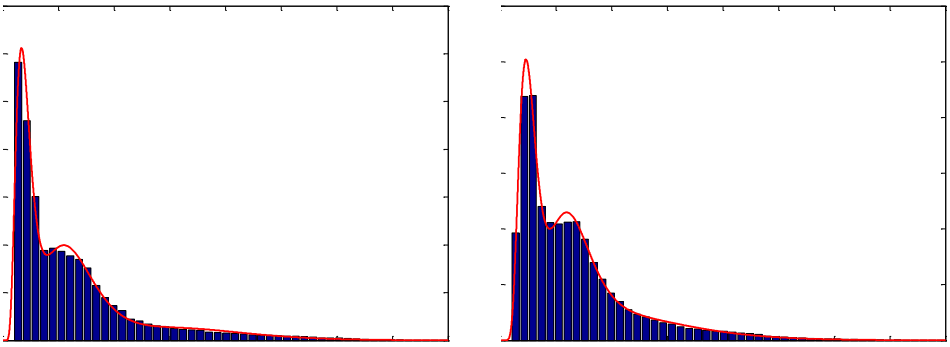

Figure D.15: Station G005 years 2006 (left) and 2007 (right)

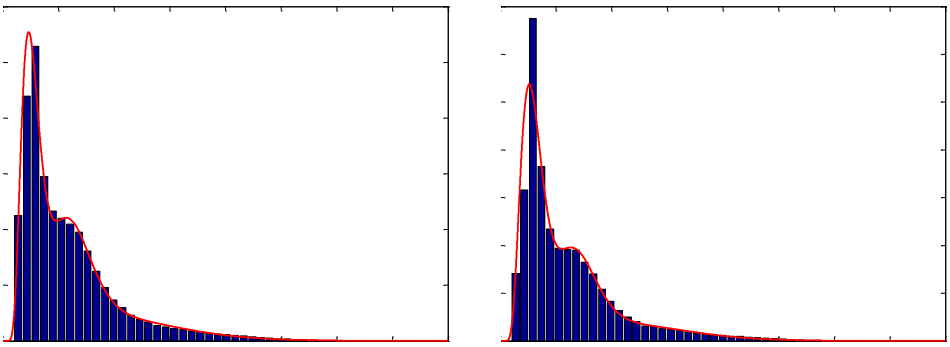

Figure D.16: Station G005 years 2008 (left) and 2009 (right)

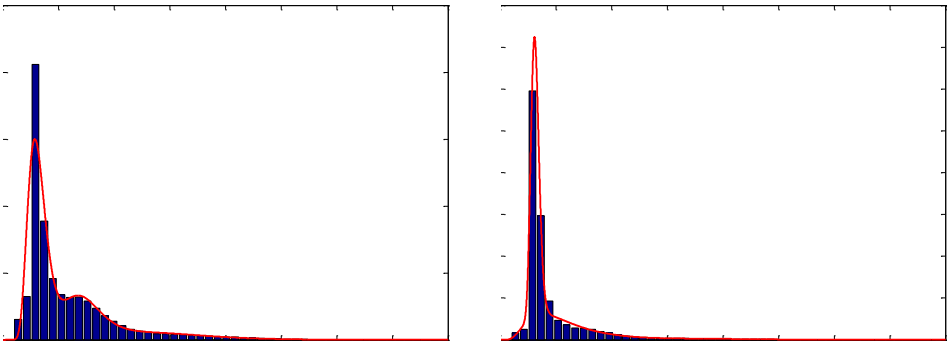

Figure D.17: Station G005 years 2010 (left) and 2011 (right)

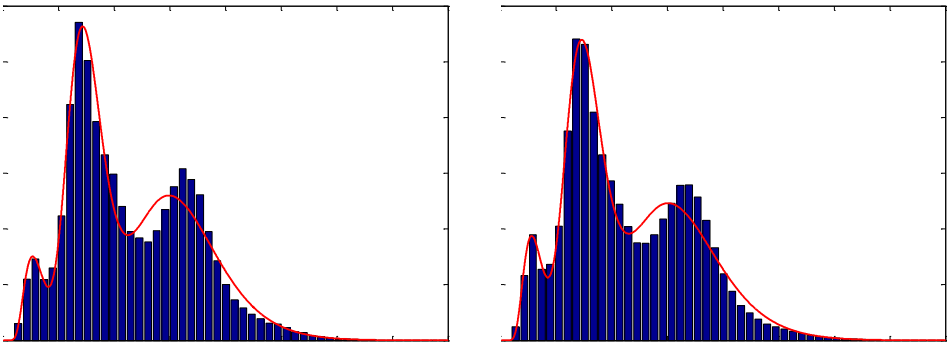

Figure D.18: Station R001 years 2000 (left) and 2001 (right)

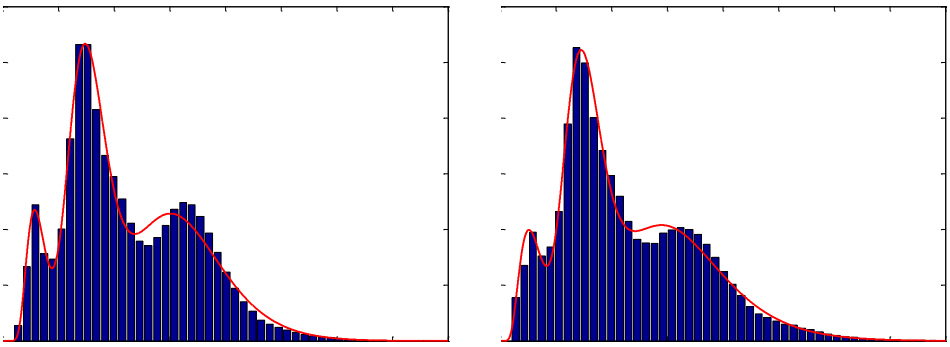

Figure D.19: Station R001 years 2002 (left) and 2003 (right)

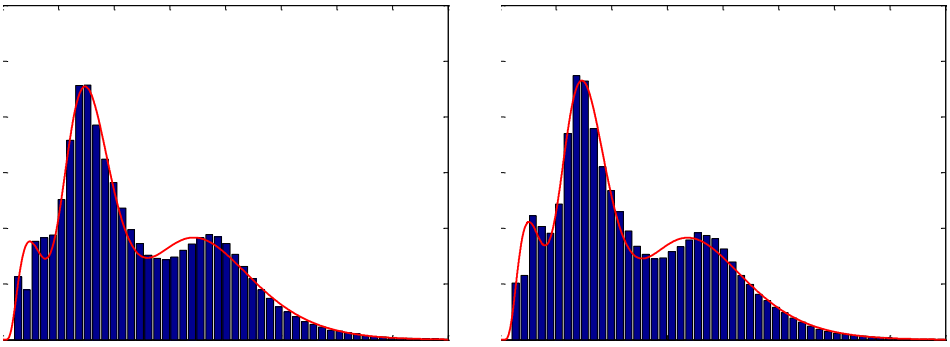

Figure D.20: Station R001 years 2004 (left) and 2005 (right)

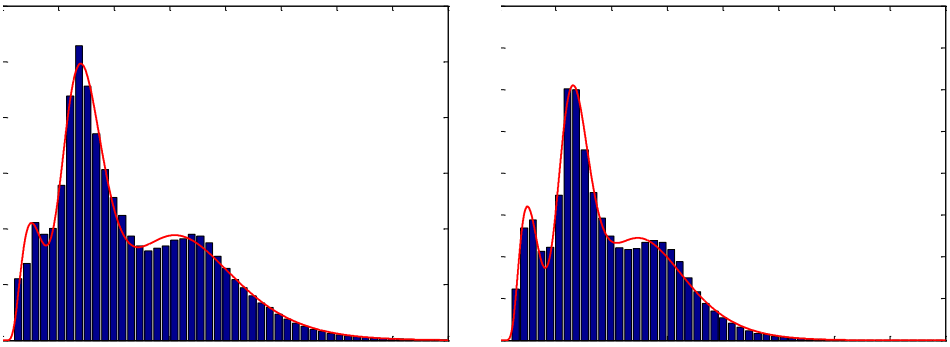

Figure D.21: Station R001 years 2006 (left) and 2007 (right)

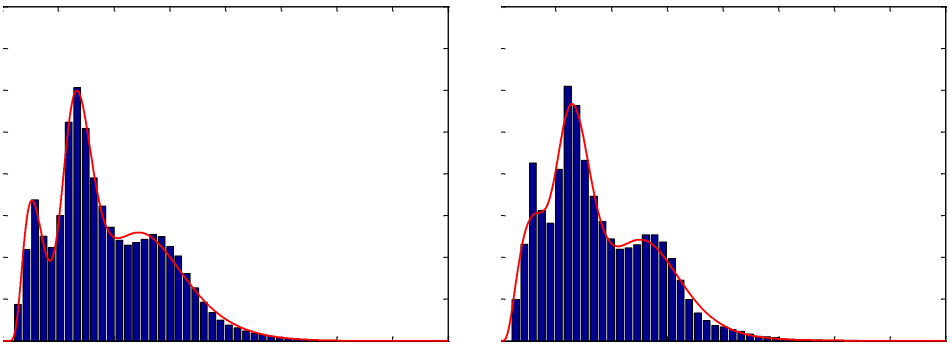

Figure D.22: Station R001 years 2008 (left) and 2009 (right)

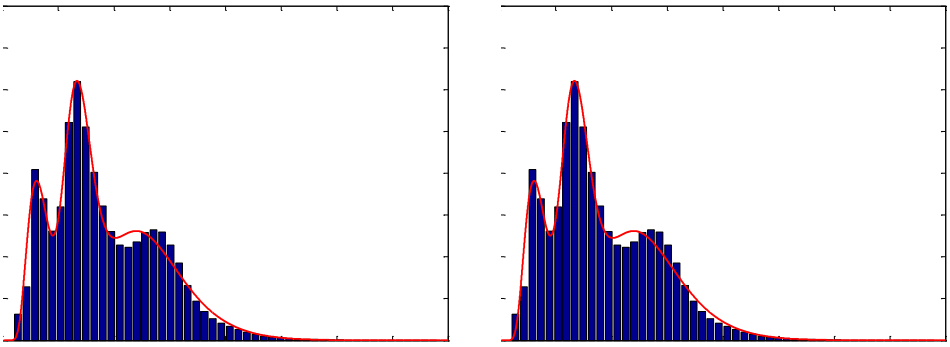

Figure D.23: Station R001 years 2010 (left) and 2011 (right)